STUDIES ON SOME PROPERTIES OF PHOTON INDUCED COSMIC RAY AIR SHOWERS

A THESIS

SUBMITTED TO THE GAUHATI UNIVERSITY

FOR THE AWARD OF THE DEGREE OF

DOCTOR OF PHILOSOPHY

IN PHYSICS

IN THE FACULTY OF SCIENCE

BY

PUNAM PATGIRI

DEPARTMENT OF PHYSICS

GAUHATI UNIVERSITY

2016

Dr. (Mrs) Kalyanee Boruah
Professor
Department of Physics
GAUHATI UNIVERSITY
Guwahati – 781 014
Assam, INDIA

Ph: +91-361-2570531 (O)
+91-361-2674537 (R)
Mobile: 9435543920
E-mail: kalyanee1@rediffmail.com
kalyaneeboruah@gmail.com
Residence: Qr. No. 45, GU Campus

CERTIFICATE

This is to certify that Ms. Punam Patgiri, M.Sc. has worked under my guidance and supervision since May, 2010 for her thesis entitled "Studies on some properties of photon induced cosmic ray air showers" which is being submitted to the Gauhati University for the award of the Degree of Doctor of Philosophy.

This thesis is based on original work done by Ms. Punam Patgiri. She has fulfilled all the requirements under the Ph.D regulation of Gauhati University and has published a few original research papers in reputed Journals and Conference Proceedings. She has also presented research papers in the Regional and National Conferences.

The whole research work incorporated in her thesis is original work done by her and no part is submitted to any University for any other degree.

8-8-16

(Kalyanee Boruah)

Professor & Research Guide

Professor
Department of Phys.
Gauhati University

DECLARATION

The thesis entitled "***Studies on some properties of photon induced cosmic ray air showers***" is an original work done by me and I am submitting this as a fulfillment of the requirements for the award of Degree of Doctor of Philosophy in Physics of Gauhati University. I hereby, declare that no portion of this work incorporated here has been submitted to Gauhati University or anywhere else by me or by any other person for the award of any degree.

Date : 08/08/16

Punam Patgiri.
(Punam Patgiri)

Place : Guwahati

DEDICATED TO

My parents, sisters

and brother

ACKNOWLEDGEMENT

First and foremost, I express my sincere thanks and gratitude to my respected supervisor Prof. Kalyanee Boruah, Department of Physics, Gauhati University, for her kind and sincere help and invaluable guidance and supervision all throughout my Ph.D work, which finally enabled me to complete my thesis. I am also indebted to Prof. Pradip Kr. Boruah, Department of Instrumentation and USIC, G.U., who offered his valuable suggestions and discussions during my work.

I am also indebted to Prof. Anurup Gohain Barua, Head, Department of Physics, Gauhati University for providing necessary Departmental Laboratory and Library facilities during the course of my study.

I also acknowledge my gratitude to all the esteemed faculty members of Department of Physics, and also Prof. N. Nimai Singh, Ex-Head of the Department of Physics, G.U., who actively participated during all my presentations about this work and solicited their valuable suggestions which helped me to improve my work to a large extent. I will ever remain grateful to all the members for their motivation and encouragement.

I am grateful to Dr. D. Heck and his team for giving permission and guidance to use the simulation code CORSIKA in this work.

I express my deepest regard for my co-workers: Dr. Dipsikha Kalita, Dr. Chabin Ch Thakuria, Ms. Bonita Das, Dr. M Rahman, Dr. Bandita Choudhury for their constant support and kind co-operation during the tenure of my research work. It has indeed been a fruitful experience for me that helped me in carrying out my research work and I am deeply indebted to everyone for that.

I gratefully acknowledge the University Grant Commission (UGC), New Delhi for providing financial assistance.

My heartfelt thanks goes to Kunjalata Kalita and Nipan Das of Department of Instrumentation and USIC for their assistance and encouragement during my research period. I thank staff members of Physics Department, Seminar Library, K K Handique Library and Administration for their timely help.

I sincerely acknowledge the constant encouragement and support of my parent Late Bhupendra Nath Patgiri and Mrs. Charulata Patgiri which immensely helped me in completing my research work and writing thesis. In addition, I offer my special gratitude to my sisters Juri Patgiri and Rubi Patgiri, brother Pritam Patgiri, brother in laws Dr. Pabitra Rajbongshi and Ananta Rajbongshi for being supportive in my field. I express my deep love and affection to my nieces Janisha, Nerissa, Tanisha and Krishangi whose every activities were the source of inspiration for me during my research work. Last but not the least, I express my thanks to my roommate Suman Agarwalla for her encouragement and support.

CONTENTS

List of Figures:

List of Tables:

CHAPTER-1

INTRODUCTION

High energy Cosmic Ray (CR) physics is an important branch of Astroparticle Physics since its discovery in 1912. Research on cosmic rays is being carried out over 100 years to resolve the unsolved problems relating to their origin, acceleration and transport to the earth's atmosphere. The study of cosmic ray physics opens a wide range for research in the field of astronomy, astrophysics and particle physics. The extensive air showers produced by the cosmic ray particles on the earth's atmosphere provide information on the properties of different primary particles coming from the outer space. The study of gamma ray induced showers can furnish information on the sources of high energy cosmic rays. Supernova remnants, pulsars, X-ray binaries, radio galaxies, quasars etc. are the potential sources of cosmic rays as well as the high energy gamma rays. So in order to predict the sources, gamma ray induced showers should be separated from hadron induced showers. In this thesis we have investigated the properties on which gamma ray induced showers are different from hadron induced showers.

1.1 Cosmic Rays

Earth is subjected to a constant bombardment of charged particles having energy ranging from about GeV to beyond 10^{20} eV [1] from Galactic and Extra-Galactic sources. They are usually a proton, an electron, or an atomic nucleus, produced by various astrophysical processes that are taking place in the universe. The primary particles collide and interact with the atmospheric nuclei and give rise to a cascading shower of secondary particles which is known as the Extensive Air Shower (EAS). At energies above 10^{14} eV, primary cosmic rays can be studied only by detecting these air showers [2]. Various groups of cosmic ray physicists have been conducting experiments to solve the problems relating to nature of different physical processes that are taking place in the universe and the origin of ultra high energy particles.

1.1.1 Discovery of Cosmic Rays

Until the discovery of cosmic rays, it was believed that the ionization of particles occurred only due to the phenomenon of radioactivity. In 1912, the Austrian physicist, Victor Hess found that the ionization rate increases with height. His famous balloon flight was consisted of three enhanced accuracy Wulf electrometers to measure the ionization radiation. After a series of observations, to his surprise, found that ionization rate had increased approximately three times more at an altitude of 17,400 feet (5,300 meters) than

the ground [3]. Hess concluded that this ionization is due to some radiations coming from the outer space.

Soon after Victor Hess' balloon flight, in 1913-14, W. Kolhorster conducted the same experiment at an altitude of 9 km. His findings were same as that of Hess, which confirmed that the increase of ionization with altitude was due to arrival of penetrating radiation from outside the earth's atmosphere [4]. In 1925, these extra-terrestrial radiations were termed as cosmic rays by Robert Millikan. In 1936, Victor Hess was awarded the Nobel Prize in Physics for his discovery.

After the discovery of cosmic rays, a new field of research had emerged. Several experiments were carried out by various physicists to establish the properties of cosmic rays and their origin. During the period of 1930 to 1945, it was confirmed that the composition of primary cosmic rays are mainly protons. The observations carried out by balloons containing nuclear emulsions at the top of the atmosphere showed that the primary cosmic ray also composed of helium nuclei (about 10%) and heavier nuclei (about 1%) [5]. Many fundamental discoveries had been made from the study of cosmic rays. In 1933, Anderson discovered positrons the antiparticle of electrons. Pierre Auger in 1939 observed the existence of extensive air shower particles in the atmosphere from the detection of coincidence between the horizontally placed scintillation counters [6].

1.1.2 Origin of Cosmic Rays

The mystery behind the origin of cosmic ray physics remained unsolved even after 100 years of its discovery. The high energy cosmic rays must have originated in the interstellar medium with acceleration mechanism. The Sun and Milky Way are considered to be sources of low energy cosmic rays particles. The ultra high energy cosmic rays are of extra-galactic origin. The exploding stars, known as supernovae, gamma ray burst, pulsars, X-ray binaries, radio galaxies, quasars etc. are considered to generate these high energy particles. The origin of ultra high energy cosmic rays sources can be explained with the help of two models. One is bottom-up and other is top-down model [7].

In bottom-up scenario, protons and ions get accelerated from lower to higher energies within the strong magnetic field. Basically two different acceleration mechanisms exist. One is diffusive or stochastic shock acceleration, proposed by Fermi [8], occurs in supernovae remnants, gamma ray bursts (GRBs), active galactic nuclei (AGNs), hot spots of colliding galaxies and radio galaxies. In this process particles get accelerated to high energies by repeated collisions with the magnetic clouds. The power law spectrum of the cosmic rays is an important consequence of this mechanism [9]. The other process is known as the one shot model or inductive acceleration mechanism. Here acceleration of particles takes place by strong electric fields, during the rotation of compact objects such as accretion disks of black holes or highly magnetized neutron stars [10]. This diffusive acceleration mechanism is relatively slower than the inductive mechanism.

While in top-down scenario, no acceleration mechanism is involved. In this process, high energy particles get created by the decay of unstable heavy elements which have originated in the very early universe. Here again two different processes are involved. One can be described by the topological defects and other by cold dark matter. Topological defects have originated from the phase transition of early universe and are related to monopoles, cosmic strings and superconducting strings which are considered to be the potential sources of ultra high energy cosmic rays [11]. The second process is based on the decay of long lived heavy relics which were created in the early universe. By the formation of clusters, relic particles behave like cold dark matter particles which can produce ultra high energy particles [10]. The composition of UHE cosmic rays should be dominated by electrons and photons in top-down model as they are the decay products of super heavy relics. So this model contradicts with the bottom-up model.

Based on the energy content, cosmic ray particles can be classified into four main categories as, Solar Cosmic Rays, Galactic Cosmic Rays, Extra Galactic Cosmic Rays and Anomalous Cosmic Rays.

Solar Cosmic Rays:

The Sun is a source of cosmic ray in our neighbourhood. The energy of solar protons, electrons and ions varies from 10^7 to 10^{10} eV [12]. So they must be measured by space borne instruments. The high energy solar particles are produced from the activity of solar flares and coronal mass ejection. These particles can be observed directly at Earth or in interstellar medium.

Galactic Cosmic Rays:

The cosmic ray particles that originate within our own galaxy Milky Way but outside the Sun are known as Galactic cosmic rays. They can have energies from 10^{10} to 10^{18} eV i.e. they can be observed upto the second knee of energy spectrum. They are mainly generated by the Supernovae explosion [13]. The expanding shock front accelerates the cosmic ray particles to higher energies i.e. nearly the speed of light. The composition of galactic cosmic rays is heavier than solar components as it contains heavier atomic nuclei.

Extra-Galactic Cosmic Rays:

Cosmic rays originating from outside our galaxy are known as Extra-galactic cosmic rays. They evolve with energy higher than 10^{18} eV and produced by acceleration in the extragalactic shocks. The sources of these high energy particles are considered to be active galactic nuclei, pulsars, quasars and gamma ray bursts.

Anomalous Cosmic Rays:

Anomalous cosmic rays are component of nuclear radiation beyond the heliosphere. They are component with lowest energy i.e. 10^{7} to 10^{8} eV originating from neutral interstellar atoms [14]. Neutral atoms such as helium, oxygen, nitrogen undergo single ionization on entering the heliosphere by the ultra violet radiation emitted by the sun. The

charged particles are carried to the solar wind termination shock and get accelerated to higher energies [15].

1.1.3 Acceleration

The study of acceleration mechanism of high energy particles is of great importance for the scientists. As mentioned in section 1.1.2, the acceleration of cosmic ray particles is associated with the bottom-up model. The theory on the acceleration of cosmic ray particles was postulated by Enrico Fermi in 1949 for the first time [8]. The Fermi acceleration is of two types. One is first-order Fermi acceleration also known as diffusive shock acceleration and other is second-order Fermi acceleration. Both types of mechanisms describe the evolution process of high energy particles in the universe.

1.1.3.1 First order Fermi Acceleration

The first order Fermi acceleration theory can be applied to interpret the distribution of non thermal synchrotron radiation in various astrophysical shock waves. According to this mechanism acceleration of cosmic ray particles occurs in collisionless environment. A charged particle diffuse from upstream to downstream in a shock wave through collision with the magnetic turbulence of plasma. This particle again collides with the magnetic turbulence of plasma and gets reflected back to upstream. This process of reflection continues and as a result, particle emerges with an increased velocity [16].

The average energy gain $(\Delta E/E)$ per collision in this process is

$$\frac{\Delta E}{E} = \frac{4}{3}\frac{v}{c} \tag{1.1}$$

where v is speed of the magnetic turbulence of plasma and c is speed of the moving charged particle [17].

This theory plays a pivotal role in the interpretation of acceleration mechanism associated with shock waves like supernova remnants and solar flares.

1.1.3.2 Second order Fermi Acceleration

According to this model, charged particles gain or lose energy by head-on and tail-end collisions with the interstellar magnetic clouds. As the probability of head-on collision is more so the particles get accelerated to high energy by repetitive collision with the magnetic clouds which act as magnetic mirrors. In this process the average energy gain $(\Delta E/E)$ is given by [17]

$$\frac{\Delta E}{E} = \frac{8}{3}\left(\frac{v}{c}\right)^2 \tag{1.2}$$

where v is speed of the magnetic clouds and c is the speed of the moving charged particle. This process is called second order as the average energy gain is proportional to $(v/c)^2$.

1.1.4 Energy Spectrum

The total flux of cosmic ray follows a simple power law equation over an energy range of 1 GeV to above 10^{20} eV,

$$\frac{dN}{dE} = E^{-\gamma} \qquad (1.3)$$

where the exponent, γ is called the slope of the energy spectrum.

At lower energies, below 10^{14} eV primary particles can be measured easily by means of satellite and balloon borne detectors due to their very high flux [18]. It has been found that at an energy about 10^{11} eV, one particle hits per square meter of the earth's surface per second. Here composition is believed to be lighter and of solar origin. Above 10^{14} eV, the cosmic ray flux decreases rapidly to a point, where direct detection becomes almost impossible. The ground based arrays measuring the extensive air showers produced by primaries in the atmosphere can derive the energy of these high energy cosmic ray particles. The variation of the cosmic ray flux with primary energy is shown in Fig. 1.1. From this figure one can observe the change of slope of the energy spectrum at two distinct points which are known as knee (~5×10^{15} eV) and ankle (~5×10^{18} eV). Various groups of scientists had measured the wide range of energy spectrum as shown in Fig. 1.2. Here the structure is enhanced by multiplying the energy spectrum by a factor $E^{2.5}$.

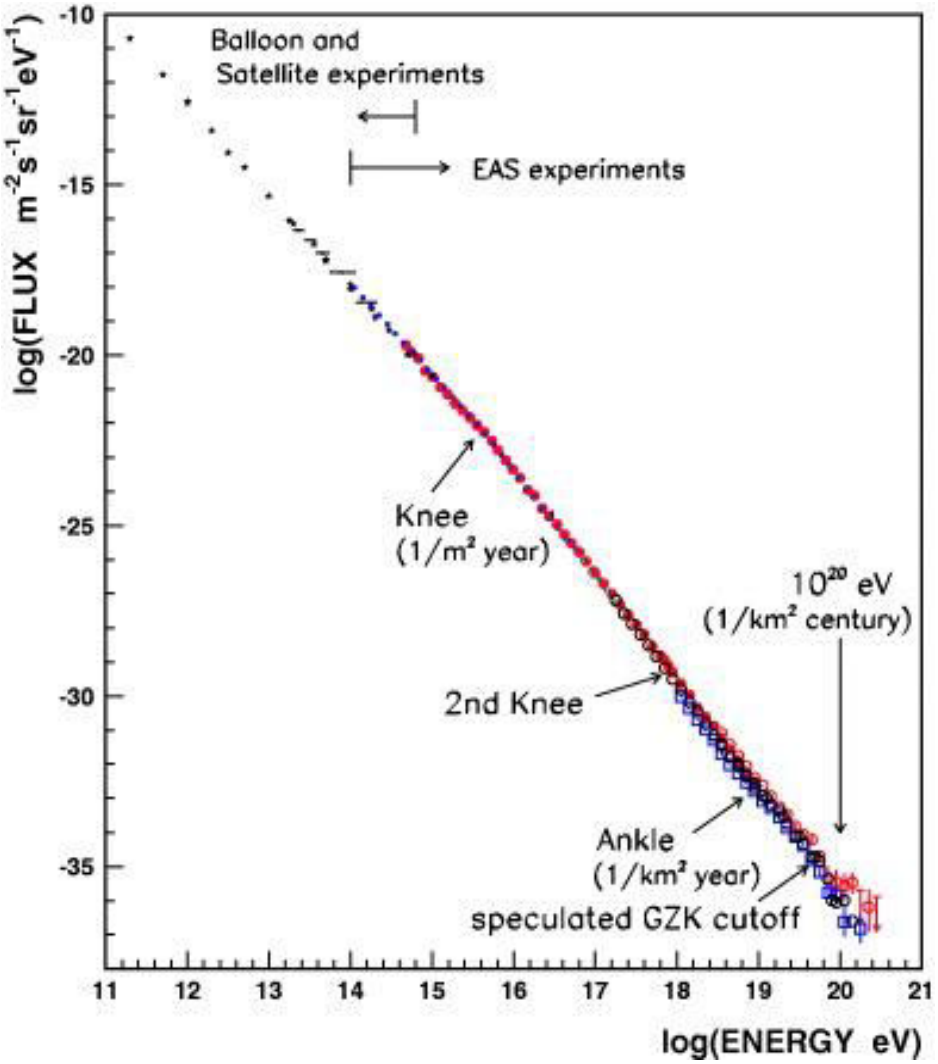

Figure 1.1: Energy spectrum of primary cosmic rays [19]. The red closed and open circles represent Akeno-AGASA results, dots represent the direct observations with balloon- and satellite-borne detectors, blue circles represent Tibet results below and above the knee, open black circles and open blue squares represent the results from HiRes and Auger observatories.

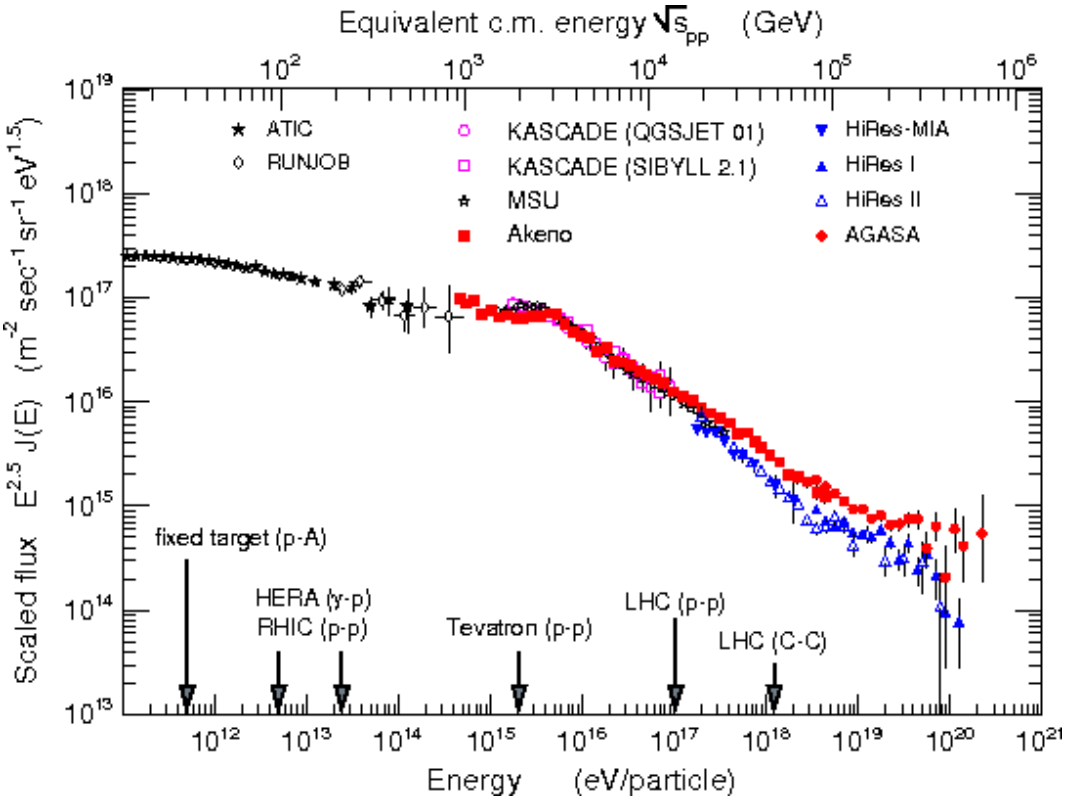

Figure 1.2: Differential energy Spectrum of the cosmic ray flux [20] multiplied by a factor $E^{2.5}$.

The composition of primary cosmic ray and the steepening of energy spectrum are inter-related. It has been considered that the cosmic ray mass composition changes from lighter to heavier at around 5×10^{15} eV. This particular point is called as the knee where steepening of the slope occurs from 2.7 to 3.0 due decrease of flux i.e. only one particle per square meter per year [21]. Again a second knee is observed at around 5×10^{17} eV with

spectral index 3.3. Here the origin of cosmic ray is outside the solar system but within our galaxy. The Galactic cosmic rays mainly originate from the supernovae explosions. Further the slope flattens to 2.7 at an energy 5×10^{18} eV, which is known as the ankle [22]. At this position the composition again changes from heavier to lighter due to extra-galactic origin.

Near 5×10^{19} eV, another steepening of the energy spectrum is observed due to further decrease of cosmic ray flux. This particular effect is called as the GZK cut-off as predicted by Greisen, Zatsepin and Kuzmin in 1966 [1]. The high energy protons interact with the photons of cosmic ray microwave background within a distance of 150 million light years and produce pions. In this process they lose much of their energy and so not able to reach the earth. Above 10^{19} eV the flux is much reduced to one particle per square kilometer per century [23].

1.1.5 Cosmic Ray Composition

The cosmic ray composition study can help in solving the questions relating to the origin and acceleration of high energy particles. Nearly all the elements of periodic table are found in cosmic ray composition. Generally the dominant composition is nucleonic i.e. proton to heavier elements with about 95% to 99% (about 89% protons, 10% helium and 1% other heavier nuclei). The remaining percentage is covered by leptons and other exotic particles. Primary electrons comprise about 1%, and gamma photons about 10^{-4} of the nuclear flux. The chemical composition keeps changing with the energy spectrum. In the

energy range 0.1-100 TeV, the observed composition is 50% protons, 25% helium nuclei, 13% iron nuclei and 13% CNO [24]. Fig. 1.3 shows the relative abundance of various elements found in cosmic rays and in the solar system.

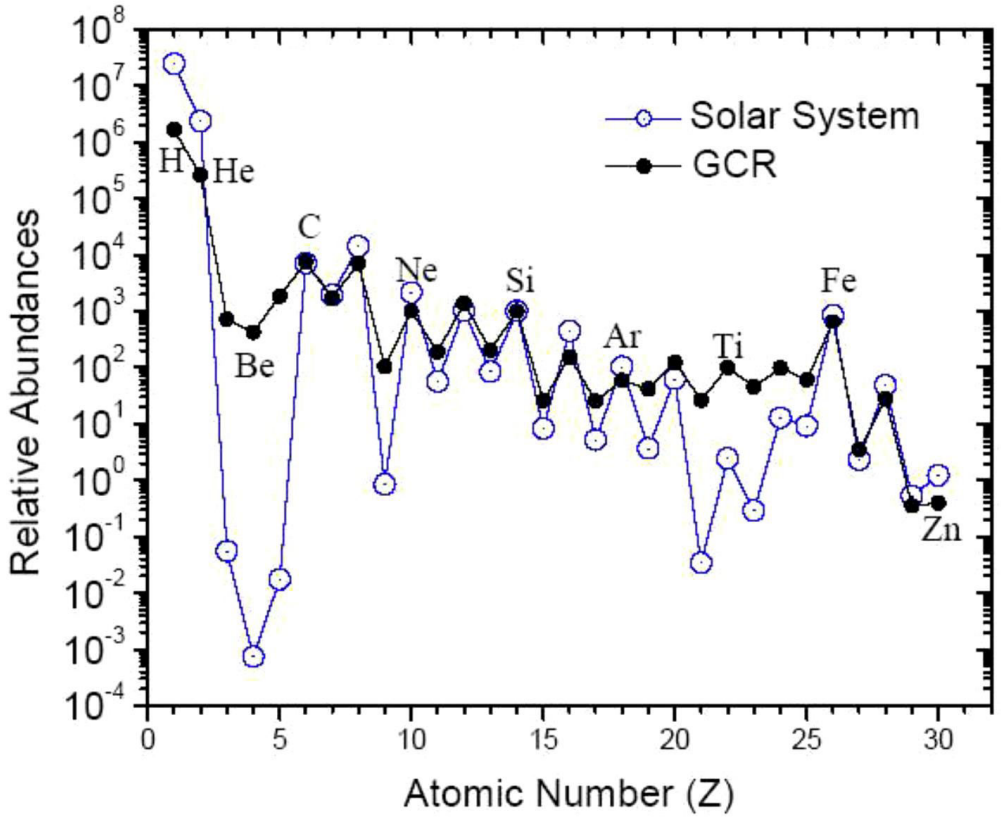

Figure 1.3: The composition of low energy cosmic ray particles along with the composition in the Solar System.

From the above Fig. 1.3, it is clear that the relative abundance of the normally found elements such as carbon, oxygen, silicon and iron are same in both cosmic ray and solar system. However the rarely observed elements such as lithium, beryllium, boron show higher abundances in GCR than in the solar system. During the collision of heavier nuclei with the interstellar gas, these rare elements are produced. Due to high ionization energy, lighter elements such as hydrogen and helium cannot get accelerated and hence they are less abundant in galactic cosmic rays than the solar system [25]. These differences in composition can furnish valuable information about the origin and acceleration of cosmic rays.

1.2 Extensive Air Showers

The high energy primary cosmic ray particles coming from the outer space suffer different types of nuclear interactions at the earth's atmosphere and as a result, generate secondary particles. These secondary particles interact again and again with the air nuclei until their energy is sufficient for further interactions. As a result, a large number of secondaries are produced and this process is termed as the Extensive Air Shower. At energies above 10^{14} eV, cosmic ray flux decreases to a point where direct detection of the high energy particles is not possible. The only practical method to study these high energy cosmic ray particles is to detect air showers [2]. The phenomenon of air shower was discovered by Bruno Rossi in 1934 [26]. With the help of coincidence circuit, Rossi found that many particles had arrived simultaneously at the detector level only within few meters.

And thus he had estimated the arrival direction and number of particles at the detector surface.

The first interaction usually takes place in the upper atmosphere producing different types of particles which are mostly pions, kaons, baryons and anti baryons. The energy of the primary particle is shared in between the secondaries which further interacts or decay to generate new particles [1]. The neutral pions with a mean life time of 10^{-16} s decay into two gamma photons in a process

$$\pi^0 \rightarrow \gamma + \gamma \qquad (1.4)$$

The charged pions with a mean life time of 10^{-8} s decay into muons and neutrinos in a process

$$\pi^{\pm} \rightarrow \mu^{\pm} + \nu_{\mu}^{\mp} \qquad (1.5)$$

The charged kaons also decay into muons and neutrinos by the mode

$$K^{\pm} \rightarrow \mu^{\pm} + \nu_{\mu} \qquad (1.6)$$

Again kaons may decay into charged and neutral pions as follows [27]

$$K^{\pm} \rightarrow \pi^{\pm} + \pi^0 \qquad (1.7)$$

The air shower is composed of mainly three components as follows [shown in Fig. 1.4]

(i) Electromagnetic or the soft component (e^+, e^-, γ)

(ii) Hadronic component (nucleon, anti-nucleon, $K^{\pm}$, $\pi^{\pm}$)

(iii) Muonic or the hard component ($\mu^{\pm}$, ν_{μ}, ν_e)

The gamma photon produced by the decay of neutral pions initiates the electromagnetic showers mainly by the process of bremsstrahlung and pair creation. The particles produced in these processes are electrons, positrons and gamma photons which constitute the electromagnetic component. The hadrons (mainly kaons, pions and baryons) form the hadronic component of air shower. Muons are mainly produced by the decay of charged pions and kaons which constitute the muonic component, the most penetrating component of air shower. These are the most observed component of cosmic rays at Earth's surface because of their longer life time and weak interaction with matter.

Initially the electromagnetic and hadronic components of air shower grow in size and then decreases after reaching a maximum development in the atmosphere. But the muonic component only grows and maximize in size while propagating down into the atmosphere.

In addition to these three components, electromagnetic radiation component is also associated with the air showers. They are mainly Cherenkov Radiation, Fluorescent Light and Radio Emission.

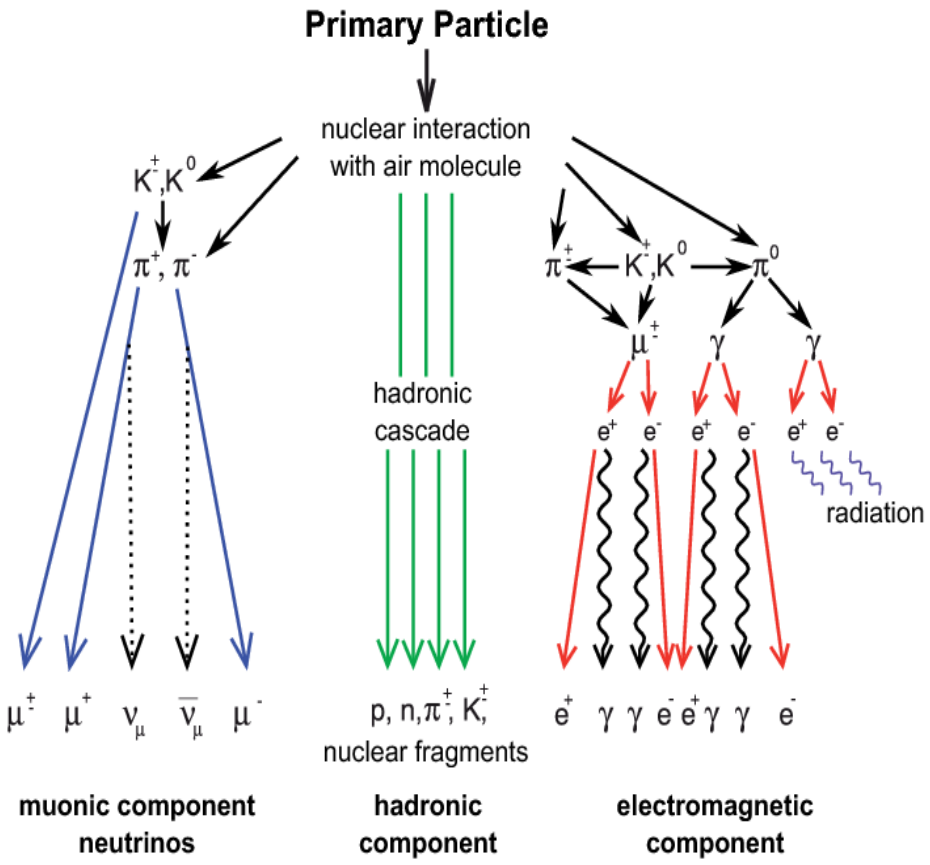

Figure 1.4: Schematic Development of extensive air showers describing the main three components.

1.2.1 Electromagnetic component

The electro-magnetic component also known as soft component of an extensive air shower (EAS) consists of electrons, positrons and photons. The neutral pions produced by the hadronic collisions in the atmosphere immediately decay into two gamma photons [28].

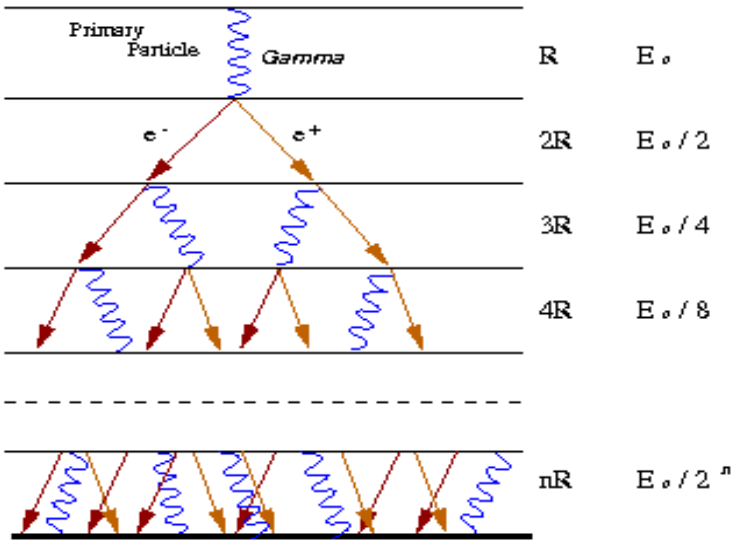

Figure 1.5: Development Extensive Air Shower (EAS) in the atmosphere.

These gamma photons produce a pair of electron and positron by the process of pair production. The energy of the gamma photon is shared between the pair in the form of kinetic energy. The process of pair production only occurs at higher energy (E >1.02 MeV).

$$\gamma \rightarrow e^{+} + e^{-} \qquad (1.8)$$

These electrons and positrons give rise to new photons via Bremsstrahlung

$$e^{\pm} = \gamma + e^{\pm} \qquad (1.9)$$

Each particle loses $1/e$ fraction of its average energy while crossing every radiation length (R) during their propagation through the atmosphere. These two processes alternate until the ionisation losses of the electrons are comparable to the energy loss due to bremsstrahlung. Thus the resulting cascade of electrons and photons constitute the electromagnetic component of air showers as shown in Fig. 1.5. This is the most abundant component observed in the lower atmosphere which constitutes approximately 90% of the charged particles of an Extensive Air Shower.

1.2.2 Hadronic component

The hadronic component consist of strongly interacting particles i.e. mesons (kaons and pions), nucleons and antinucleons. It contributes only about 1% to the total particle flux in an air shower. Hadrons are produced with large longitudinal momentum at the top of atmosphere by the collision of primary particle with the air nuclei or as decay products of short living resonances. The secondary hadrons are produced with a small transverse momentum of about 400 MeV/c, so they remain close to the shower core. As other components of air shower have originated from this component, so it can be considered as the backbone of extensive air shower. Hadronic showers develop later and travel deeper into the atmosphere compared to electromagnetic showers. They have larger lateral spread than electromagnetic showers [28].

1.2.3 Muonic component

The muonic component arises from the decay of high energy charged pions and kaons. Muons are the main component of cosmic rays which contributes about 10% to the total particle flux of an air shower at ground level. Muons with higher energy (E >100 GeV) that originate at the early development stage of an air shower can travel longer distances due to relativistic time dilation [29]. They lose energy only by ionization on their way through the atmosphere at a rate of about 2 MeV per g/cm^2 [30]. Being least

interacting, most of the muons survive and travel almost straight to the observation level. So it is also known as the penetrating component of cosmic ray air shower. The low energy muons descended from a later development stage of an air shower, eventually decay via the weak force into electrons and neutrinos with a mean life of 10^{-6} s.

$$\mu^{\pm} \rightarrow e^{\pm} + \nu_{\mu} + \nu_{e} \tag{1.10}$$

The lateral spread of the muons is larger and depends on the transverse momenta of the parent charged mesons as well as on multiple scattering and deflection of geomagnetic field. The lateral spread of muons can be parameterized by the following function given by Greisen [27]

$$\rho_{\mu}\,(N_e, r) = 18\left(\frac{N_e}{10^6}\right)^{3/4} r^{-3/4}\left(1 + \frac{r}{320}\right)^{-2.5} \tag{1.11}$$

Where $\rho_{\mu}\,(N_e, r)$ is the density of muons (E_{μ} >1 GeV) as a function of shower size (N_e) and core distance (r). The number of muons (N_{μ}) of energy >E_{μ} produced in a shower of primary mass A is related by the function

$$N_{\mu}(A) \propto A\left(\frac{N_e}{A}\right)^{\alpha_{\mu}} \propto A^{1-\alpha_{\mu}} \tag{1.12}$$

The value of the exponent α_{μ} varies from (0.8-0.9) for E_{μ} ~ 1GeV to 0.7 for E_{μ} ~ 200 GeV.

As muons originate at the early stage of EAS development, they retain valuable information regarding the hadronic interactions and mass of the primary particle.

1.2.4 Radiation component

The main electromagnetic processes that appear as bulk effects are Cherenkov radiation, fluorescence and radio emission.

1.2.4.1 Cherenkov radiation

If a relativistic charged particle travels through a medium with a velocity greater than the phase velocity of light in that medium, a faint radiation is produced by the medium which is known as Cherenkov radiation. It is named after Soviet physicist, Pavel Cherenkov who detected this effect experimentally in 1934 while studying effect of radioactive substances on liquids. Soon after its discovery, I. E. Tamm and I. M. Frank gave theoretical interpretation of this effect. In 1958, the Physics Nobel Prize was awarded to Cherenkov, Tamm and Frank for their discovery and interpretation of the "Cherenkov effect" [31, 32].

When a charge particle moves through a medium, it polarizes the nearby atoms and the electromagnetic radiation is emitted. Generally the dipole fields created along the

direction of particle track interfere destructively and no radiation is emitted. However if a particle moves with a velocity v (so that, $v > c/n$), c is the velocity of light in vacuum and n is the refractive index of the medium) greater than the velocity of light in a medium (c/n), then the wavefronts interfere constructively according to Huygen's principle. As a result, Cherenkov light is emitted around the particle's trajectory forming a cone [33] as shown in Fig. 1.6.

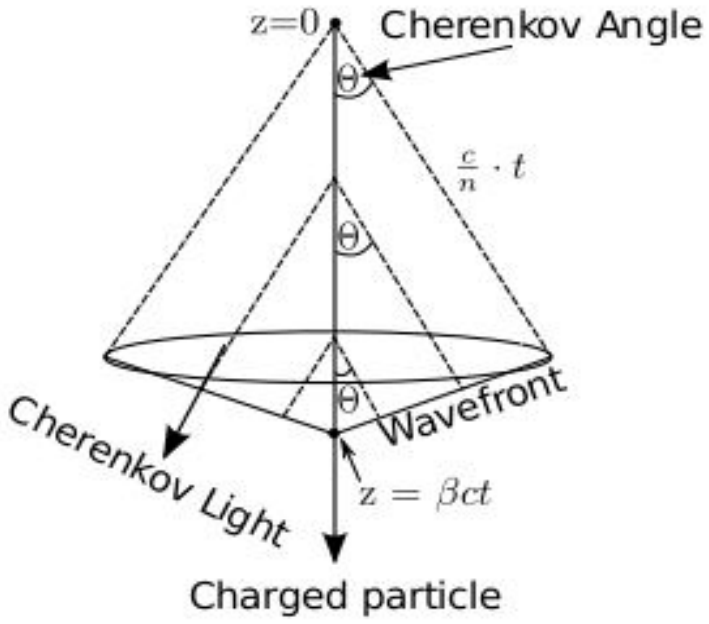

Figure 1.6: Emission of Cherenkov Radiation through a cone.

The angle (θ_c) between the particle trajectory and emitted radiation is given by

$$cos\theta_c = \frac{c'}{v} = \frac{1}{\beta n} \tag{1.13}$$

where $c' = c/n$ and $\beta = v/c$

The condition that has to be satisfied for the emission of Cherenkov radiation is $\beta \geq 1/n$, since $cos\theta_c \leq 1$ [29]. The maximum Cherenkov emission angle $\theta_{c,max} = arc\ cos\left(\frac{1}{n}\right)$ with $\beta \approx 1$ for ultra-relativistic particles.

The threshold energy for the emission of Cherenkov radiation by a charged particle is

$$E_{th} = \frac{mc^2}{\sqrt{1-\beta^2}} = \frac{mc^2}{\sqrt{1-n^{-2}}} \tag{1.14}$$

Cherenkov radiation in EAS

In 1953, W. Galbraith and J. V. Jelly made the detection of Cherenkov light flashes in the atmosphere [2] for the first time. Electrons and positrons are the main component of EAS which emit Cherenkov radiation mostly in the visible region of electromagnetic

spectrum. Cherenkov radiation produced in an air shower can reach the ground level with much less absorption. Hence it carries information about the origin and energy of primary particle [34]. Since the refractive index (n) of the atmosphere keeps changing due to variation of air density so the emission angle is lower at the high altitude (low density region) and higher at the low altitude (high density region). It is a function of altitude as it depends on pressure and temperature of the atmosphere. Equation (1.14) implies that with increasing altitude refractive index decreases and hence the threshold energy increases. At the sea level threshold energy of an electron for emission of Cherenkov radiation is about 21 MeV with $n = 1.00029$ and increases to about 35 MeV at an altitude of 7.5 kilometers above the sea level [34].

As Cherenkov radiation is emitted through a cone, so its lateral spread is sensitive to the longitudinal shower development. From the lateral distribution of Cherenkov light, depth of shower maximum can be estimated. The lateral extension of Cherenkov radiation is more symmetric around its particle trajectory for gamma ray induced showers than hadron induced showers. Based on this difference, gamma and hadron showers can be identified on the ground.

1.2.4.2 Fluorescent radiation

The air molecules get ionized and exited by the passage of high energy charged particles through the atmosphere. The de-excited nitrogen molecules emit a light mainly in the UV region (300-400nm) which is known as fluorescent light. In the atmosphere most of the fluorescent light is produced by low energy secondary electrons during ionization processes. X-rays emitted from the inner-shell ionization of air molecules also contribute to fluorescent radiation in a small amount [35].

In the middle of 1960's, Kenneth Greisen and his group made an attempt to observe fluorescent light from the Extensive Air Showers. And in 1976, the fluorescence emission from cosmic rays was detected for the first time by the Physicists of University of Utah [36].

Due to forward emission, Cherenkov light is restricted to small regions around the shower axis. So it can be easily distinguished from largely extended isotropic fluorescent light. As the yield of fluorescence photons are due to energy loss of exited molecules, their number is directly related to energy deposit in the atmosphere. So, the longitudinal profile of a shower can be estimated by measuring the rate of fluorescent photon emission [37]. The estimation of primary energy by fluorescence technique is more accurate than other techniques due to smaller fluctuations and hence this technique is used by many groups of scientists including Fly's Eye and Pierre Auger Observatory.

1.2.4.3 Radio emission

The radiation emitted by the electromagnetic component of an Extensive Air Shower at radio frequency range is known as radio emission of air showers. The radio pulse generated is of nanosecond timescale and covers a broad frequency spectrum. The theory of coherent radio emission was proposed by Askaryan in 1961 [38]. And based on this, in 1965, Jelly and his collaborators detected the phenomenon of radio emission experimentally at a frequency of 44 MHz [39].

The emission of radio pulses occurs mainly due to two processes – (i) geomagnetic emission and (ii) charge excess emission. The main contribution to this radiation emission mechanism is driven by the geomagnetic field. In this process, opposite drift of electrons and positrons occurs due to the action of Lorentz force exerted by Earth's magnetic field. The second contribution comes from the excess electrons in the shower front as they are knocked out from the air molecules due to collision with charged particles [40]. The geomagnetic radiation gets polarized along the direction of shower axis whereas the charge excess radiation gets radially polarized. Thus these two components are easily distinguishable from each other. Several experiments such as CODALEMA [41], LOPES [42], AERA [43], Tunka-Rex [44] and LOFAR [45] have recorded radio pulses in order to study properties of cosmic ray air showers.

1.2.5 Longitudinal profile of EAS

The longitudinal development of air showers can clarify the nature of primary particle and their interaction in the atmosphere. The longitudinal profile of a shower normally refers to the number of charged particles as a function of atmospheric depth which signifies the characteristics of the secondary particles [46]. The longitudinal profile mainly refers two important parameters. One is the depth of shower maximum, X_{max} and other is the number of particles at the maximum development, $N(X_{max})$. From the reconstruction of X_{max}, the mass, energy and elongation rate of primary particle (A) can be estimated. The longitudinal developments of secondary particles are different for different primary particles depending on their type and primary energy [47].

Most of the cosmic ray secondary particles are generated through electromagnetic processes. W. Heitler described a model for the development of electromagnetic cascades in the atmosphere in 1954, [48] which is also known as the Toy Model. In this model, Heitler assumed that after crossing a distance equal to the mean free path λ, a photon produces a pair of electron and positron by the process of pair production. In this process, each created electron carries half of primary energy E_0. The process of bremsstrahlung takes place by these electrons after travelling a distance λ. The mean free path λ for both the processes i.e. pair production and bremsstrahlung is considered to be the same for this model [48]. These two processes continue until their energy is enough for further creation

of new particles. The value of this critical energy E_c is about 84.2 MeV [27] in air. Fig. 1.7 illustrates the development of electromagnetic cascades with the help of Toy Model.

Considering "n" number of branching nodes before reaching to the critical energy, E_c, the maximum yield of shower particles $N(X)$ as a function of atmospheric depth, X can be expressed as

$$N(X) = 2^n = 2^{x/\lambda} \tag{1.15}$$

with each particle having an average energy of

$$E(X) = \frac{E_0}{N(X)} \tag{1.16}$$

After reaching maximum, the shower decreases exponentially. The development of the longitudinal profile of a shower is shown in Fig. 1.7, i.e. the shower particles first increases with depth, reaches a maximum value and then begin to fall in number.

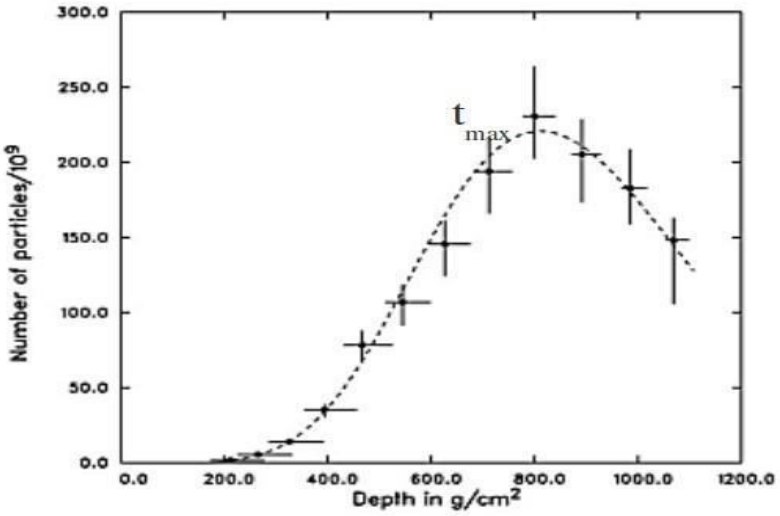

Figure 1.7: Longitudinal profile describing rise and fall of air shower.

The depth where maximum number of particles are generated is known as the depth of shower maximum X_{max}, after which the shower particles reaches to their critical energy, so the shower begin to decline. The depth of shower maximum X_{max} and number of particles at this depth can be related to the primary energy E_0 [49] as

$$X_{max} = \lambda \frac{\ln\left(\frac{E_0}{E_c}\right)}{\ln 2} \tag{1.17}$$

$$N(X_{max}) = \frac{E_0}{E_c} \tag{1.18}$$

The depth of shower maximum is a logarithmic function of primary energy whereas the number of particles at shower maximum, N_{max} is linearly dependent on the primary energy E_0.

The development of the hadronic showers can also be explained with the help of model similar to Heitler. The original Heitler model is extended for hadronic showers by J. Matthews in his paper in 2005 [50]. He assumed that after traversing a fixed distance of $\lambda \ln 2$, primary hadron produces charged and neutral pions. The number of produced charged pions ($\pi^{\pm}$) is N_{ch} and neutral pions (π^0) is $N_{ch}/2$.

The charged pions interact again after crossing another distance of $\lambda \ln 2$. And this process continues until their ene rgy become equal to the critical energy. After which, they begin to decay by producing muons and neutrinos [50]. The neutral pions immediately decay into two gamma photons which then initiate the electromagnetic cascades. Fig. 1.8 explains both the processes of electromagnetic and hadronic cascades developed in the atmosphere.

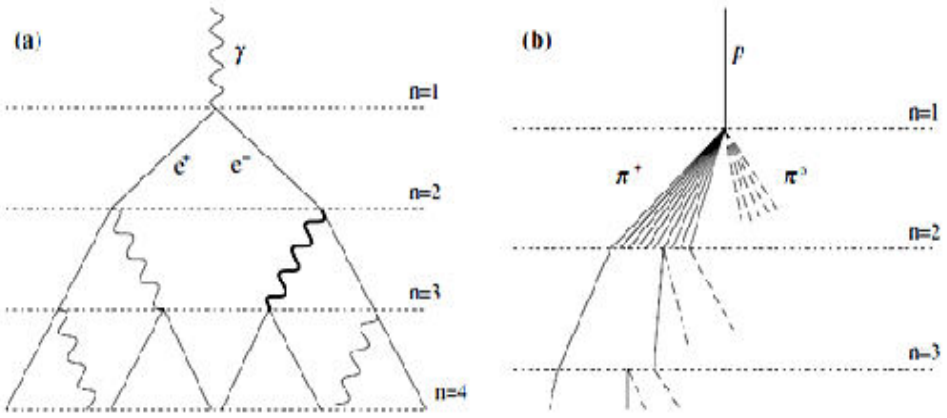

Figure 1.8: Schematic diagram of (a) electromagnetic and (b) and hadronic cascades in the atmosphere [50].

In order to describe the longitudinal profile of a shower, Gaisser and Hillas introduces a function which depends on the essential characteristics of an air shower, defined as [51]

$$N(X) = N_{max}\left(\frac{X - X_0}{X_{max} - X_0}\right)^{\left(\frac{X_{max}-X_0}{\lambda}\right)} exp\left(\frac{X_{max} - X}{\lambda}\right) \qquad (1.19)$$

where X_0 is the first interaction point and λ is the shower decay length.

The distribution of the number of charged particles as a function of atmospheric depth for different primaries is found to follow a Gaussian pattern. So they can be well fitted by the Gaussian function as follows

$$n(s) = exp\left(-\frac{(s-1)^2}{2\sigma^2}\right) \tag{1.20}$$

where σ is standard deviation and s is the longitudinal shower age [52] which can be defined as

$$s_L = \left(\frac{3X}{X+2X_{max}}\right) \tag{1.21}$$

Here X is the atmospheric depth (in g/cm^2). Depending on the value of shower age the different development stages of longitudinal profile of a shower can be estimated.

For $s < 1$, the shower is at its development stage and known as young showers

$s = 1$, shower is at its maximum development i.e. at the depth of shower maximum

$s > 1$, shower is beyond its maximum development and can be classified as old showers [53].

1.2.6 Lateral profile of EAS

Due to the multiple Coulomb scattering, the air shower also spreads laterally i.e. in a direction perpendicular to the incident primary particle [27]. The lateral profile of secondary particles at the observational level is described by the number of particles as a function of core distance (r). The number of particles is maximum near the shower axis and gradually falls with increasing core distance. The density of charged particles in the Extensive Air Shower as a function of distance from the shower axis can be represented as lateral distribution function (LDF). The Nishimura-Kamata-Greisen (NKG) function is a reasonable approximation to the lateral distribution of charged particles and has been very useful in the analysis of experimental data [54].

The lateral distribution of electrons can be fitted with the Nishimura-Kamata-Greisen (NKG) function given by

$$\rho_{NKG}(r, s_{\perp}, N_e) = \frac{N_e}{2\pi r_0^2} C_{s_{\perp}} \left(\frac{r}{r_0}\right)^{s_{\perp}-2} \left(\frac{r}{r_0}\right)^{s_{\perp}-4.5} \qquad (1.22)$$

Where r_0 is the Moliere radius which is nearly equal to 80 m at sea level [55], N_e is the shower size, $s_{\perp}$ is the lateral shower age parameter and the normalization factor $C_{s_{\perp}}$ is given by

$$C_{s_\perp} = \frac{\Gamma(4.5-s)}{\Gamma(s)\Gamma(4.5-2s)} \tag{1.23}$$

The lateral distribution of the muonic component can be described by the function proposed by Greisen [56]

$$\rho_\mu(N_e, r) = C\left(\frac{r}{r_G}\right)^{-0.75}\left(1+\frac{r}{r_G}\right)^{-2.5} \tag{1.24}$$

where $\rho_\mu(N_e, r)$ is the density of muons with core distance (r), C is the scaling parameter and r_G is the Greisen radius.

The lateral distribution of Cherenkov photons can be fitted either by an exponential function or by a power law function.

The exponential function is given by [57]

$$Q(r) = A\exp\left(\lambda\frac{r}{10^4}\right) \tag{1.25}$$

where $Q(r)$ is the Cherenkov photon density and λ is the steepness parameter.

Again the power law function [58] as proposed by Protheroe and Turver is

$$Q(r) = C\ (r + 50)^{-\delta} \qquad (1.26)$$

Where δ is the shape parameter of the Cherenkov lateral distribution function.

1.3 Observation Techniques of Air Showers

As the flux of cosmic rays is sufficiently large below 10^{14} eV, they can be studied directly with the help of detectors like emulsion stacks, calorimeters and scintillation detectors mounted on satellites or balloons. However at higher energies above 10^{14} eV, due to low flux, direct detection is not practical. Hence we have to rely on the information obtained from the longitudinal and lateral development of Extensive Air Showers by the high energy primary particles.

There are different methods of detection for particle and radiation component of EAS. For the detection of particles on the ground, scintillation detectors or muon counters are used. Again the radiation components are collected by Cherenkov light detectors, fluorescence light detectors and radio detectors. Fig. 1.9 shows the schematic diagram of different experimental techniques used for study of EAS parameters.

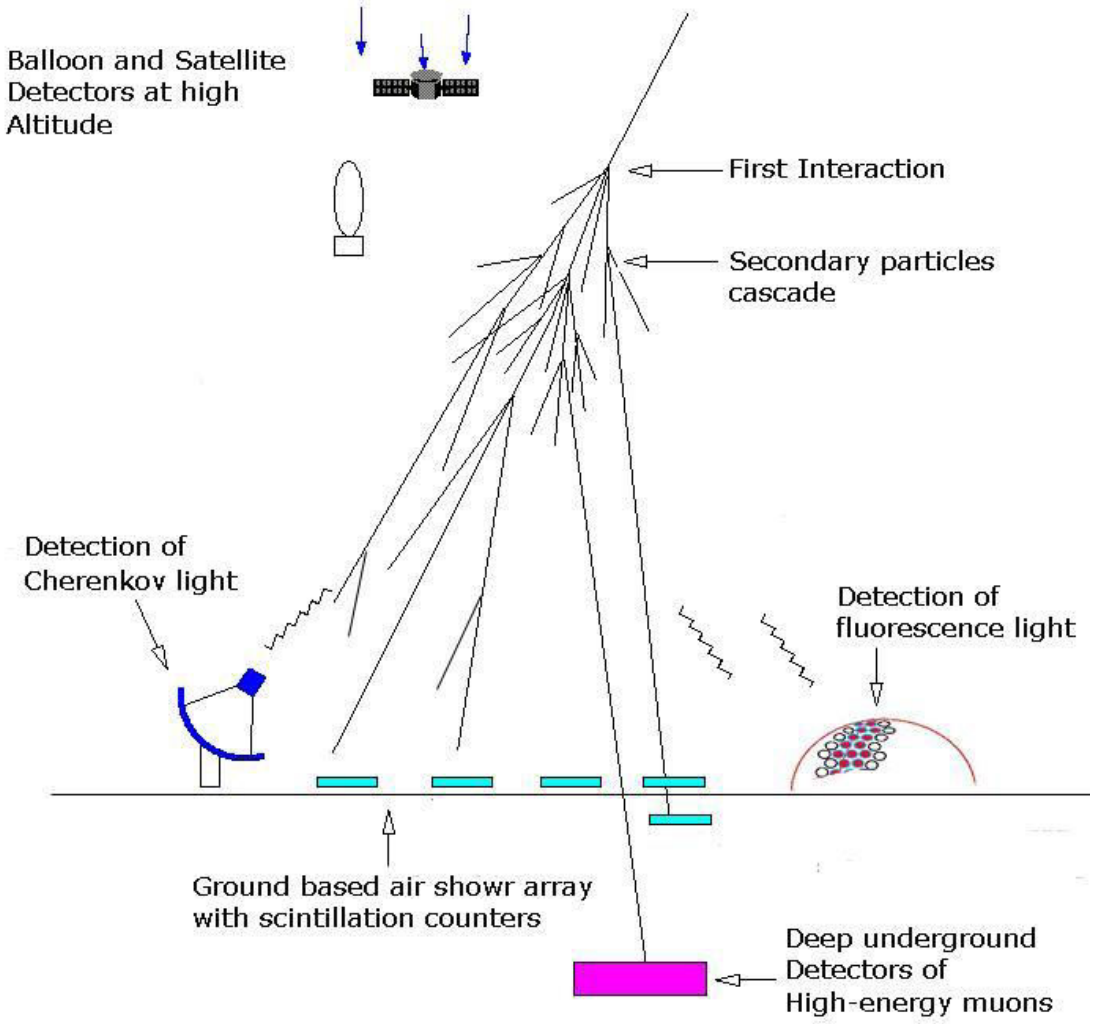

Figure 1.9: Schematic diagram of cosmic ray detection methods for cosmic ray showers.

1.3.1 Particle Detector Arrays

Particles arriving at the ground level can be measured with the help of ground based detector arrays. Here main contribution comes from the muonic component of air shower as they can reach the ground. This method measures the lateral distribution of the air shower particles. The detectors which are being used for particle detection mainly include scintillation counters, water Cherenkov counters and resistive plate chambers [10]. These detectors can reconstruct the energy and arrival direction of the primary particles by measuring the detected number of particles or, amount of light produced and arrival time of these particles. Again particle number and radius of shower front can be derived from the energy measurements [59]. The KASCADE-Grande experiment [60], AGASA experiment [61], and Auger experiment [62] employ this technique for deriving various EAS parameters. In India, a large particle detector array (GRAPES) [63] is constructed by the TIFR group in Ooty, to detect TeV cosmic rays. In order to detect the air shower particles, the detector area should be large enough. Detectors are uniformly placed apart from each other over the detection area. By recording the coincidence between adjacent detectors, various parameters relating to air shower can be reconstructed. In order to achieve appropriate measurements by the ground based arrays, their location, detection area and spacing between various detectors should be chosen accordingly. The water Cherenkov detectors measure Cherenkov emission that occurs while passage of particles through the water tanks within the detectors. As these detectors possess bigger aperture due to their larger acceptance zenith angle, are more preferable than the scintillation detectors.

The Pierre Auger Observatory contains 1600 water Cherenkov detectors covering an area of 3000 km^2 with 1.5 km spacing each [64]. Another example of water Cherenkov detector was Haverah Park array [65] in England with an area of about 12 km^2. This array was operated for 20 years and turned off in 1987. The ARGO-YBJ experiment at Yangbajing in Tibet (China) has been designed utilizing the Resistive Plate Counters (RPCs) to study the gamma ray astronomy [66]. Presently the most used particle detectors are scintillation and water Cherenkov detectors. However in early days Geiger counters were widely used for particle detection at the ground level.

1.3.2 Air Cherenkov Detector Arrays

The Cherenkov light emitted by charged particles in the atmosphere can be detected at the surface of the earth with the help of air Cherenkov detector arrays. An air Cherenkov detector consists of a parabolic mirror, at the focus of which, light sensors like PMTs are placed. Having large aperture and wide angle acceptance they work more or less in the same way as that of particle detectors. Advantage is that they contain more number of photons at the ground and hence carry more information about the longitudinal development. However they can be operated only in moonless, dark and clear nights with the help of optical telescopes. These arrays can function independently or in combination with particle detector arrays [2].

Some of the important examples of Cherenkov arrays are Tunka array and AIROBICC array. The Tunka array situated near lake Baikal in Siberia [67] measures showers initiated by high energy cosmic rays or gamma rays. The arrival direction and primary energy of particles may be derived from these measurements. The High Energy Gamma Ray Astronomy (HEGRA) experiment consists of AIROBICC (AIRshower Observation By angle Integrating Cherenkov Counters) array [68] covering an area more than 32000 m. The HAGAR (High Altitude GAmma-Ray) telescope system [69], HESS (High Energy Stereoscopic System) [70] and CTA (The Cherenkov Telescope Array) [71] employ Imaging Cherenkov Telescopes for investigation of TeV gamma ray sources.

1.3.3 Air Fluorescence Detectors

From the isotropically emitted fluorescent light by exited Nitrogen molecules, air showers can be detected at larger distances from the shower axis. Fluorescent light produces around 4 to 5 photons per ionizing particle and emitted near 300 to 400 nm band [10]. The longitudinal profile of shower is generally studied by this technique and hence by estimating depth of shower maximum (X_{max}), information about mass composition can be inferred. The photomultiplier tubes mounted on telescopes can detect particle's track from which primary energy can be reconstructed. Due to isotropic nature fluorescent light can be measured from all directions. Thus these detectors are more advantageous than the Cherenkov detectors. But can be operated only in clear moonless nights.

The air fluorescence technique was used in Fly's Eye experiment for the first time. The High Resolution Fly's Eye or HiRes which is an extension of original Fly's Eye experiment detected the phenomenon of GZK cutoff for ultra high energy cosmic ray particles [72]. This experiment was carried out by physicists of University of Utah for the period 1997 to 2006. The fluorescence detector of Pierre Auger Observatory consists of 24 large telescopes which are employed to measure the atmospheric fluorescent light.

1.3.4 Radio Detectors

Measuring the radio frequency pulses emitted by charged particles in the electromagnetic component of air showers, high energy cosmic ray particles can be detected. Radio signals are not affected much by the atmospheric conditions and so can be measured in both day and night. Radio detection technique provides higher duty cycle than the other optical techniques [25]. As radio pulses are continuous, it becomes easier to derive the arrival directions with more accuracy by their arrival time detection.

During 90's two radio detection experiments were set up. One is the Chicago Air Shower Array (CASA) in conjunction with the MIchigan Anti Array (MIA) array, with the name CASA-MIA [73] situated in Utah. And the other is at KASCADE site. From these experiments no satisfactory results were found. The first result came from the CODALEMA [74] experiment situated in France. The north-south asymmetry in particle track was detected by this experiment. The LOPES (LOFAR PrototypE Station) project

located at Karlsruhe, Germany, was a phased digital array operated for about 10 years. With the advanced technology of radio interferometry, Lopes array successfully reconstructed the air shower parameters [75]. LOFAR (Low Frequency Array) is the first radio telescope build up at core of Netherlands. It uses large number of omnidirectional antennas, from which signals get digitalized and further processed by digital computers [25]. The main objectives of this experiment are to detect radio emission (i) from the high energy cosmic ray particles in the earth's atmosphere and (ii) from the interaction of neutrinos and cosmic ray particles with the lunar surface [45].

1.4 Gamma Ray Astronomy

Gamma Ray Astronomy plays a pivotal role in exploring the non-thermal phenomenon of the Universe. Gamma rays cover a huge range in the electromagnetic spectrum with energy from 0.1 MeV to 10000 MeV. They carry information regarding the various violent processes occurring in the Universe. Traveling undeflected from original site, gamma rays are capable of locating the high energy cosmic ray sources. They may get produced by both electromagnetic and hadronic interaction processes.

The electromagnetic process includes three mechanisms namely synchrotron radiation, inverse Compton scattering, and bremsstrahlung.

(i) Synchrotron Radiation: Synchrotron radiation is emitted by the energetic moving electrons in the weak interstellar magnetic field. This mechanism is not suitable for production of high energy photons as large amount of energy get lost during this process.

(ii) Inverse Compton Scattering: In this process, a photon of comparatively low energy collides with high energy electron and emerges with increased energy.

(iii) Bremsstrahlung: When a high energy electron interacts with the electromagnetic field of the nucleus, gets accelerated and emits a photon. This process is known as Bremsstrahlung [27].

The hadronic process occurs mainly by the decay of neutral pions. Through proton-proton or proton-necleus collisions, neutral pions are produced which then decay into gamma photons. The hadrons because of their heavy mass do not loss much of their energy by synchrotron radiation and hence get accelerated to high energies. So the high energy gamma rays are considered to be produced mainly by the hadronic processes [2].

Penetrating through the galactic and intergalactic magnetic fields, gamma rays reach to the earth surface and can be detected by satellite based and ground based detectors. Due to low flux, only very few atmospheric showers are photon initiated. The showers initiated by gamma ray generally differ from hadron initiated showers.

1.4.1 Difference between Photon and Hadron induced showers

The study involving separation of photon induced showers from cosmic ray background would be highly beneficial in searching ultra high energy sources of standard gamma ray emission. Fig. 1.10 shows the schematic development of photon and hadron initiated showers.

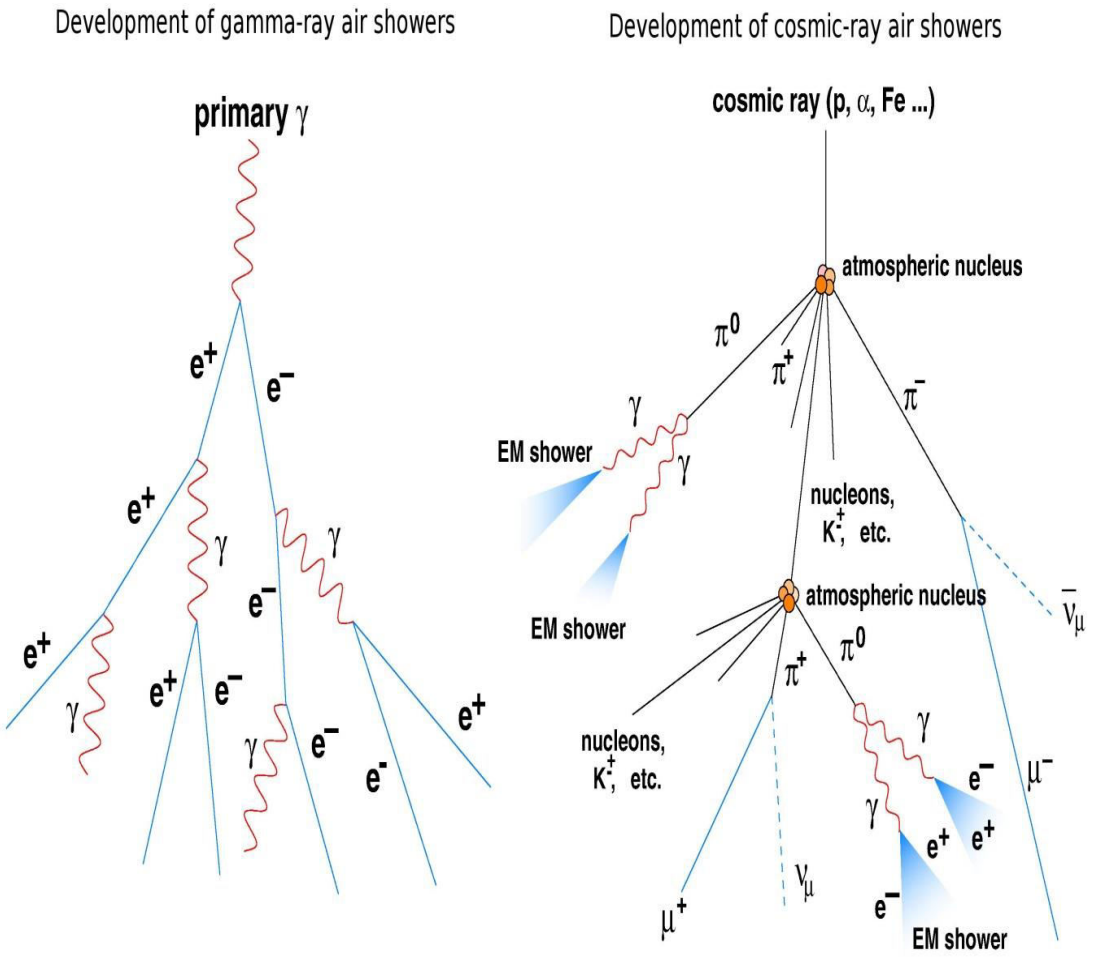

Figure 1.10: Development of showers induced by primary gamma ray and hadron.

The observed differences between gamma and hadron induced showers are:

(i) The spatial structure of gamma and hadron showers is different. Gamma showers are more symmetric and lie close to shower axis than the hadron showers. This can be explained as electrons and photons are main component of gamma induced showers, which do not possess large transverse momentum and hence concentrated within small region.

(ii) The gamma induced showers evolve through the process of pair production and bremsstrahlung. So they contain mainly electromagnetic components and hence their hadronic content is negligible.

(iii) Due to strong bunching of particles in gamma induced showers they can generate a narrow pulse of 3 to 5 ns duration while passing through thin detectors [2].

(iv) Gamma ray induced showers are known as muon poor due to their small muon content. However the hadron induced showers contain large number of muons as they get produced through hadronic interactions.

(v) The hadron induced showers undergo more fluctuations during their development stages compared to photon induced showers.

1.5 Plan of the thesis

In this thesis an attempt is made to study the properties of photon induced cosmic ray air showers using simulation and to identify some parameters that are sensitive for separation of photon induced showers from hadron induced showers. The present study has been performed using a standard EAS simulation program called CORSIKA (COsmic Ray SImulations for KAscade) code [76].

The plan of the thesis is as follows:

Chapter - 1 contains a brief description about the origin, acceleration, composition, energy spectrum of Cosmic Rays. It is followed by a brief description on Extensive Air Shower phenomenon and its various components (particle and radiation) along with EAS detection techniques at the ground level. In the last part we have discussed some general properties in which photon and hadron induced showers are different.

Chapter - 2 contains a brief description about the Monte Carlo Simulation method, Random number generators using different distribution functions. The general features of CORSIKA code with different high and low hadronic interaction models and various options that can be incorporated while installing and running of this code have been discussed.

In Chapter - 3, zenith angle variation of the secondary charged particles at different atmospheric depths have been studies by means of simulated data using photon and hadron

primaries. The differential zenith angle distribution parameter is related with asymmetry of the secondary charged particles. Again from the study of shower rate spectrum, attenuation lengths are obtained beyond their shower maximum.

In Chapter - 4, we have performed a study on the longitudinal and lateral development of photon induced showers and results are compared with hadron induced showers. The interaction lengths have been evaluated for gamma and proton primaries at different primary energies from the simulated data using Gaisser-Hillas fit. Again from the fit of lateral distribution of secondary electrons with the Nishimura-Kamata-Greisen (NKG) function, the lateral age parameter has been evaluated for different primaries. The variation of local age parameter (LAP) with radial distance is also studies in this chapter.

In Chapter - 5, a study on the relative fluctuation of secondary electrons and muons have been performed using both longitudinal and lateral profiles of shower for gamma and hadron primaries. In the later part, the polar angle distribution of secondary electrons and muons for gamma and hadron showers have been used to study fluctuation by applying the Principal Component Analysis (PCA) method.

In Chapter - 6, the average lateral density distribution of Cherenkov photons for gamma and hadron primaries are fitted with a power law function. The variation of the obtained lateral shape parameter with the depth of shower maximum is being studied.

Chapter - 7 contains the summary and discussion of results obtained in previous chapters along with future perspectives.

REFERENCES

[1] K. Greisen, *Phys. Rev. Lett.,* **16**, 748, (1966)

[2] P. K. F. Grieder, *Extensive Air Showers: High Energy Phenomena and Astrophysical Aspects- A Tutorial, Reference Manual and Data Book,* **Vol. I**, Springer, 254, (2010)

[3] Victor Hess, *Phys. Z.* **13**, 1084, (1912)

[4] P. Kiraly, *23rd European Cosmic Ray Symposium,* **409,** 012001, (2013)

[5] P. Freier et al., *Physical Review*, **74** (12), 1828–1837, (1948)

[6] P. Ehrenfest, *Review of Modern Physics*, **11,** (1939)

[7] M. Lemoine and G. Sigl, *Physics and Astrophysics of Ultra High Energy Cosmic Rays*, Springer, (2001)

[8] E. Fermi, *Physical Review* **75**, 1169, (1949)

[9] David Scott Barnhill, Ph. D Thesis, "Composition Analysis of Ultrahigh Energy Cosmic Rays Using the Pierre Auger Observatory Surface Detector", University of California, Los Angeles, (2005)

[10] Chihwa Song, Ph.D Thesis, "Study of Ultra High Energy Cosmic Rays with the High Resolution Fly's Eye Prototype Detector", Columbia University, (2001)

[11] V. Berezinsky, B. Hnatyk and A. Vilenkin, *Phys. Rev. D*, **64**, 043004, (2001)

[12] L. Miroshnichenk, *Solar cosmic rays*, **260**, Springer, (2001)

[13] V. L. Ginzburg & V. S. Ptuskin, *Physics Reviews*, **4**, 161-256, (1985)

[14] B. Klecker et al., *Space Science Reviews*, **83** (1-2), 259-308, (1998)

[15] P. K. F. Grieder, Cosmic Rays at Earth, Gulf Professional Publishing, (2001)

[16] M. G. Baring*, arXiv:astro-ph/9711177v1*, (1997)

[17] M. Bustamante, http://cern.ch/PhysicSchool/LatAmSchool/2009/Presentations/pDG1.pdf

[18] Radomir Smida, Ph. D Thesis, "Cosmic-Ray Physics with the Pierre Auger Observatory" Institute of Physics, Academy of Sciences of the Czech Republic, Charles University, Prague, (2009)

[19] M. Nagano, Search for the end of the energy spectrum of primary cosmic rays, *New J Phy*. **11,** 065012, (2009)

[20] Fabian Schussler, Ph. D Thesis, "Top-Down Reconstruction of Ultrahigh Energy Air Showers measured with the Pierre Auger Fluorescence Detector", Pierre Auger Observatory (2005)

[21] Ralph Engel*, Proc. Supp. Nuclear Physics,* **151** (1), 437-461, (2006)

[22] P. Bhattacharjee and G. Sigl, *Phys. Reports*, **327**, 109, (2000)

[23] Todor Stanev, SLAC Summer Institute on Particle Physics (SSI04), (2004)

[24] M. S. Longair, High Energy Astrophysics, Cambridge Univ. Press, (1981)

[25] Andreas Horneffer, Ph. D Thesis "Measuring Radio Emission from Cosmic Ray Air Showers with a Digital Radio Telescope", Bonn, (2006)

[26] K. Greisen, *Ann. Rev. Nucl. Sci*., **10**, 63, (1960)

[27] M. V. S. Rao and B. V. Sreekantan, *Extensive Air Shower*, World Scientific, (1998)

[28] Arne Schonwald, Ph. D Thesis "Measurement of the cosmic ray flux with H.E.S.S", Humboldt University, (2008)

[29] P. Luczak, Ph. D Thesis, "Investigation of muons in extensive air showers with the KASCADE-Grande Muon Tracking Detector", Department of Cosmic Ray Physics, Lodz, Poland (2012)

[30] D. Atri and A. L. Melott, *arXiv:1011/4522v3* (2011)

[31] A. A. Watson, *Nuclear Physics B (Proceeding supplements),* 212-213, 13-19, (2011)

[32] P. A. Cherenkov, Nobel Lecture, http://nobelprize.org/nobel_prizes/physics/laureates/1958/ cerenkov -lecture.pdf

[33] Heike Prokoph, Ph. D Thesis, "Investigations on gamma-hadron separation for imaging Cherenkov telescopes exploiting the time development of particle cascades", Leipzig University (2009)

[34] Cherenkov Radiation in EAS, www.gae.ucm.es/~emma/docs/tesina/node9.html

[35] A. S. Lidvansky, Institute for Nuclear Research, Russian Academy of Sciences, 60th October Anniversary pr. 7a, Moscow, 119312 Russia

[36] Jaime Rosado Velez, Ph. D Thesis "Analysis of the air Fluorescence induced by electrons for application to cosmic-ray detection", (2011)

[37] J. Abraham et al., *Nuclear Instruments and Methods in Physics Research Section A*, **620**, 227–251, (2010)

[38] G. A. Askaryan, *Soviet Phys. JETP*, **41**, 616, (1961)

[39] J. V. Jelly, J. H. Fruin, N. A. Porter, T. C. Weekes, F. G. Smith and R. A. Porter, *Nature*, **205**, 327, (1965)

[40] P. Schellart et al., *arXiv:1406.1355v2 [astro-ph.HE]*, (2014)

[41] D. Lebrunand and the CODALEMA Collaboration, *Proc. of 30th International Cosmic Ray Conference*, Mexico, **4** (HE part 1), 187–190, (2008)

[42] T. Huege et al. *Nuclear Instruments and Methods in Physics Research A*, **662**, S72–S79, (2012)

[43] F. G. Schroder (Pierre Auger Collaboration), *33rd ICRC*, Rio de Janeiro, (2013)

[44] D. Kostunin et al., *Nuclear Instruments and Methods in Physics Research A*, **742**, 89–94, (2014)

[45] J. R. Horandel et al., *Nuclear Physics B (Proc. Suppl.)*, **196,** 289–292, (2009)

[46] T. K. Gaisser, *Cosmic Rays and Particle Physics*, Cambridge University press, 202 (1992)

[47] A. A. Ahmed, Al-Mustansiryah. *J. Sci*. **Vol 20 (1)**, 62-69, (2009)

[48] Guofeng Yuan, Ph. D Thesis "Hadronic Physics From Extensive Air Showers", Louisiana State University, (2012)

[49] A. A. Watson, Lectures given at a Summer School in Mexico, 2002

[50] J. Matthews, *Astroparticle Physics* **22**, 387–397, (2005)

[51] T. K. Gaisser and A. M. Hillas, *15th Int. Cosmic Ray Conf.,* Plovdiv, Bulgaria, **358**, (1977)

[52] Z. Cao (HiRes/MIA Collaboration), *ICRC Proceedings*, (2001)

[53] Sonali Bhatnagar, *Physics Education*, (2009)

[54] K. Kamata, J. Nishimura, *Progr. Theoret. Phys., Supp*. **93,** (1958)

[55] T. Abu-Zayyad et al., *Astropart. Phys*., **16**, 1, (2001)

[56] W. D. Apel et al., *Astropart. Phys*., **65,** 55-63, (2015)

[57] J. D. Kuhlmann and R. W. Clay, *17th ICRC*, Paris, France, **6** , 96-99, (1981)

[58] R. J. Protheroe and K. E. Turver, *Nuovo Cimento*, **51A**, 277, (1977)

[59] Lukas Middendorf, Ph. D Thesis "Search for Ultra-High Energy Photons from Centaurus A with the Pierre Auger Observatory", (2012)

[60] T. Antoni et al. (KASCADE Collaboration), *Nucl. Instr. Meth. A*, **513**, 490, (2003)

[61] N. Chiba et al., *Nuclear Instruments and Methods in Physics Research A*, **311**, 338–349, (1992)

[62] L. Collica, *Proc. 34th Intern. Cosmic Ray Conf.*, Hague (Netherlands), (2015)

[63] S. K. Gupta et al., *Nuclear Instruments and Methods in Physics Research A*, **540**, 311– 323, (2005)

[64] M. Aglietta et al., *29th International Cosmic Ray Conference*, Pune, 101–104, (2005)

[65] D. Andrews et al., *Proc. 11th Int. Conf. on Cosmic Rays*, Budapest, (1969)

[66] A. Surdo et al., *28th International Cosmic Ray Conference*, (2003)

[67] N. M. Budnev et al., *Proc. 29th ICRC*, Pune, **6**, 257, (2005)

[68] L. Padilla et al., *arXiv:astro-ph/9807342v1* (1998)

[69] L. Saha et al., *Astroparticle Physics*, **42**, 33, (2013)

[70] HESS website: http://www.mpi-hd.mpg.de/hfm/HESS/

[71] CTA website: http://www.mpi-hd.mpg.de/hfm/CTA/

[72] J. N. Matthews and C. C. H. Jui, *Nuclear Physics B* (Proc. Suppl.), **87**, 411-413, (2000)

[73] L. J. Rosenberg et al., *Proc. Int. Conf. on High Energy Gamma-Ray Astronomy*, (1990)

[74] D. T. Machado, *23rd European Cosmic Ray Symposium*, **409**, 012074, (2013)

[75] H. Falcke et al., LOPES Collaboration, *Nature*, **435**, 313–316, (2005)

[76] D. Heck and T. Pierog, *Extensive Air Shower Simulation with CORSIKA – A Users Guide Version 6.990*, (Germany: Karlsruher Institut Fur Technologie (KIT)), (2011)

CHAPTER-2

CORSIKA - A MONTE CARLO SIMULATION CODE

Monte Carlo simulation method is a statistical technique giving the solutions of problems that are difficult to solve analytically. Now a days the computer simulation has become one of the most important technique used in various fields such as research, finance, engineering, project management, insurance etc. For the understanding of the general behaviour and design of particle detector arrays, method of simulation is used. High energy cosmic ray particles give rise to complex extensive air shower (EAS) phenomenon which is very difficult to analyze physically. In such a situation, method of simulation is essential to estimate the various EAS parameters. Till date a number of computer based air shower simulation programs have been developed. One such reliable and widely used program is the CORSIKA (Cosmic Ray SImulation for KAscade) code [1]. In this chapter we explain the general features of the Monte Carlo code CORSIKA.

2.1 The Monte Carlo Method

The Monte Carlo simulation method solves the complex physical and mathematical problems through random sampling of variables. This method was invented by Nicholas Metropolis and Stanislaw Ulam during World War II as a code for the secret work at Loss Alamos National Laboratory [2] and was named after the Monte Carlo Casino of Monaco city. Further, development on this method was made by Von Neumann and Fermi [3].

With the advent of electronic computers, this method had been utilized significantly in different areas to model a variety of physical and conceptual systems. This method generates an individual event or values of a parameter using random numbers from probability distribution functions. The computer generated random numbers are uniformly distributed between 0 and 1 [4]. The outcomes of a Monte Carlo event cannot be predicted earlier. It typically undergoes a series of statistical tests and random samplings.

The main steps involved in Monte Carlo simulation are [5]

(i) Generation of a parametric model.

(ii) Generation of a set of random inputs.

(iii) Evaluation of the model.

(iv) Repetition of the steps.

(v) Analysis of the result.

This technique provides possible comprehensive outcome of a complex physical situation.

2.1.1 Random Numbers

Assuming some analytical functions computer generates a sequence of random numbers. They are often referred to as pseudo random numbers as they are not truly random being generated by an algorithm. However, they satisfy all requirements of a random number. J. Neumann suggested the algorithm for generation of random variables for the first time [3].

For the simulation of a system, random variables are required which depends on some probability functions. A uniform random number generator produces a uniform distribution in the interval (0, 1) [6]. This standard generator is used to simulate other distributions. A random number generator is considered as good if it follows the property of uniformity, independence and should have long sequence length.

2.1.2 Generation of Random numbers

2.1.2.1 Computer generated random numbers

The most common pseudo random generator used by computers is the linear Congruential generator.

For a n^{th} random number, I_n, the next random number is given by [7]

$$I_{n+1} = (a\, I_n + c)\, mod\, m \qquad (2.1)$$

Where a is the multiplier, m is very large positive integer and c is another integer. The value of constants should be chosen properly. The integer I_n obtained from Eq. 2.1 is then divided by m to get random sequence in the interval $(0, 1)$ and this can be used for the derivation of any other probability distribution function.

The middle square method is another simple method for generating random numbers. This method was suggested by John von Neumann [8]. This method has several disadvantages and gives output of poor quality.

2.1.2.2 Generation of random numbers from distribution function

There are a number of methods of generating random variables following a particular distribution function, using the standard uniform random numbers, $0 < R < 1$.

Inverse Transform Method

In inverse transform method [9], the probability distribution function $f(x)$ is integrated to an area so that the cumulative distribution, $F(X) = \int_{-\infty}^{X} f(x)dx$, lies in between 0 and 1. This function is equated to standard random number 'R' and the required random variable is obtained from the inverse function $X = F^{-1}(R)$.

Acceptance-Rejection Method

In this method, a uniformly distributed random number 'x' is drawn from the range x_{min} to x_{max} , and a second one 'y' is drawn from y_{min} to y_{max}. If y < f(x), then x is accepted as the required random variable, otherwise rejected and the algorithm is repeated [10].

Box Muller Method

It is a method of generating random numbers from a Gaussian distribution [11]. From two random numbers R_1 and R_2, two normally distributed independent values of x_1 and x_2 can be obtained as [4]

$$x_1 = \sqrt{-2lnR_1}\sin(2\pi R_1) \quad (2.2)$$

$$x_2 = \sqrt{-2lnR_2}\sin(2\pi R_2) \quad (2.3)$$

2.2 Monte Carlo Simulation of Air Shower Cascade

The high energy cosmic ray particles can be measured only by the detection of Extensive Air Shower (EAS). For designing of experiments and analysis of data, a detailed theoretical modeling of air shower cascade is required. So, in order to predict and study the various parameters of Extensive Air Shower, the method of Monte Carlo simulation is used. The air shower simulation program should take care of all interactions and decay processes of high energy particles. One such reliable Monte Carlo code is the CORSIKA code. This code is operated with the random number generator RANMAR [12] as implemented in the CERN program library [13]. Here the random number generator is written in standard FORTRAN code. In this code, particles are generated through successive collision and decay processes until they reach the observation level or their energy falls below the critical value.

2.3 The CORSIKA code

CORSIKA is a Monte Carlo simulation code developed to study of evolution and properties of Extensive Air Showers initiated by primary particles in the atmosphere. Initially this code was developed to perform the simulations for the KASCADE (KArlsruhe Shower Core and Array DEtector) experiment [14, 15] at Karlsruhe in Germany. Based on three well established programs, this code has been developed. The first program consists of ISOBAR routines, which can be used as an alternative for low energy hadronic interactions. This program was written by P. K. Grieder in 1970s [16]. The second program is based on the interaction generator HDPM (Hybrid Dual Parton Model), written by Capdevielle [17]. The third program describes the electromagnetic components of air showers with EGS4 [18] code. With these three programs, the first version of CORSIKA was developed in 1989.

This code can deal with the interaction and decay of more than fifty elementary particles such as hadrons, muons, photons and lighter to heavier nuclei in the atmosphere upto 10^{20} eV. Various informations regarding the properties of secondary particles such as their type, energy, location, direction and arrival times can be predicted by this program.

Basically there are 4 main parts in the CORSIKA program [1]. They are

(i) The first part deals with the input and output profiles, performs decay of particles along with ionization loss and multiple scattering of particles.

(ii) The second part describes the hadronic interactions of particles in the atmosphere at higher energies.

(iii) The third part describes the hadronic interactions at lower energies.

(iv) The fourth part describes interactions and transport of electrons, positrons and photons.

The CORSIKA code has been modified several times and extensions are added to meet the requirements of KASCADE experiment. And it had become one of the most used simulation tool for the study of EAS.

2.4 Interaction Models in CORSIKA

2.4.1 Hadronic Interactions: The hadronic interaction models can be divided into high energy hadronic interaction model and low energy hadronic interaction model. The first model deals with the interaction of high energy particles and second one deals with hadronic interactions at low energy particles i.e. below 80 GeV.

2.4.1.1 High Energy Models

DPMJET: DPMJET (Dual Parton Model with JETs) is a high energy model based on two component Dual Parton Model [19, 20, 21] containing multiple soft chains and multiple minijets. This model describes high energy hadronic interactions of hadron-nucleus and nucleus-nucleus collisions.

EPOS: EPOS (Energy conserving quantum mechanical multi-scattering approach, based on Partons, Off-shell remnants and Splitting parton ladders) is a high energy model based on the NEXUS framework with improved hard interactions and high density effect. It combines the features of VENUS and QGSJET01 models in order to treat the high energy interactions. The recent RHIC data can be parameterized with this model.

VENUS: VENUS [22] (Very Energetic NUclear Scattering) is a program developed to treat the ultra-relativistic collision between nucleon-nucleon, nucleon-nucleus, and nucleus-nucleus. This model is based on the Gribov-Regge theory, that includes the process of Pomeron exchange for high energy hadron-hadron collisions.

NEXUS Option: NEXUS [23] (NEXt generation of Unified Scattering approach) model uses the features of VENUS and QGSJET models. This model can be extrapolated to higher energies in order to treat the high energy hadronic interactions. The NEXUS model

describes the universal behaviour of high energy interactions as it originates from the universality hypothesis [24].

HDPM: HDPM is a simple Monte Carlo routine that is used to simulate the high energy hadronic interactions. This method is fairly adjustable with the available experimental data. The simulated events of proton-proton interactions from this model are found to be in agreement with other simulation methods. In CORSIKA code, HDPM routine is present in the default option.

SIBYLL: SIBYLL [25, 26] is a program based on the QCD mini-jet model which can simulate the extreme high energy hadronic interactions. This model generates a number of secondary particles. The short lived particles immediately decay into other particles. Nucleons, antinucleons, charged pions and kaons are treated as projectiles by this model.

QGSJET: QGSJET [27, 28] (Quark Gluon String model with JETs) is an extension of the QGS model. This model uses the quasi-eikonal Pomeron parameterization for elastic hadron-nucleon scattering to describe the high energy hadronic interactions. Here hadronization process is related to the quark gluon string model. In this model, two strings are formed by cutting down the Pomerons according to the Abramovskii-Gribov-Kancheli rule. The QGSJET model also consists of minijets which describes the hard interactions at highest energies. Different versions of this model are available such as QGSJET01, QGSJETII-03 and QGSJET-II-04. The earliest and the most used model QGSJET01 is based on Pomeron exchanges that describes the multiple hadronic interaction processes.

The QGSJETII model includes the non linear parton effects through Pomeron interactions. QGSJET-II-04 is the most recent version of QGSJET with much improvements.

2.4.1.2 Low Energy Models

FLUKA: FLUKA [29] (FLUctuating KAscade) is a low energy hadronic interaction model based on the Monte Carlo technique. This model incorporated with CORSIKA, is able to generate secondary particles and perform their interactions in the atmosphere. A detailed description on the FLUKA model can be obtained from the FLUKA webpage: http://www.fluka.org/. For CORSIKA simulation, FLUKA is the most relevant package. It includes many detailed information regarding the development of air showers and de-excitation of target nucleus.

GHEISHA: GHEISHA [30] (Gamma Hadron Electron Interaction SHower code) is a widely used low energy hadronic interaction model. This model can be implemented for describing hadronic collisions upto 100 GeV in GEANT [31] program. In CORSIKA, this package mainly deals with the elastic and inelastic cross sections of the hadrons below 80 GeV and their interaction and production mechanisms.

UrQMD: UrQMD [32] (Ultra-relativistic Quantum Molecular Dynamics) package deals with the low energy hadron-nucleus and nucleus-nucleus interactions in air. In CORSIKA, UrQMD 1.3_cors version is incorporated.

2.4.2 Electromagnetic Interactions

The interactions of electrons and photons in CORSIKA code can be described either with EGS4 (Electron Gamma Shower) [18] option or with the analytical NKG (Nishimura-Kamata-Greisen) option [33].

The EGS4 program performs full simulation of electromagnetic components considering pair production, bremsstahlung, Moller scattering, Compton scattering and photoelectric reactions. It also provides detailed information on various properties of electromagnetic components such as momentum, propagation time and space coordinates and hence requires large computing times almost increasing linearly with primary energy.

The NKG program considers electron densities at a particular position. It works faster giving results analytically. This option cannot be used considering the Landau-Pomeranchuk-Migdal effect above 10^{17} eV.

2.5 Cherenkov Options

The emission of Cherenkov radiation by the atmospheric charged particles can be treated with the Cherenkov option. With the selection of the Cherenkov option, the EGS4 program gets activated automatically. The various options incorporated within CORSIKA for generation of Cherenkov radiation are as follows:

Cherenkov Standard Option: The routines treating the Cherenkov radiation have been supplied by the HEGRA Collaboration [34] and considerably improved by K. Bernlohr [35]. Within a wave length band Cherenkov radiation is emitted. To reduce the computational time, Cherenkov photon bunch is treated as single particles. This option records only arriving photons at the detector level.

Cherenkov Wavelength Option: According to this option, the refractive index of air is wavelength dependent. Photons with shorter wavelengths will form larger emission cone and hence give rise to larger bunch size.

Imaging Atmospheric Cherenkov Telescope Option: The routines treating the Cherenkov radiation for Imaging Atmospheric Cherenkov Telescopes (IACT option) have been supplied by K. Bernlohr [36].

Imaging Atmospheric Cherenkov Telescope extension Option: This option extends parameters for describing radiation emitting particles. Thus the extended information is stored after the normal information in an additional photon bunch.

Cherenkov light reduction option: In this option the absorption of light is taken into account within the atmosphere, telescope mirror, or detecting photomultiplier tubes. The computing time as well as the output storage space get reduced with selection of this option.

INTCLONG and NOCLONG option: With this option, longitudinal distribution of Cherenkov photons can be recorded in differential mode and thus it requires extra computing time.

STACEE option: Here the output file for Cherenkov light is generated in a format used for STACEE (Solar Tower Atmospheric Cerenkov Effect Experiment) experiment [37].

2.6 Installing and Running of CORSIKA

For obtaining the CORSIKA versions, a request has to be sent either to Tanguy Pierog or Dieter Heck. On getting permission this code can be downloaded with a secure server from the web site (http:// www-ik.fzk.de/corsika/). The CORSIKA code can be installed in UNIX and LINUX environments with GNU C/C++ compiler. The installation commands are as follows

> tar zxvf corsika-6990.tar.gz

> cd corsika-6990/

> ./coconut

.

.

The previous versions of CORSIKA code are installed using ./corsika-install command.

After installation of CORSIKA code, the parameters of input file have to be selected according to ones choice to run the simulation.

2.7 Input file

The general structure of CORSIKA input file with Cherenkov option:

RUNNR	1	number of run
EVTNR	100400	number of first shower event
SEED	100401 0 0	seed for Hadronic part
SEED	100402 0 0	seed for EGS4 part
SEED	100403 0 0	seed for Cherenkov part
NSHOW	1000000	number of showers to generate
PRMPAR	14	particle type of prim. particle
ESLOPE	-2.7	slope of primary energy spectrum
ERANGE	2.00E4 4.00E4	energy range of primary particle
THETAP	0. 70.	range of zenith angle (degree)
PHIP	0. 360.	range of azimuth angle (degree)
OBSLEV	110.E2	observation level (in cm)
ELMFLG	T T	em. interaction flags (NKG, EGS)
RADNKG	200.E2	outer radius for NKG elect.distrib.
ARRANG	0.	rotation of array to north
CERARY	10 8 1200. 1500. 80. 50.	Definition of Cherenkov array grid
CERSIZ	0.	bunch size Cherenkov photons
CERFIL	F	Cherenkov output to extra file

CWAVLG	300. 450.	Cherenkov wavelength band
CSCAT	5 1000. 1000.	scatter Cherenkov events
FIXHEI	0. 0	first interaction height & target
FIXCHI	0.	starting altitude (g/cm**2)
MAGNET	16.4 -53.4	magnetic field south pole
HADFLG	0 1 0 1 0 2	flags for hadr. interaction
GHEISH	T	use gheisha for low energy hadrons
VENUS	T	use venus for high energy hadrons
VENSIG	T	use VENUS hadronic cross sections
ECUTS	3 .3 .015 .015	energy cuts for particles
MUADDI	T	additional info for muons
MUMULT	T	muon multiple scattering angle
LONGI	T 20. T	longit.distr. & step size & fit
MAXPRT	0	max. number of printed events
ECTMAP	100	cut on gamma factor for printout
STEPFC	1.0	mult. scattering step length fact.
DEBUG	F 6 F 1000000	debug flag and log.unit for out
VENDBG	0	venus debug option
DIRECT	/home/user/corsika/run/	output directory
USER	you	user name for database file
HOST	your_host	host name for data base file
EXIT		terminates input

2.8 Output files

The important output files that are generated in CORSIKA run are as follows [1]:

list file: This file contains all information about simulation time, version of code, interaction models, physical constants, steering keywords, generated particles along with the input parameters.

DATnnnnnn file: This file possess various information of the particles that are capable of reaching the observation level. Here data exists in the form of binary numbers, so this file must be executed using (corsikaread) option.

DATnnnnnn.long file: This file contains information regarding the longitudinal distribution and energy deposits of showers at each atmospheric depth.

DATnnnnnn.tab file: This file gives tabular output of binned γ, $e^{\pm}$ and $\mu^{\pm}$ particles at the observation level.

DATnnnnnn.dbase file: The output of this file can be used as a data base in order to examine the content of an air shower library.

REFERENCES

[1] D. Heck and T. Pierog, *Extensive Air Shower Simulation with CORSIKA - A Users Guide Version 6.990,* (Germany: Karlsruher Institut Fur Technologie (KIT)), (2011)

[2] N. Metropolis and S. Ulam, *Journal of Am. Stats. Asso*., **Vol. 44**, No. 247 (1949), p. 335-341

[3] I. M. Sobol, *The monte carlo method*, Mir Publishers, Moscow, (1984)

[4] M. V. S Rao & B. V. Sreekantan, *Extensive Air Showers*, World Scientific, (1998)

[5] J. W. Wittwer, (2004), *A Practical Guide to Monte Carlo Simulation Basics*, http:// www.Vertex42.com/ExcelArticle/me.MonteCarloSimulation.html

[6] D. P. Kroese, (2011), Lecture notes on Monte Carlo Methods, Summer School of the Australian Mathematical Sciences Institute (AMSI) http://www.maths.uq.edu.au/~kroese

[7] R. L. Harrison, *AIP Conf Proc*., 1204, 17–21, (2010)

[8] H. Rahimov, M. Babaie and H. Hassanabadi, *Applied Mathematics*, **2**, 482-486, (2011)

[9] K. Hagiwara et al., Physical Review D, **66**, 010001-1, (2002)

[10] The Numerical Algorithms Group, "G05 – Random Number Generators" NAG Library Manual, Mark 23

[11] W. H. Press, S. A. Teukolsky, W. T. Vetterling and B. P. Flannery, *Numerical Recipes in Fortran77*, 2nd Edition, Cambridge University Press, (1994)

[12] G. Marsaglia and A. Zaman, *Report FSU–SCRI–87–50* (1987), Florida State University

[13] F. James, *Report CERN DD/88/22* (1988), CERN, Geneva

[14] P. Doll et al., *The Karlsruhe Cosmic Ray Project KASCADE*, *Report KfK 4686* (1990), Kernforschungszentrum Karlsruhe; *Nucl. Phys. B (Proc. Suppl.),* **14A** (1990)

[15] H. O. Klages for the KASCADE Collaboration, *Nucl. Phys. B (Proc. Suppl.),* 52B, 92, (1997), ; *Proc. 25th Int. Cosmic Ray Conf*., Durban, **6**, 141, (1997)

[16] P. K. F. Grieder, *Report INS–J125* (1970), Inst. for Nuclear Studies, Univ. of Tokyo; P. K. F. Grieder, *Proc. 16th Int. Cosmic Ray Conf*., Kyoto, **9**, 161, (1979)

[17] J. N. Capdevielle, *J. Phys. G*: *Nucl. Part. Phys*., **15** 909, (1989)

[18] W. R. Nelson, H. Hirayama, and D. W. O. Rogers, *Report SALC 265*, Stanford Linear Accelerator Center, (1985)

[19] J. Ranft, *Phys. Rev. D*, **51**, 64, (1995)

[20] P. Aurenche, F. W. Bopp, A. Capella, J. Kwiecinski, M. Maire, J. Ranft and J. Tran Thanh Van, *Phys. Rev. D*, **45**, 92 (1992)

[21] F. W. Bopp, D. Petermann, R. Engel and J. Ranft, *Phys. Rev. D*, **49,** 3236 (1994)

[22] K. Werner, *Phys. Rep*., 232, 87, (1993)

[23] H. J. Drescher et al., *Phys. Rep*. 350, 93, (2001)

[24] D. Heck et al., Recent Additions to the Extensive Air Shower Simulation Code, *Proc. 26th ICRC*, Salt Lake City, USA, (1999)

[25] R. S. Fletcher, T. K. Gaisser, P. Lipari and T. Stanev, *Phys. Rev. D*, **50**, 5710, (1994)

[26] J. Engel, T.K. Gaisser, P. Lipari and T. Stanev, *Phys. Rev. D*, **46**, 5013, (1992)

[27] A. B. Kaidalov and K. A. Ter-Martirosyan, *Sov. J. Nucl. Phys*., **39**, 979, (1984)

[28] A. B. Kaidalov, K. A. Ter-Martirosyan and Yu.M. Shabelsky, *Sov. J. Nucl. Phys*., **43**, 822, (1986)

[29] A. Ferrari, P. R. Sala, A. Fasso and J. Ranft, *"FLUKA: a multi-particle transport code",* Report CERN- 2005-10 INFN/TC_05/11 SLAC-R-773, (2005)

[30] H. Fesefeldt., PITHA-85/02 (RWTH, Aachen), (1985)

[31] Application Software Group, GEANT, CERN Program Library (1994)

[32] S. A. Bass et al., *Prog. Part. Nucl. Phys*., **41**, 225, (1998)

[33] A. A. Lagutin, A. V. Plyasheshnikov, and V. V. Uchaikin, *Proc. 16th ICRC*, Kyoto, Japan, **7**, 18, (1979); J. N. Capdevielle et al. (KASCADE collaboration), *Proc. 22nd ICRC*, Dublin, Ireland, **4**, 405, (1991)

[34] S. Martinez et al., *Nucl. Instr. Meth. A*, 357, 567, (1995)

[35] K. Bernlohr, internal report MPI-Heidelberg (1998); *Astropart. Phys*., **12**, 225, (2000); *Astropart. Phys*. **30**, 149, (2008)

[36] K. Bernlohr, Simulation of Imaging Atmospheric Cherenkov Telescopes with CORSIKA and sim_telarray, *arXiv: 0808.2253*

[37] C. E. Covault et al., Proc. 27th Int. Cosmic Ray Conf., Hamburg (Germany), 2810, (2001)

CHAPTER 3

STUDY ON ANGULAR VARIATION OF COSMIC RAY SECONDARY PARTICLES WITH ATMOSPHERIC DEPTH

The study of zenith angle distribution of secondary charged particles provides information on the various development stages of Extensive Air Showers through the atmosphere. Again, from this study, the shower attenuation length can be estimated. The distribution of the secondary cosmic ray charged particles in the atmosphere as a function of zenith angle of the primary particle depends on various factors such as atmospheric depth, latitude & longitude of the place of observation and possibly other atmospheric conditions. Apart from type, direction and energy of primary particles, the investigation of Air Shower events also provide information on environmental effects due to atmospheric condition, geomagnetic field or atmospheric thickness on the development of secondary particles in the atmosphere [1].

The secondary charged particles produced in an EAS are absorbed and scattered in the atmosphere, which acts as a part of the detector medium. Hence, at any observation

level, the distribution of the secondary particles with respect to the arrival direction (zenith angle) of the primary cosmic ray, show asymmetry. The asymmetry parameter is the power index, n(X) of the differential zenith angle distribution of the secondary charged particles, which may be derived from the simulated data and compared with experimental measurement. Moreover, the study of the variation of the shower frequency with zenith angle is also crucial as it gives valuable information about attenuation of EAS in the atmosphere beyond shower maximum. This can be related to the shower attenuation length, λ [2].

In the present work, the distribution of secondary charged particles in different zenith angle bins are fitted with a differential distribution function from which the asymmetry parameter and attenuation length have been derived at different atmospheric depths considering pure and mixed primary compositions, using CORSIKA code. Effort is made to distinguish between gamma and hadron primaries on the basis of their zenith angle distribution. The discovery of high energy gamma-ray sources has increased the interest for the study of the gamma induced air showers [3]. As gamma rays are not deviated from their original direction, their detection may furnish information about high energy cosmic ray sources. Air showers also find application in TeV gamma ray astronomy observatories (HAGAR telescope system [4]), Imaging Cherenkov Telescope systems (HESS [5], CTA [6]), that investigate TeV gamma ray sources by recording the Cherenkov light emitted by air shower particles in the upper atmosphere. Supernova remnants, pulsars, X-ray binaries, radio galaxies, quasars etc. are the potential sources of cosmic rays as well as the high energy gamma rays. So to identify the measurable parameters in which gamma and hadron showers are different, a detailed study on various stages of development of the shower

particles is needed and to derive these primary parameters from experimental observations, method of simulation is widely used [7-10].

3.1 Zenith Angle Dependence of shower intensity

Distribution of air shower based on zenith angle is related to the arrival direction and origin of primary particles [2]. At a given observation level, longitudinal development of showers can be derived from the variation of the shower intensity with zenith angle. It can provide information about the nature of primary cosmic rays and their interactions in the atmosphere.

Generally the zenith angle distribution of the arrival rate of a shower is related to $\cos^n\theta$. Again in CORSIKA, the default primary intensity distribution is taken as, $I \propto \sin\theta\cos\theta$. Here θ represents the zenith angle. The 'sine' term defines the solid angle element, while the 'cosine' term takes into account the geometrical efficiency of a flat horizontal detector [11]. Hence we have chosen the following distribution function for fitting with our simulated data

$$dN_{sp}/d\theta = A(X)\sin\theta\cos^{n(X)}\theta \qquad (3.1)$$

Here the power index n(X) is a function of atmospheric depth, X.

3.2 Simulation of zenith angle distribution using CORSIKA

In this work two versions of CORSIKA, viz., CORSIKA 6.990 [11] with high energy model QGSJET01, and CORSIKA 7.3500 [12] with QGSJET II-04 have been considered. The low energy hadronic interactions are simulated with FLUKA [13]. We simulate 2000 showers (each), with zenith angles from 0^0 to 60^0 at the ground level considering pure primary composition (photon, proton and iron nucleus) and mixed composition (92%p + 6%He + 2%Fe) and (80%p + 20%γ). The primary energy range chosen is 10 TeV to 1 PeV with an energy spectral shape of a power law with index -2.7. The secondary charged particles considered are, electrons, positrons, positive and negative muons with threshold energies (> 0.3 GeV) for muons and (> 0.003 GeV) for electrons both for the two models. Further, the recent version is tested with lower energy thresholds for muons and electrons (> 0.1 GeV and > 0.001 GeV respectively).

3.3 Estimation of the power index n(X)

As the zenith angle increases the secondary cosmic ray particles get absorbed through greater distances in the atmosphere. For observation levels below the shower maximum (~500 g/cm^2) the number of shower particles first increases with zenith angle owing to increase in solid angle, attains a maximum value and then decreases at higher zenith angles due to atmospheric absorption [14]. In our first approach, differential distribution $dN_{sp}(\theta,X)/d\theta$ is obtained where $N_{sp}(\theta,X)$ is the number of secondary charged

particles as a function of the zenith angle, θ and atmospheric depth, X. This is done by considering 12 zenith angle bins of width 5^0, in the range $0^0 - 60^0$, for 52 atmospheric depths from 20 g/cm^2 to 1040 g/cm^2 in steps of 20 g/cm^2, as shown in Fig. 3.1(a-f). Here, the differential distribution i.e. the number of secondary charged particles in zenith angle bins is plotted as a function of the zenith angle at different depths. From these figures, it is seen that the number of secondary particles increases with zenith angle for lower atmospheric depths. This can be explained as the slant depth increases, more number of interactions takes place and as a result the number of secondary particles also increases. But in case of higher atmospheric depth, the number of particles initially raises to a maximum and then decreases as the shower is absorbed in the atmosphere.

Again as seen from Fig. 3.1(a-f), for gamma induced showers the number of secondary charged particles are less in comparison to proton and iron induced showers at lower depths, as gamma-photons penetrate deep into the higher depths without producing much secondaries. As the shower penetrates deeper, the photon induced showers, being purely electromagnetic, produce a larger number of secondaries compared to proton and iron induced showers. Further for higher depths, secondaries begin to fall in number due to atmospheric absorption. Hence, once again the number of secondary particles becomes less for photon induced showers compared to proton and iron induced showers. As such, the distributions of secondary particles are different at different atmospheric depths which reveal that the absorber thickness i.e, the atmosphere affects the development of a shower in the atmosphere. The obtained distributions are fitted with (Eqn. 3.1) and the power index, n(X) and the amplitude parameter A(X) have been evaluated for each atmospheric depth from 1040 g/cm^2 in steps of 20 g/cm^2 [1].

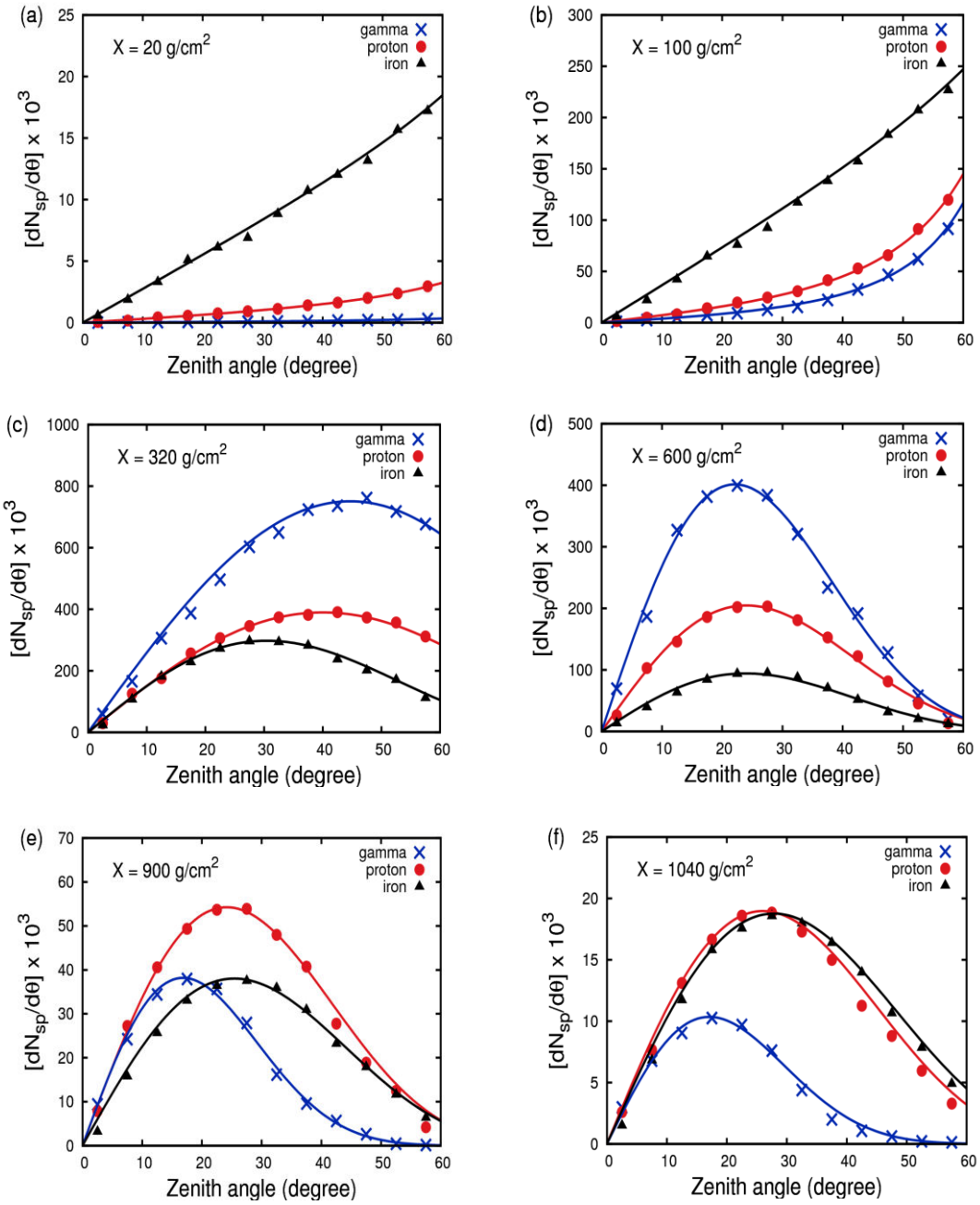

Fig. 3.1 Differential zenith angle distribution of secondary charged particles at atmospheric depths **(a)** 20 g/cm^2, **(b)** 100 g/cm^2, **(c)** 320 g/cm^2, **(d)** 600 g/cm^2, **(e)** 900 g/cm^2 and **(f)** 1040 g/cm^2 using CORSIKA 6.990 with QGSJET01.

To test the effect of high energy interaction models and secondary particle energy threshold on 'n', the above procedure is repeated using CORSIKA 7.3500 with QGSJET II-04 and with lower energy thresholds for muons and electrons (> 0.1 GeV and > 0.001 GeV respectively). The results obtained are exhibited in Fig. 3.2 and Fig. 3.3. It is found that beyond the shower maximum, the difference of this parameter 'n', between gamma and hadron (proton and iron) induced showers increases with atmospheric depth. The amplitude parameter is also significantly higher for gamma shower in the range of about 300 to 800 g/cm2.

Next, we consider a mixed primary composition model, by taking (92%p + 6%He + 2%Fe), and (80%p + 20%γ), for finding the power index of the zenith angle distribution. The results for pure and mixed composition using QGSJET01 with $E\mu > 0.3$ GeV and $Ee > 0.003$ GeV [Fig. 3.2(a)] are compiled in Table 3.1, along with experimental values at different atmospheric depths and selected energy range.

Table 3.1 Comparison of simulated values of power index n(X) with available experimental data:

Experiment				Present work n(X) with single primary n(X) ± σ		Present work n(X) with mixed composition	
Reference	Atm. depth , X (g/cm^2)	Energy range (TeV)	Power index n(X)	Gamma	hadron	(92%p + 6%He + 2%Fe)	(80%p + 20%γ)
MAKET-ANI detector array [15]	639	> 100 10^2-10^4	6	6.7 ±0.98	5.3 ±0.61 (p) 5.2 ±0.72 (Fe)	5.89±0.56	5.92±0.74
University of Puebla array, Mexico [16]	800	10^2-10^4	6.6	9.78±1.28	5.4 ±0.53 (p) 4.9 ±0.63 (Fe)	6.2 ±0.51	6.53±0.58
Scintillation array, Tehran, Iran [17]	890	> 100	5.85	10.7±1.25	5.19±0.51 (p) 4.59±0.60 (Fe)	5.64±0.55	5.83±0.47

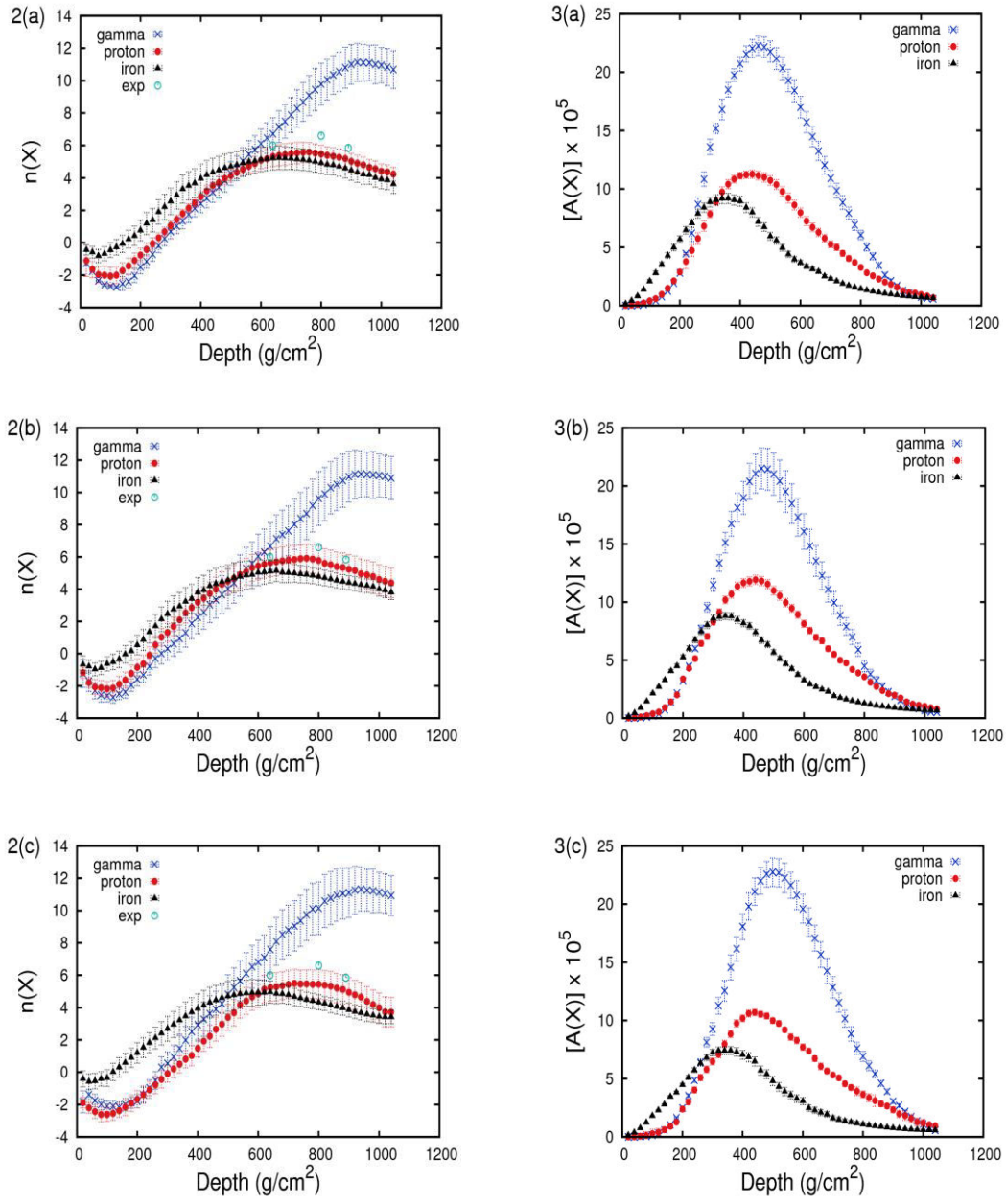

Fig. 3.2 Variation of n with atmospheric depth using **(a)** QGSJET01 with $E_\mu > 0.3$ GeV and $E_e > 0.003$ GeV, **(b)** QGSJET II-04 with $E_\mu > 0.3$ GeV and $E_e > 0.003$ GeV and **(c)** QGSJET II-04 with $E_\mu > 0.1$ GeV and $E_e > 0.001$ GeV.

Fig. 3.3 The values of A vs atmospheric depth using **(a)** QGSJET01 with $E_\mu > 0.3$ GeV and $E_e > 0.003$ GeV, **(b)** QGSJET II-04 with $E_\mu > 0.3$ GeV and $E_e > 0.003$ GeV and **(c)** QGSJET II-04 with $E_\mu > 0.1$ GeV and $E_e > 0.001$ GeV.

3.4 Estimation of attenuation length

The longitudinal development of the air shower is characterized by exponential decline of the shower particles beyond their maximum development. The magnitude of this effect may be measured by a parameter called attenuation length λ defined as,

$$F(\theta, > N, X_0) = F(0, > N, X_0)\exp[-X_0(\sec\theta-1)/\lambda] \qquad (3.2)$$

where $F(\theta, > N, X_0)$ is the frequency of showers with zenith angle θ, shower size > N, and vertical atmospheric depth X_0 [18]. For a given depth, a plot of log[F(θ)] vs sec(θ) is a straight line (Fig. 3.4), from the slope of which the value of λ may be estimated.

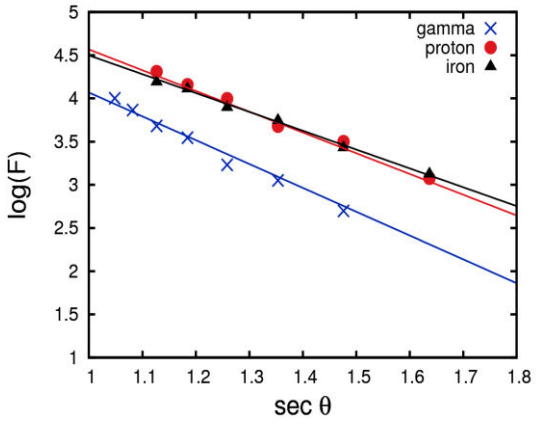

Fig. 3.4 The variation of log(F) with sec(θ) for gamma, proton and iron primary at 1040 g/cm^2.

From the zenith angle distribution of the total number of charged particles at different atmospheric depths beyond shower maximum, frequency spectra as function of zenith angle have been estimated for pure and mixed primary compositions. Simulations are carried out using (a) QGSJET01 with $E_\mu > 0.3$ GeV and $E_e > 0.003$ GeV, (b) QGSJET II-04 with $E_\mu > 0.3$ GeV and $E_e > 0.003$ GeV & (c) QGSJET II-04 with $E_\mu > 0.1$ GeV and $E_e > 0.001$ GeV.

The variations of attenuation length (λ) with atmospheric depth for these cases are depicted in Fig. 3.5(a), (b) & (c) respectively. Irrespective of atmospheric depth, this parameter is found to be greater for proton and iron primaries, as compared to gamma primary. Attenuation length for gamma shower is found to be minimum at all depths. Available experimental results on measurement of attenuation length by various detector arrays are presented in Fig. 3.5 and compiled in Table 3.2 along with the results from present work for pure and mixed composition models using QGSJET01. Typical values of λ, as estimated for atmospheric depth of 1040 g/cm^2 using QGSJET01 with $E_\mu > 0.3$ GeV and $E_e > 0.003$ GeV, are found to be,

$$\lambda(\text{gamma}) = 171.62 \pm 16 \text{ g/cm}^2$$

$$\lambda(\text{proton}) = 197.54 \pm 11 \text{ g/cm}^2$$

$$\lambda(\text{iron}) = 200.42 \pm 14 \text{ g/cm}^2$$

$$\lambda[\text{mixed (92\%p + 6\%He + 2\%Fe)}] = 199.62 \pm 14 \text{ g/cm}^2$$

$$\lambda[\text{mixed (80\%p + 20\%}\gamma\text{)}] = 186.64 \pm 14 \text{ g/cm}^2$$

Table 3.2 Comparison of simulated values of attenuation length (λ) with available experimental data:

Experiment				Present work λ (g/cm^2)			
Reference	Atm. depth, X (g/cm^2)	Energy range (TeV)	Attenuation Length, λ (g/cm^2)	Gamma	hadron	(92%p + 6%He + 2%Fe)	(80%p + 20%γ)
MAKET-ANI detector. [19]	700	Knee	240±30	211.35±11	243.25±13 (p) 255.78±10 (Fe)	245.93±14	237.81±12
EAS-TOP array. [20]	820	Knee	219±3	197.94±16	227.93±6 (p) 239.78±13 (Fe)	226.56±10	219.23±16
KASCADE array. [21]	1022	10^2–10^4 Knee	175-196±13	172.21±19	199.87±14 (p) 203.64±16 (Fe)	203.7 ±16	189.87±13
Buckland Park array. [14]	1030	< knee	185	171.62±16	197.54±11 (p) 200.42±14 (Fe)	199.62±14	186.64±14

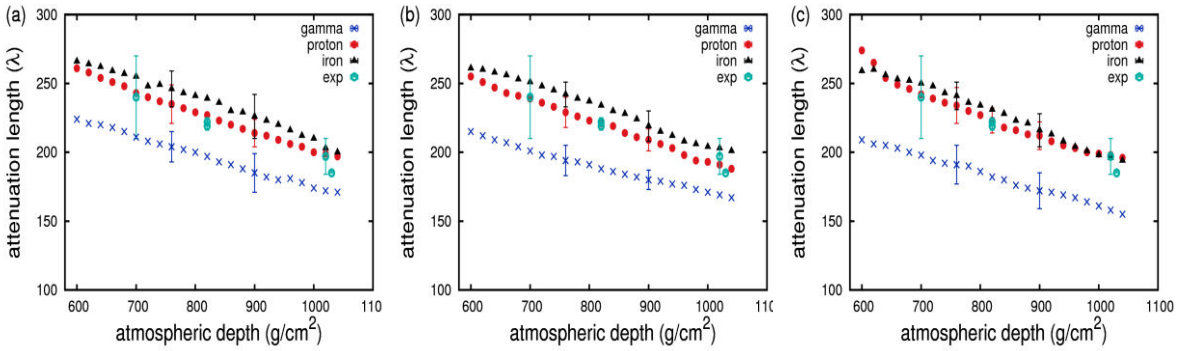

Fig. 3.5

(a) The variation of attenuation length (λ) with atmospheric depth using QGSJET01 with $E_\mu > 0.3$ GeV and $E_e > 0.003$ GeV.

(b) The variation of attenuation length (λ) with atmospheric depth using QGSJET II-04 with $E_\mu > 0.3$ GeV and $E_e > 0.003$ GeV.

(c) The variation of attenuation length (λ) with atmospheric depth using QGSJET II-04 with $E_\mu > 0.1$ GeV and $E_e > 0.001$ GeV.

3.5 Results and discussion

In this work, zenith angle distribution of the secondary cosmic ray charged component for different primaries have been studied using simulated data. Simulation is carried out assuming primary energy range (10TeV–1PeV) with pure primary composition (photon, proton and iron nucleus) as well as mixed compositions (92%p + 6%He + 2%Fe) & (80%p + 20%γ). Two different versions of QGSJET model of high energy hadronic

interactions have been tested considering threshold energies (E_μ > 0.3 GeV and E_e > 0.003 GeV) and (E_μ > 0.1GeV and E_e > 0.001 GeV) of the secondary particles. The differential zenith angle distributions, derived from 2000 simulated showers (for each configuration) are fitted with a power law in cos(θ), where the power index is related to attenuation. The fitted parameters, 'n(X)' and 'A(X)' are plotted in Figs. 3.2 and 3.3 respectively. Experimental values of the parameter 'n', as published by three air shower arrays operating in the same energy range (below the knee of the primary energy spectrum) are tabulated in Table 3.1, and plotted in Fig. 3.2, along with this work. The results are found to agree with a proton dominant mixed composition within experimental error.

The variation of the shower rate [F(θ)] with zenith angle (θ), for threshold shower sizes are deduced for different atmospheric depths. Optimum value of the threshold shower size for this work is found to be 500. A plot of log[F(θ)] versus sec(θ) is linear as depicted in Fig. 3.4. The slope of the graph gives the parameter 'λ', for all the composition models. Variation of this parameter with atmospheric depth for different primary compositions and different versions of interaction model QGSJET with different threshold energies of the secondary electrons and muons are shown in Fig. 3.5 (a), (b) & (c). It has been observed from Fig. 3.5(a) & (b), a change of the versions of hadronic interaction model without changing the secondary threshold energies, produce no significant difference for the results of proton or iron induced showers. However, from Fig. 3.5(b) & (c), which have been derived for the same interaction model (QGSJET II-04), but with different threshold energies of the secondary particles, a difference is observed. At higher threshold energies [Fig. 3.5(b)], the difference between proton and iron primaries is about (4% to 6%) and for

lower threshold energies [Fig. 3.5(c)], this difference is much reduced (0.5% to 3.5%). Comparing present result with experimental data of arrays detecting secondary charged particles having lower energy threshold, there is reasonable agreement with proton dominated mixed composition [Table 3.2].

The present simulation work is based on assumption of different primary compositions and high energy hadronic interaction characteristics. As a convention we have considered as our primary model of high energy hadronic interaction, the earlier version, QGSJET01, which is also widely used. The study of attenuation length of hadrons from measurement by scintillator array of KASCADE experiment [22], shows some deficits in this model which needs modification. Later, measurements of attenuation length of muons by KASCADE-Grande observatory [23] and analyses of the muon component by Pierre Auger Collaborations [24] also pointed out a possible discrepancy between the measured values and those predicted by newer versions of QGSJET model. Since the improved version of the QGSJET model is QGSJETII, we have chosen to compare these two versions. However, no significant difference is observed between the two.

A correlation between the two parameters (n & λ) purely based on CORSIKA Simulation is presented in Fig. 3.6. Pure gamma showers show a negative correlation, where as hadron showers show a slight positive correlation. When showers with a mixed composition (92%p + 6%He + 2%Fe) is compared with proton showers, the change of the value of 'n' is found to be only about 0.4% to 1% for lower attenuation lengths (< 220 g/cm^2), corresponding to higher atmospheric depths (> 850 g/cm^2, lower altitude). Whereas

for higher attenuation lengths (lower atmospheric depths, higher altitude) the change in 'n' varies from about 7% to 10%.

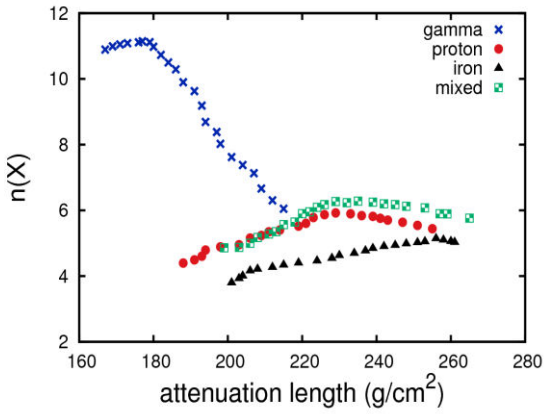

Fig. 3.6 The variation of power index, n(X) with attenuation length, λ.

3.6 Conclusion

Measurement of zenith angle distribution of secondary shower particles in the atmosphere is important for understanding the properties of longitudinal development of an EAS. It is now possible to examine the zenith angle distribution with both good angular resolution and statistics. Zenith angle distribution of extensive air showers can therefore be measured very accurately with high angular resolution arrays presently under operation or under construction. It is observed that using this method, the absorption of the shower

particles in the atmosphere may be studied by simply measuring zenith angle distribution without having to measure shower size. It may be noted that the present simulation study has found no significant difference between the old and new versions of QGSJET hadronic interaction model, which are based on Gribov–Regge theory. In a real experiment, if the composition is measured by other means, then the present method can be used to test any hadronic interaction model. Further, our simulation study shows that the arrays situated at lower atmospheric depths (higher altitudes) are in a better position to infer about average mass composition based on zenith angle distribution.

REFERENCES

[1] S. M. H. Halataei, M. Bahmanabadi, M. Khakian Ghomi and J. Samimi, *Physical Review D,* **77,** 083001, (2008)

[2] P. K. F. Grieder, *Extensive Air Showers: High Energy Phenomena and Astrophysical Aspects- A Tutorial, Reference Manual and Data Book,* **Volume I,** Springer, 254, (2010)

[3] B. D'Ettorre Piazzoli and G. Di Sciascio, *Astroparticle Physics,* 199, (1994)

[4] L. Saha *et al., Astroparticle Physics,* **42,** 33, (2013)

[5] HESS website: http://www.mpi-hd.mpg.de/hfm/HESS/

[6] CTA website: http://www.mpi-hd.mpg.de/hfm/CTA/

[7] K. Boruah, *Phys Rev. D,* **56,** 7376, (1997)

[8] U. D. Goswami and K. Boruah, *Indian J. Phys.,* **78,** 1253, (2004)

[9] D. Kalita and K. Boruah, *Indian J. Phys.,* **87(3)**, 289, (2013)

[10] M. Rahman and K. Boruah, *Indian J. Phys.,* **90(3)**, 253, (2015)

[11] D. Heck and T. Pierog, *Extensive Air Shower Simulation with CORSIKA: A users guide version 6.990,* [Karlsruhe, Germany: Karlsruher Institut Fur Technologie (KIT)], (2011)

[12] D. Heck and T. Pierog, *Extensive Air Shower Simulation with CORSIKA: A users guide version 7.3500,* [Karlsruhe, Germany: Karlsruher Institut Fur Technologie (KIT)], (2012)

[13] A. Ferrari, P. R. Sala, A. Fasso and J. Ranft, *"FLUKA: a multi-particle transport code",* Report CERN-2005-10(2005) INFN/TC_05/11 SLAC-R-773

[14] D. Ciampa and R. W. Clay, *J. Phys. G: Nucl. Phys.,* **14,** 787, (1988)

[15] A. Chilingarian, G. Gharagyozyan, G. Hovsepyan and G. Karapetyan, *Astropart. Phys.,* **25**, 269, (2006)

[16] J. Cotzomi, O. Martnez, E. Moreno, H. Salazar and L. Villase, *Rev. Mex. Fis.,* **51(1),** 38, (2005)

[17] M. Khakian Ghomi, M. Bahmanabadi and J. Samimi, *Astron. Astrophys.,* **434,** 459, (2005)

[18] T. Hara *et al., Phys. Rev. Lett.,* **50**, (1983)

[19] A. A. Chilingarian *et al., arXiv:astro-ph/0002076,* (2000)

[20] M. Aglietta *et al., Astropart. Phys.,* **10,** 1, (1999)

[21] T. Antoni *et al., Astropart. Phys.,* **19,** 703, (2003)

[22] W. D. Apel *et al., Physical Review D,* **80,** 022002, (2009)

[23] J. C. Arteaga-Velazquez *et al., Proc. 34th Intern. Cosmic Ray Conf. Hague (Netherlands),* (2015)

[24] L. Collica, *Proc. 34th Intern. Cosmic Ray Conf. Hague (Netherlands),* (2015)

CHAPTER 4

STUDY ON LONGITUDINAL AND LATERAL PROFILE OF PHOTON INDUCED SHOWERS USING CORSIKA CODE

The development of a shower in the atmosphere depends on the hadronic as well as electromagnetic interactions of shower particles with the air, their interaction cross sections, the secondary particle production, decays of unstable particles and the transport through the atmosphere, including energy loss, deflection, etc. A study associated with the characteristics of distribution of secondary particles helps to understand the nature of high energy particles. Development of a shower can be explained through two mechanisms. One is longitudinal and other is lateral development of secondary particles.

The longitudinal profile of a shower normally refers to the number of charged particles as a function of atmospheric depth which signifies the characteristics of the secondary particles [1]. The study of longitudinal development provides information about the nature of primary cosmic rays and their interactions in the atmosphere. Air showers have a lateral spread due to multiple Coulomb scattering that differs for different shower

components as well as for the various primary particles. The study of lateral distribution of secondary electrons and muons in Extensive Air Showers (EAS) represents one of the techniques to obtain the cosmic ray composition.

In the photon electron cascade theory, the number of shower particles initially increases with atmospheric depth, reaches a maximum and then decreases. The stage of longitudinal development of a cosmic ray cascade in the atmosphere is described by a parameter called age parameter (s_L, longitudinal age). The lateral development of electrons in cosmic ray extensive air shower (EAS) is usually approximated by the well known Nishimura-Kamata-Greisen (NKG) structure function and the slope of this distribution is described by the lateral age parameter, $s_\perp$. Theoretically $s_\perp$ is supposed to be equal to s_L. However, it is found that the NKG function does not give a good fit to the lateral experimental distribution of electrons for a single value of the lateral age parameter and this parameter varies with the radial distance. The concept of local age parameter was introduced in order to study the radial variation of age parameter.

In this chapter, we study the longitudinal and lateral profile of gamma, proton and iron induced showers and try to find some parameters sensitive for gamma-hadron separation. As gamma rays carry information about high energy sources, so they must be distinguished from hadron background. Longitudinal profile is fitted with the Gaisser-Hillas function and the values of interaction length have been estimated for the three primaries. Next, the lateral distribution of electrons is fitted with the Nishimura-Kamata-

Greisen (NKG) function, and the variation of lateral shower age parameter with zenith angle is studied. The mean lateral age parameter is derived as a function of shower size for all the primaries considered. Local age parameter is also calculated from the simulated data and its variation with core distance is studied. Finally, lateral distributions of the muon to electron density ratio have been derived for proton and gamma showers.

4.1 Longitudinal development of air showers

The growth of the secondary particles from the top of the atmosphere to the observation level is known as longitudinal development of shower. The characteristic parameters of longitudinal profile of extensive air showers are the maximum number of particles reached (N_m) and the corresponding depth (X_m). The shower size increases rapidly as it develops in the atmosphere until it reaches its maximum, N_m, then it starts decreasing as shower electrons begin to lose more energy by ionization than by radiation [2]. The shape of longitudinal profile of a shower can be fitted with several well known trial functions such as the Gaisser-Hillas [3], Greisen [4] and a Gaussian forms. In this work we have used the Gaisser-Hillas function.

4.1.1 Gaisser-Hillas function

In order to describe the characteristics of the shower longitudinal development, Gaisser and Hillas [3] introduced a function which depends on the essential characteristics of an air shower, defined as

$$N(X) = N_m \left(\frac{X-X_0}{X_m-X_0}\right)^{\frac{X_m-X_0}{\lambda_i}} e^{\frac{X_m-X}{\lambda_i}} \tag{4.1}$$

Where X_0 is the first interaction point and λ_i is the interaction length.

The longitudinal shower age parameter s_L is expressed as a function of atmospheric depth, X.

$$s_L = \frac{3X}{X+2X_m} \tag{4.2}$$

The number of secondary charged particles may be normalized as function of longitudinal age parameter,

$$n(s_L) = \frac{N(s_L)}{N_m} \tag{4.3}$$

here, $N(s_L)$ is the total no. of charged particle at s_L.

The depth X in the Gaisser-Hillas function given by eqn. (4.1) is translated to longitudinal shower age s_L and using the normalized shower size $N(s_L)$, eqn. (4.1) becomes

$$n(s_L) = \left(1 - \frac{1-s_L}{3-s_L}\frac{3T_m}{T_m-T_0}\right)^{T_m-T_0} e^{3T_m\frac{1-s_L}{3-s_L}} \tag{4.4}$$

Where $T_m = X_m/\lambda_i$ and $T_0 = X_0/\lambda_i$.

4.2 Lateral distribution of air showers

As the shower particles propagate downward through the atmosphere, they also spread laterally around the shower axis due to multiple Coulomb scattering and this phenomenon is known as the lateral development of air shower. The secondary particles are distributed to several hundred meters from the core of the shower. The density of the charged particles in the EAS as a function of distance from the shower axis can be represented as lateral distribution function (LDF). Usually, the lateral density distribution of secondary electrons at the observation level is approximated by the well known Nishimura-Kamata-Greisen (NKG) function [5].

4.2.1 Nishimura-Kamata-Greisen function and lateral shower age

The three dimensional cascade problem was solved numerically by Nishimura and Kamata and this was approximated by a function known as, Nishimura-Kamata-Greisen (NKG) function [5], suggested by K Greisen. The NKG function is given by

$$f(r) = \frac{N_e}{2\pi r_0^2} C(s_\perp) \left(\frac{r}{r_0}\right)^{(s_\perp - 2)} \left(1 + \frac{r}{r_0}\right)^{(s_\perp - 4.5)} \quad (4.5)$$

Where r_0 is the Moliere radius which is nearly equal to 80m at sea level [6], N_e is the shower size i.e. total number of electrons in a shower and $s_\perp$ is the lateral shower age parameter and the normalization factor $C(s_\perp)$ is given by

$$C(s_\perp) = \frac{\Gamma(4.5 - s_\perp)}{\Gamma(s_\perp)\Gamma(4.5 - 2s_\perp)} \quad (4.6)$$

The lateral shower age, $s_\perp$ can be estimated from fitted density distribution of electrons with the NKG function. It is a measure of the slope of the radial distribution of secondary electrons in EAS.

4.2.2 Local age parameter (LAP)

Experimentally it has been found that the lateral density profile of a shower cannot be described properly by a constant lateral shower age parameter as it varies with the radial distances [6]. In order to study the variation of shower age parameter with radial distance, Capdevielle et al. [7] introduces the notion of local age parameter (LAP).

The LAP for two neighbouring points i and j is given by

$$s_{ij} = \frac{ln\left(F_{ij}X_{ij}^{2}Y_{ij}^{4.5}\right)}{ln\left(X_{ij}Y_{ij}\right)} \tag{4.7}$$

Where $F_{ij} = \frac{f(r_i)}{f(r_j)}$, $X_{ij} = \frac{r_i}{r_j}$, $Y_{ij} = \frac{x_i+1}{x_j+1}$ and $x = \frac{r}{r_0}$

For $r_i \rightarrow r_j$ the definition of LAP at each point is given by

$$s(r) = \frac{1}{2x+1}\left((x+1)\frac{\partial \ln f}{\partial \ln x} + 6.5x + 2\right) \tag{4.8}$$

Where $r = \frac{r_i+r_j}{2}$

4.3 Simulation of longitudinal and lateral profile

A good procedure to study the cascade development in the atmosphere is a Monte Carlo method to simulate the EAS development in the atmosphere, taking into account all knowledge of high energy hadronic and electromagnetic interactions involved [8].

For the present work we used the CORSIKA 6.990 [9] version with the high energy interaction model QGSJET01, and low energy interaction model FLUKA [10]. The electromagnetic interactions are treated by the EGS4 code. We have generated a series of 100 showers for primary gamma, proton and iron each, considering primary energies 10^{13} eV, 10^{14} eV and 10^{15} eV and a range of energy from 10^{12} to 10^{15} eV (with an energy spectral shape of a power law with index -2.7) considering zenith angle range 0^0 to 40^0. The relevant data are taken from the long output DATA files and the binary output files using FORTRAN programs.

4.4 Results

4.4.1 Longitudinal Profile

We study the longitudinal profile of photon and proton induced showers at 10^{13} eV, 10^{14} eV and 10^{15} eV. Fig. 4.1 shows the number of charged particles as a function of atmospheric depth for photon and proton induced EAS at 10^{15} eV. It is seen that the depth

of shower maximum for photon induced shower is slightly higher than the depth of shower maximum of proton induced shower. This is due to smaller interaction cross section and hence longer mean free path for gamma interaction as compared to proton interaction with air nuclei. Again the particle number at the maximum for photon induced showers is higher than that for proton induced showers.

In order to study the shape of the longitudinal development, the positions of all the shower maximum are aligned and then they are normalized by their own shower maximum size N_m. This is done by using the longitudinal shower age parameter s_L as the independent variable instead of atmospheric depth, X [eqn. 4.2].

We have fitted the simulated longitudinal profile of gamma and proton induced shower with the Gaisser-Hillas function given by eqn. (4.4) for energy 10^{13} eV, 10^{14} eV and 10^{15} eV. From these fitted functions, the values of interaction length λ_i have been evaluated for gamma and proton showers. Fig. 4.2 shows the simulated longitudinal profile for photon induced shower at 10^{15} eV fitted with the Gaisser-Hillas function. Fig. 4.3 shows the deviation of the simulated data from the Gaisser-Hillas fit. The values of the parameters of Gaisser-Hillas function are tabulated in Table 4.1 for gamma and proton induced showers.

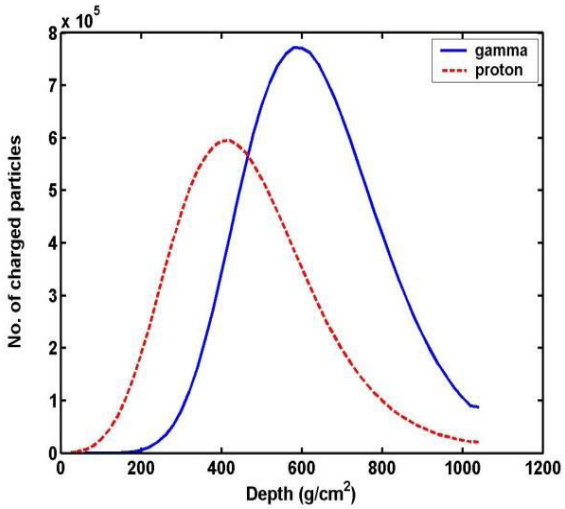

Fig. 4.1 Longitudinal profile of showers induced by gamma and proton at 10^{15} eV.

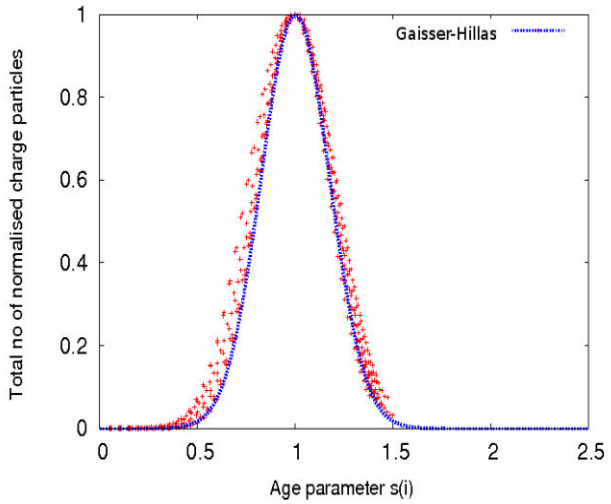

Fig. 4.2 Simulated data of photon primary fitted with the Gaisser-Hillas function at 10^{15} eV.

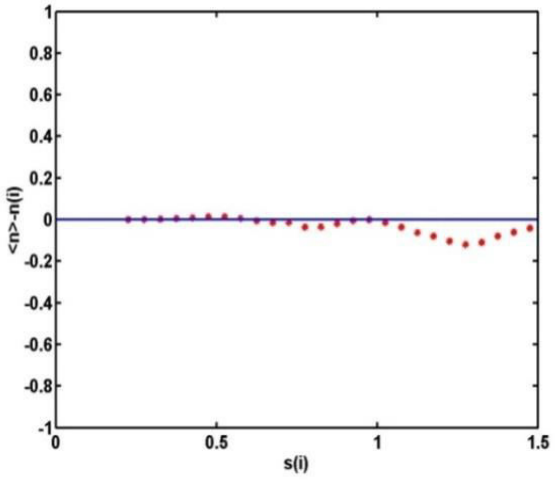

Fig. 4.3 Deviation of data from the Gaisser-Hillas fit.

Table 4.1 Parameters of GHF for gamma and proton initiated showers at different energies

Particle	$E\ (eV)$	N_{max}	X_{max}	λ_i in (g/cm^2)
Gamma	10^{13}	$(9.6 \pm 0.55) \times 10^3$	447 ± 39	76.4 ± 5.2
	10^{14}	$(8.7 \pm 0.43) \times 10^4$	515 ± 45	74.6 ± 7.5
	10^{15}	$(7.7 \pm 0.54) \times 10^5$	601 ± 67	71.2 ± 9.3
Proton	10^{13}	$(5.3 \pm 0.81) \times 10^3$	435 ± 49	52.7 ± 7.2
	10^{14}	$(5.7 \pm 0.74) \times 10^4$	490 ± 58	45.3 ± 6.7
	10^{15}	$(5.8 \pm 0.49) \times 10^5$	571 ± 63	42.6 ± 4.3

4.4.2 Lateral profile

4.4.2.1 Electron component

The lateral density distribution of electrons is fitted with the (NKG) function as given by eqn. (4.5). From the NKG fit the values of the lateral shower age parameter $s_{\perp}$ are obtained using χ^2 - minimization technique at different zenith angle bins of 5^0 from 0^0 to 40^0. The lateral shower age parameters $s_{\perp}$ are plotted with respect to the zenith angles (shown in Fig. 4.4). It is found that the lateral shower age parameter increases with the zenith angle.

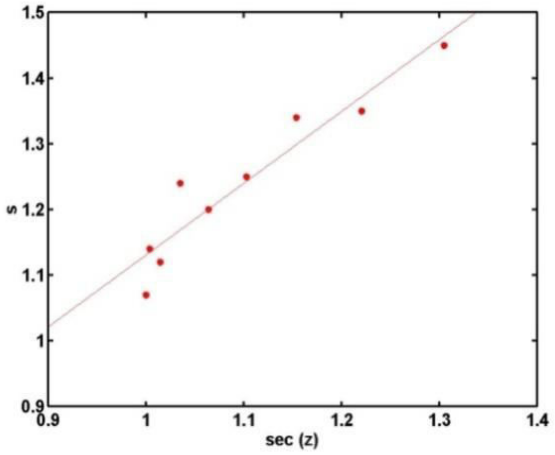

Fig. 4.4 Variation of lateral shower age with zenith angle for 10^{15} eV photon induced shower.

Again we have obtained the mean values of lateral age parameter as a function of shower size considering primary energy range from 10^{12} to 10^{15} eV for gamma, proton and iron induced showers as shown in Fig. 4.5. From the figure, it is seen that the lateral age parameter for gamma induced shower is less than the proton and iron induced showers. This shows that showers induced by heavier primaries are older compared to those generated by lighter primaries and gamma rays. A smaller lateral age parameter indicates a steeper LDF, showing that showers penetrate deeper into the atmosphere, with increasing primary energy i.e. with increasing shower size.

Fig. 4.6 shows the radial variation of local age parameter (LAP) as obtained from simulated data using eqn. (4.8) for gamma, proton and iron primaries. It is found that the local age parameter first decreases with radial distance, reaches a minimum between 30 to 50 m and then increases with radial distance, as expected from other simulation study [7]. Further, the local age parameter is found to decrease at about 300m from the core for proton and iron primaries, an effect observed by R. K. Dey et al [6] to be consistent with data of Akeno [11] and in Kascade-Grande [12]. However, for gamma shower, the local age parameter remains almost constant beyond 100m.

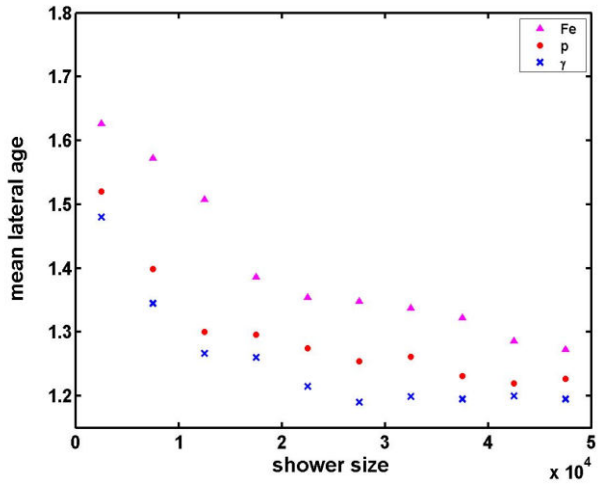

Fig. 4.5 Variation of mean lateral shower age with shower size at 10^{12}-10^{15} eV.

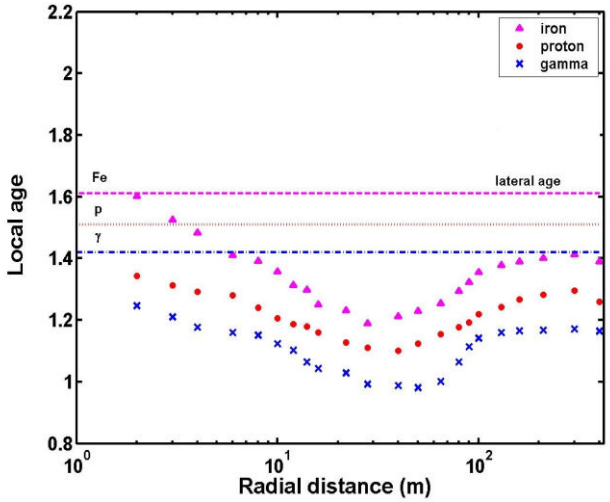

Fig. 4.6 Variation of local age parameter with radial distance.

4.4.2.2 Muon to electron ratio

The ratio of muon to electron density is an important parameter for distinguishing gamma showers from hadron background as the muon content of photon induced showers is very small compared to hadron induced showers. We have studied the lateral distribution of electrons and muons for primary photon and proton at primary energy 10^{15} eV using CORSIKA Code. The ratio of muon to electron density has been obtained as a function of core distance for both photon and proton induced showers and it is shown in Fig. 4.7. It is seen that gamma and proton primaries are well separated throughout the core distance range.

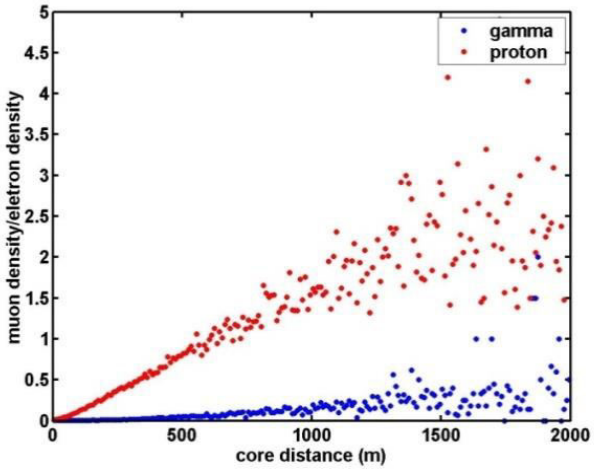

Fig. 4.7 Ratio of muon density to electron density at 10^{15} eV for photon and proton induced shower.

4.5 Conclusion

In this work, longitudinal and lateral profile of showers induced by gamma and hadron primaries have been presented. The depth of shower maximum and number of particles at maximum depth are higher for gamma induced showers than proton induced showers. The shower longitudinal profile is well fitted by the Gaisser-Hillas function. The interaction length, λ_i is found to decrease with energy and its value is more for photon showers than hadron showers.

The lateral distribution of gamma and hadron induced showers are fitted with the NKG function. The lateral shower age is found to increase with the zenith angle and decrease with shower size. It takes higher values for heavy nuclei compared to that of lighter nuclei and gamma ray primaries. From the simulation result it is found that the mean LAP is lower for gamma ray induced EAS for all core distances. This can be an effective parameter to separate out gamma ray induced showers from hadron induced showers. Variation of local age parameter with distance from the shower axis shows that this value remain constant for larger core distances (beyond 100m) for gamma showers, where as there is a decrease for hadron showers. This parameter can be measured in a closely packed EAS array and can be used for gamma hadron discrimination. Finally muon to electron density ratio is found to be sensitive to gamma proton separation.

REFERENES

[1] T. K. Gaisser, *Cosmic Rays and Particle Physics*, Cambridge University press, 202, (1992)

[2] T. Abu-Zayyad et al., *Astropart. Phys*., **16**, 1, (2001)

[3] T. Gaisser and A. M. Hillas, *Proc. 15th ICRC,* **8**, 353, (Plovdiv 1977)

[4] K. Greisen, *Annu. Rev. Nucl. Sci*., **10**, 63, (1960)

[5] K. Greisen, *Progress in Cosmic Ray Physics*, Vol.III, Amsterdam, NH publishing Co., (1956)

[6] R. K. Dey, A. Bhadra, and J. N. Capdevielle, *ICRC*, (2011)

[7] J. N. Capdevielle and J. Gawin*, J. of Physics G*, **8**, 1317, (1982)

[8] M. M. Espinosa et al., *Proc ICRC*, (2001)

[9] D. Heck and T. Pierog, *Extensive Air Shower Simulation with CORSIKA: A users guide version 6.990,* [Karlsruhe, Germany: Karlsruher Institut Fur Technologie (KIT)] (2011)

[10] A. Ferrari, P. R. Sala, A. Fasso and J. Ranft, "*FLUKA: a multi-particle transport code*", ReportCERN-2005-10(2005) INFN/TC_05/11 SLAC-R-773

[11] M. Nagano et al., *Journal of the physical society of Japan*, **vol. 53**, pp.1667-1681 (1984)

[12] J. N. Capdevielle et al., *J.Phys. G : Nucl. Part. Phys*., **31** , 507-524, (2005)

CHAPTER 5

A COMPREHENSIVE STUDY ON FLUCTUATION OF SECONDARY CHARGED PARTICLES FOR GAMMA AND HADRON PRIMARIES

The high energy cosmic ray primaries on entering the earth's atmosphere suffer multiple nuclear interactions. As a result, different types of secondary particles like electrons, muons and hadrons are produced [1]. The variations in the characteristics of secondary particles generated by same primary with same energy and direction give rise to the phenomenon of shower to shower fluctuations [2]. Fluctuations in shower may arise mainly due to the location and point of first interaction of primary particle with the air nuclei. Depth of shower maximum and multiplicity are the parameters where fluctuation is mostly observed [3]. A study on fluctuations of showers is expected to help in the measurement of air shower parameters with more accuracy. At higher energies i.e. above 10^{12} eV, majority of primary cosmic rays contain lighter to heavier atomic nuclei such as proton, helium, oxygen, iron and many others. The composition of gamma photons is only about 0.1%. The detection of primary gamma ray initiated air showers is of particular interest as their arrival direction point back to their sources. The gamma ray induced

showers mainly contain electrons and positrons along with a small number of muons. So by detecting the number of muons in a shower, gamma ray can be separated from hadrons. In real cosmic ray experiments, separation between gamma and hadron showers is a difficult task.

The present work has been divided into three sections. In the first section, the relative fluctuation ($\sigma/\overline{\mathrm{N}}$) for electron and muon components have been evaluated considering longitudinal profile of air showers for different primary particles (i.e. photon, proton and iron). In the second section, the impact of relative fluctuation on the lateral profile is studied.

In the third section, fluctuation of the secondary charged particles is studied using a statistical technique called, Principal Component Analysis (PCA) method. It reduces a data set into a new set of components with larger variance. The first component with the largest variance is called the first principal component and so on [4]. In astrophysics, PCA method is used in the analysis of spectra of Gamma Ray Bursts and in galaxy surveys [5]. Here we have applied this method for gamma hadron separation considering the number of secondary charged particles as a function of polar angle within a ring of 100 m radius.

5.1. Shower to shower fluctuation

5.1.1. Fluctuation of longitudinal profile

As the shower develops into the atmosphere the number of secondary particles goes on increasing with atmospheric depth upto a certain level, after which the shower particles began to decline in its size. The evolution of the EAS particles varies from shower to shower. The longitudinal distribution of air showers can clarify the nature of primary particle and their interaction in the atmosphere [6]. The longitudinal profile mainly refers to two important parameters. One is the depth of shower maximum and other is the number of particles at the maximum development.

In order to study the variation of secondary electron and muon components from shower to shower, we have calculated relative fluctuation, $\sigma/\overline{\mathrm{N}}$ at 52 depths from 20 to 1040 g/cm^2 by a step of 20 g/cm^2. Here σ is the standard deviation and $\overline{\mathrm{N}}$ is the average number of secondary particles.

5.1.2. Fluctuation of lateral profile

The lateral distribution of a shower normally means the spread of secondary particles perpendicular to the direction of primary particle. From the number of secondary particles and their distribution at the ground level one can estimate the energy and mass of

the primary particles [7]. The study of muon content of an air shower can furnish valuable information about the primary particle type and their interactions as they are mainly produced by hadronic interactions in the atmosphere [8]. Fluctuations in lateral shower development have been studied, by means of the distribution of secondary charged particles (i.e. electrons and muons) at the ground level as a function of core distance (r). The range of core distance chosen is (0-300) m in a step of 20 m around the shower axis. The relative fluctuation $(\sigma/\overline{\mathrm{N}})$ is obtained for secondary electrons and muons at each radial bins.

5.2. Principal Component Analysis (PCA) Method

Principal component analysis (PCA) is a well established statistical method that generates eigenvalues and eigenvectors from a covariance matrix of a set of data [9]. By this method, whole data set is transformed into a new system of coordinates with a linear function of the original variables. The advantage of this method is that it reduces the set of data into a smaller number of variables without losing much information from the original data set.

The covariance matrix can be constructed [10] as

$$C_{ij} = \frac{1}{M}\frac{\sum_{k=1}^{M}(v_{ik}-\mu_i)(v_{jk}-\mu_j)}{\sigma_i\sigma_j} \qquad (5.1)$$

where M is the number of vectors and v_{ik} is the i^{th} component corresponding to k^{th} vector of the set of variables.

μ_i and σ_i are mean and variance of the variables corresponding to the i^{th} component of the vectors defined by

$$\mu_i = \frac{1}{M}\sum_{k=1}^{M} v_{ik,} \quad \sigma_i^2 = \frac{1}{M}\sum_{k=1}^{M}(v_{ik} - \mu_i)^2$$

Solving the eigen value equation,

$$C\Psi_n = \lambda\Psi_n \tag{5.2}$$

N eigen values values (λ) and N eigen vectors can be obtained.

5.3 Simulations with CORSIKA

In order to predict the properties of atmospheric air showers created by primary cosmic ray particles, several numerical Monte Carlo simulation models have been designed [11-14]. In this work simulation of air showers have been carried out with the help of CORSIKA 6.990 [15] version employing QGSJET01 as high energy hadronic interaction model and FLUKA [16] as low energy hadronic interaction model. 500 vertical showers

(each) have been generated considering pure primary compositions (photon, proton and iron nucleus) at primary energies 10^{14} eV, 10^{15} eV and 10^{16} eV.

5.4 Results

5.4.1 Using longitudinal profile

The comparison of average longitudinal profile of secondary electrons and muons for primary photons, protons and iron nuclei at primary energy 10^{15} eV are shown in Fig. 5.1 (a) and (b) respectively.

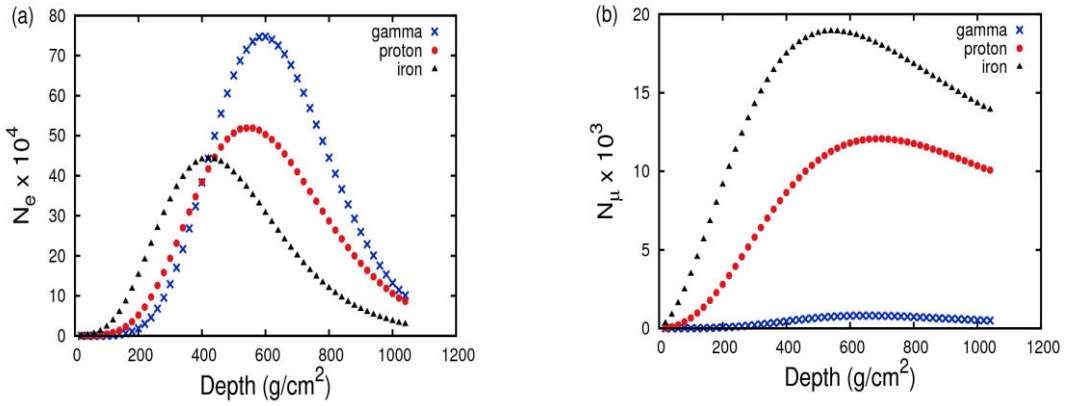

Fig. 5.1 Longitudinal development of average no. of (a) electrons and (b) muons as a function of atmospheric depth at 10^{15} eV.

From Fig. 5.1(a), it is observed that the average number of electrons are more for gamma induced showers than proton and iron induced showers. Again Fig. 5.1(b) shows that the average number of muons are very less for showers induced by gamma primaries compared to proton and iron primaries.

The relative fluctuation ($\sigma/\overline{\mathrm{N}}$) is obtained considering secondary electron and muon components for primary gamma, proton and iron at 10^{14} eV, 10^{15} eV and 10^{16} eV. These are presented in Fig. 5.2 (a), (b), (c) and Fig. 5.3 (a), (b), (c) respectively. From these figures, it has been observed that the relative fluctuation is more at lower depth, becomes minimum at the depth of shower maximum and then again increases with depth. This reveals that fluctuation is minimum at the depth where particle number is maximum i.e at the depth of shower maximum (X_{max}) for all the cases.

The electron component of iron primary shows less fluctuation at all energies, whereas gamma and proton showers show almost similar type of fluctuations. But for muons, gamma primaries show highest fluctuation independent of primary energy. Thus the study of fluctuations considering muon number can help in the separation of gamma induced showers from hadron induced showers.

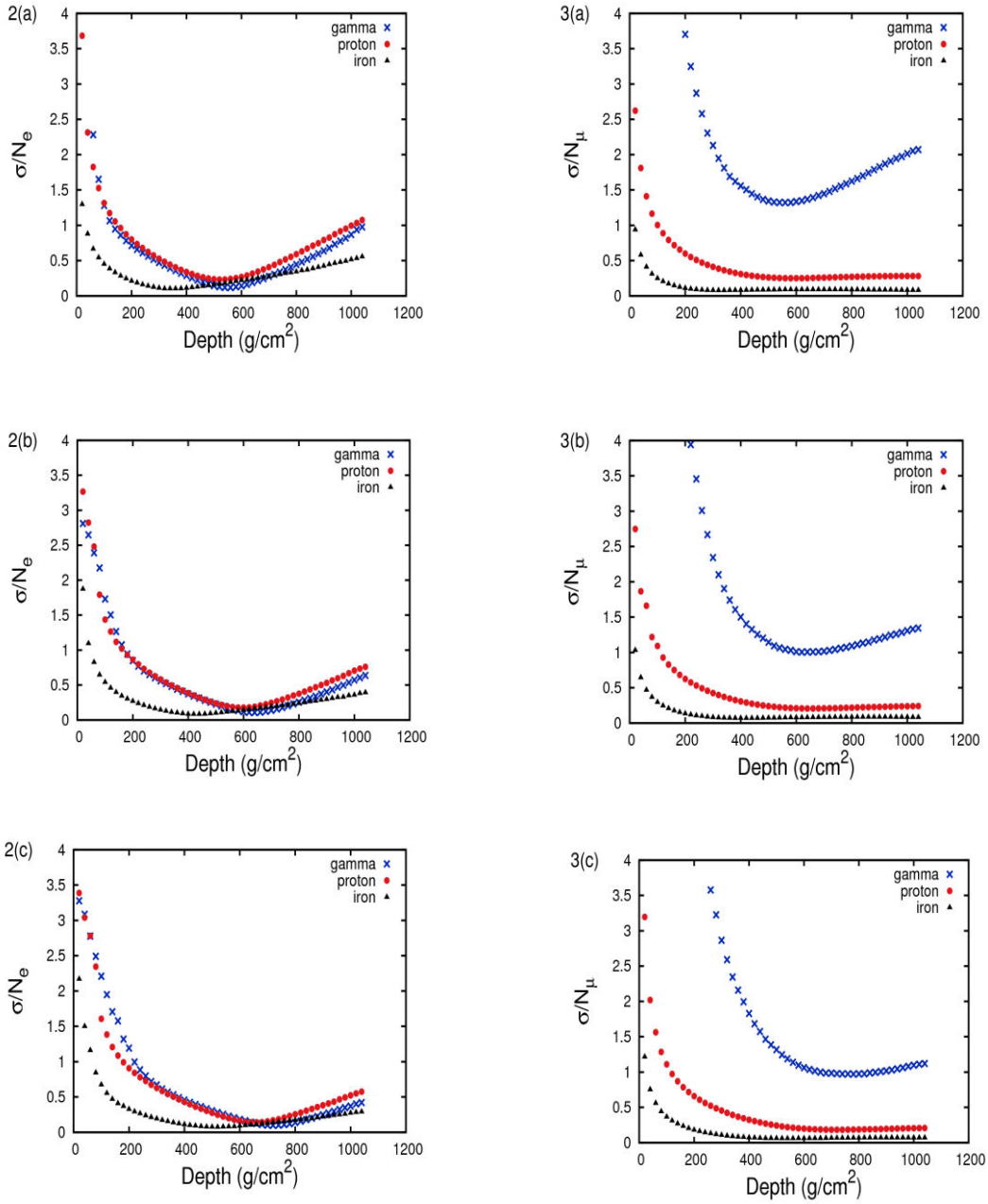

Fig. 5.2 Relative fluctuation ($\sigma/\bar{N}_e$) of secondary electrons as a function of depth at **(a)** 10^{14} eV, **(b)** 10^{15} eV and **(c)** 10^{16} eV.

Fig. 5.3 Relative fluctuation ($\sigma/\bar{N}_\mu$) of secondary muons as a function of depth at **(a)** 10^{14} eV, **(b)** 10^{15} eV and **(c)** 10^{16} eV.

5.4.2 Using lateral profile

The lateral distribution of average number of secondary electrons and muons as a function of core distance are plotted in Figs. 5.4 (a) and (b) respectively for gamma, proton and iron primaries at 10^{15} eV.

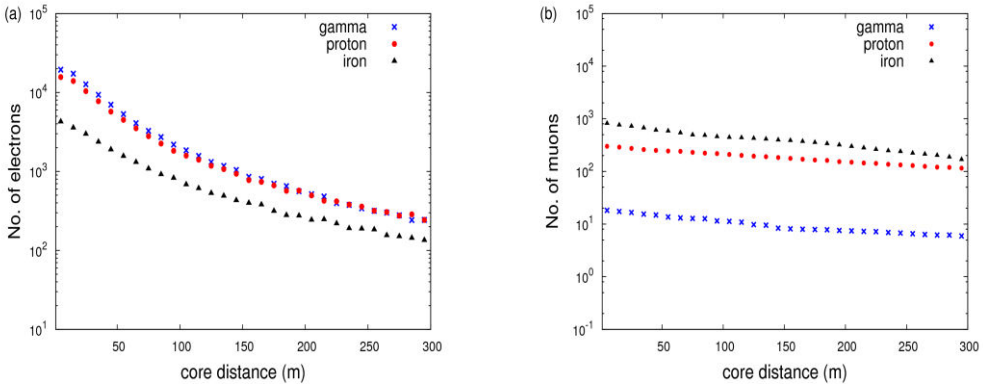

Fig. 5.4 Lateral distribution of average number of secondary (a) electrons and (b) muons for primary energy 10^{15} eV.

As gamma rays mainly undergo electromagnetic interactions while travelling through the atmosphere, their electron component is more and muon component is much less in comparison to hadrons (proton and iron). Again the muon content is found to be more for iron primary as muons are produced by hadronic interactions.

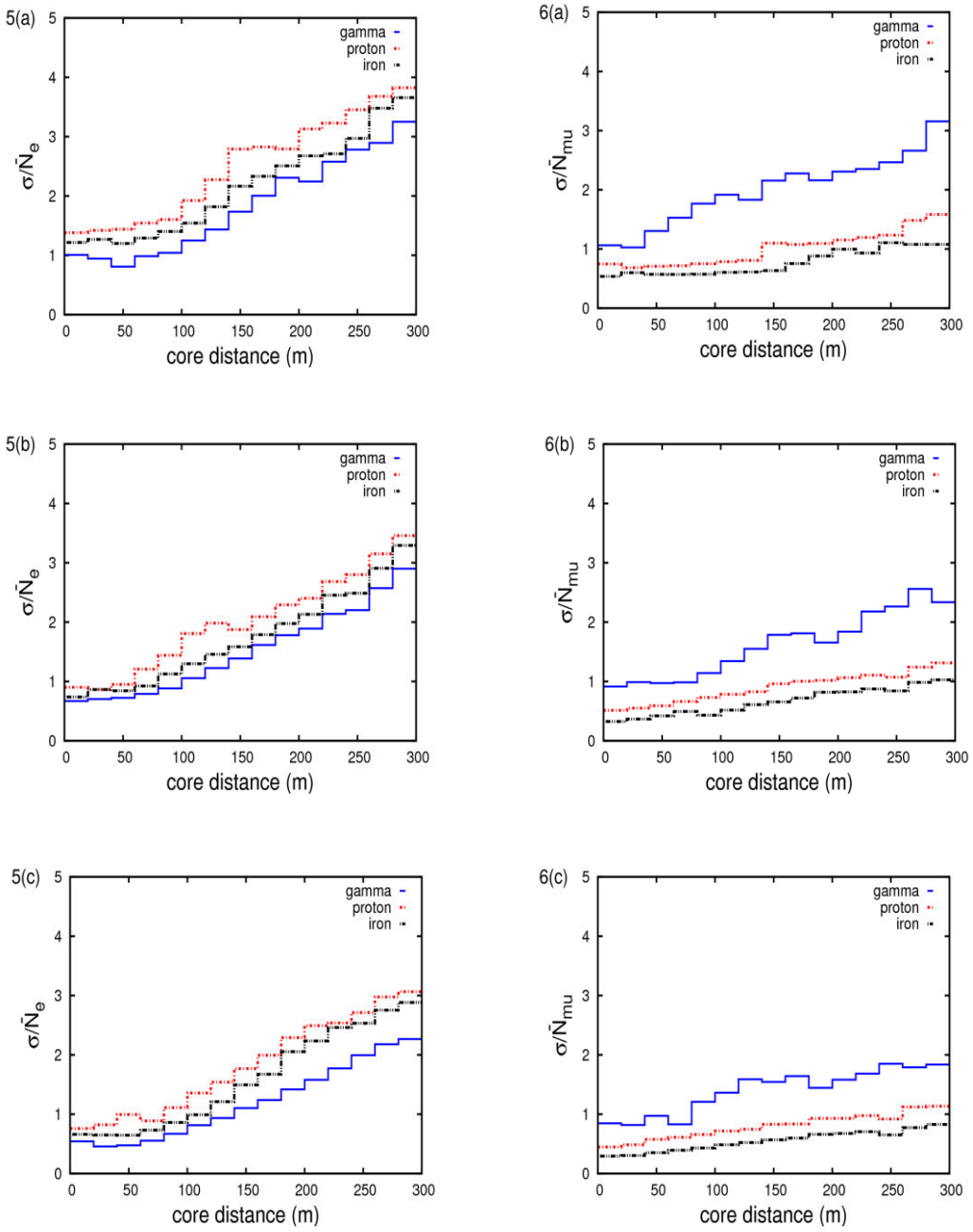

Fig. 5.5 Relative fluctuation ($\sigma/\bar{N}_e$) of secondary electrons as a function of core distance at **(a)** 10^{14} eV, **(b)** 10^{15} eV and **(c)** 10^{16} eV.

Fig. 5.6 Relative fluctuation ($\sigma/\bar{N}_\mu$) of secondary muons as a function of core distance at **(a)** 10^{14} eV, **(b)** 10^{15} eV and **(c)** 10^{16} eV.

It is found from Fig. 5.5 and Fig. 5.6, that for both the secondaries $(\sigma/\overline{N})$ is minimum near the shower axis and gradually increases with the core distance. From this study one can infer that, as the number of particles decreases with distances from the shower core, the relative fluctuation increases. For muon component, gamma primary shows maximum fluctuation. Whereas proton and iron primaries show comparatively less fluctuation. The relative fluctuation for electron component is approximately same for all the primaries. Again fluctuation is found to decrease with increasing primary energy.

5.4.3. Separation of gamma-hadron using PCA Method

At first we have considered the lateral distribution of secondary electrons and muons separately falling within a core distance of 100 meters. The selected events have been divided in 100 equal polar angle bins around the shower axis. In Fig. 5.7 (a), (b), (c) and Fig. 5.8 (a), (b), (c), the two dimensional distribution of secondary electrons and muons are shown respectively at primary energy 10^{15} eV for primary gamma, proton and iron nuclei. Again their one dimensional distributions as a function of polar angle have been presented in Fig. 5.9 (a), (b), (c) and Fig. 5.10 (a), (b), (c) respectively.

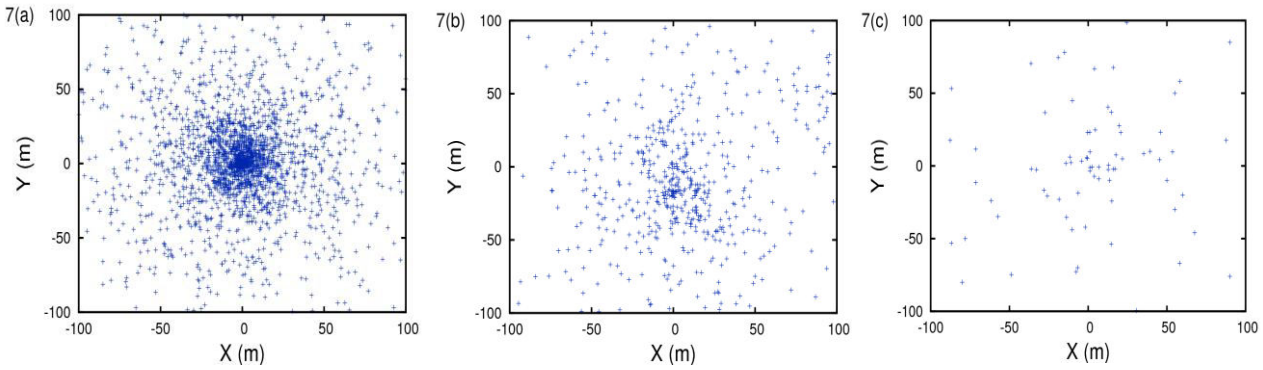

Fig. 5.7 Two dimensional distribution of electrons for (a) gamma, (b) proton and (c) iron primary at 10^{15} eV.

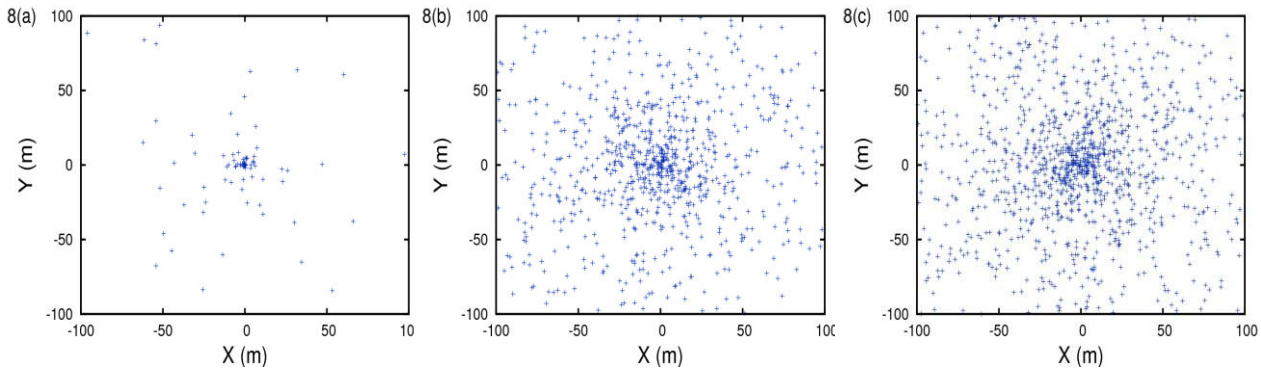

Fig. 5.8 Two dimensional distribution of muons for **(a)** gamma, **(b)** proton and **(c)** iron primary at 1

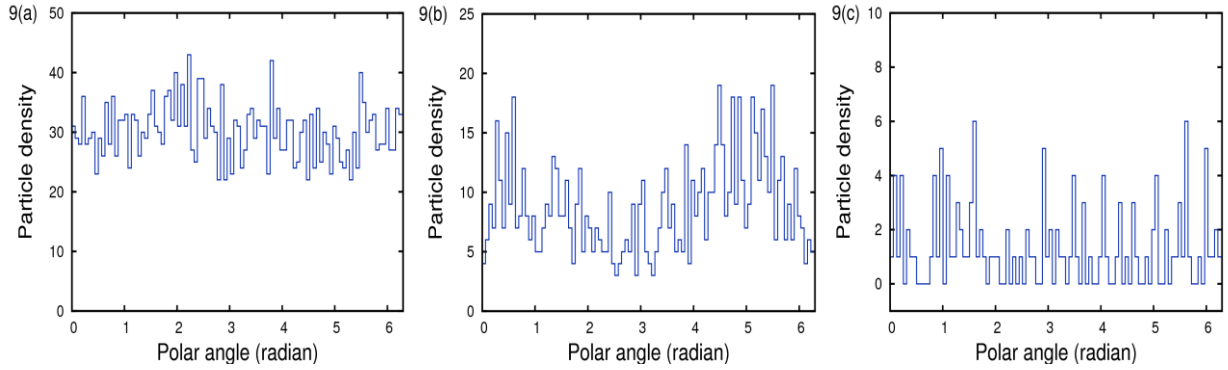

Fig. 5.9 Distribution of electrons with polar angle for **(a)** gamma, **(b)** proton and **(c)** iron primary at 10^{15} eV.

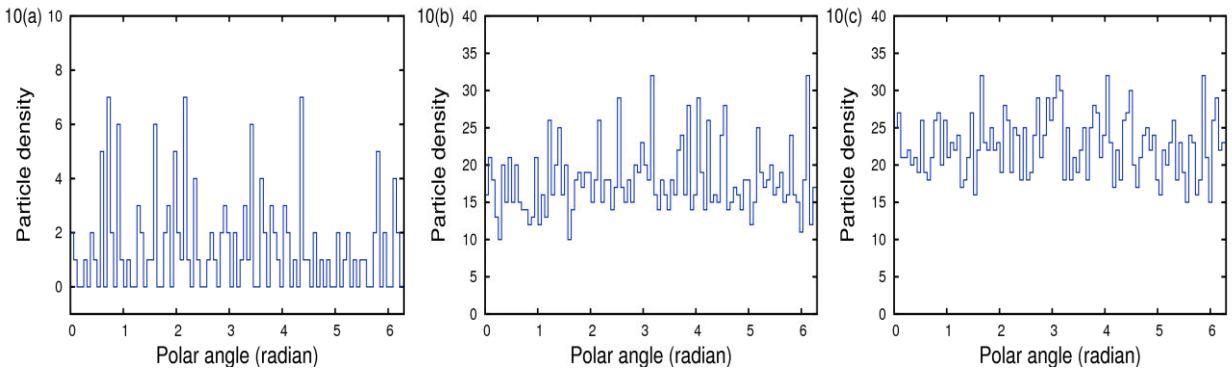

Fig. 5.10 Distribution of muons with polar angle for **(a)** gamma**, (b)** proton and **(c)** iron primary at 10^{15} eV.

As seen from the Fig. 5.7(a), (b) and (c), gamma induced showers contains more number of secondary electrons which are distributed almost evenly around the shower axis. The distributions of secondary electrons are not symmetric for proton and iron induced showers. Further, Fig. 5.8(a), (b) and (c) show the distribution of secondary muons. As the number of muons are very small for gamma primaries, they show large variation around the shower core.

To apply the PCA method, we classify the whole simulated data, with selected shower size, N_s intervals by an amplitude of ΔN_s = 50000, arriving at the ground level. Table 5.1 shows the four selected bins along with the number of primary cosmic ray particles N_p falling within these particular bins ΔN_s.

Considering 100 equal sectors of polar angle, the whole data series is cut into 10 non overlapping pieces of 10 data points each. Then eigen values are computed using Eqn. (5.1) and (5.2). Fig. 5.11 (a) and (b) shows the decreasing order of eigen value spectrum with the rank of the matrix for ΔN_2 bin for secondary electrons and muons respectively.

Table 5.1 Distribution of simulated events into ΔN_s bins along with number of primary particles, N_p falling within the particular bins

Particle	ΔN_s	N_p
Photon	$\Delta N_1 = 0 - 50000$	661
	$\Delta N_2 = 50000 - 100000$	329
	$\Delta N_3 = 100000 - 150000$	194
	$\Delta N_4 = 150000 - 200000$	179
Proton	$\Delta N_1 = 0 - 50000$	776
	$\Delta N_2 = 50000 - 100000$	271
	$\Delta N_3 = 100000 - 150000$	123
	$\Delta N_4 = 150000 - 200000$	71
Iron	$\Delta N_1 = 0 - 50000$	907
	$\Delta N_2 = 50000 - 100000$	129
	$\Delta N_3 = 100000 - 150000$	87
	$\Delta N_4 = 150000 - 200000$	64

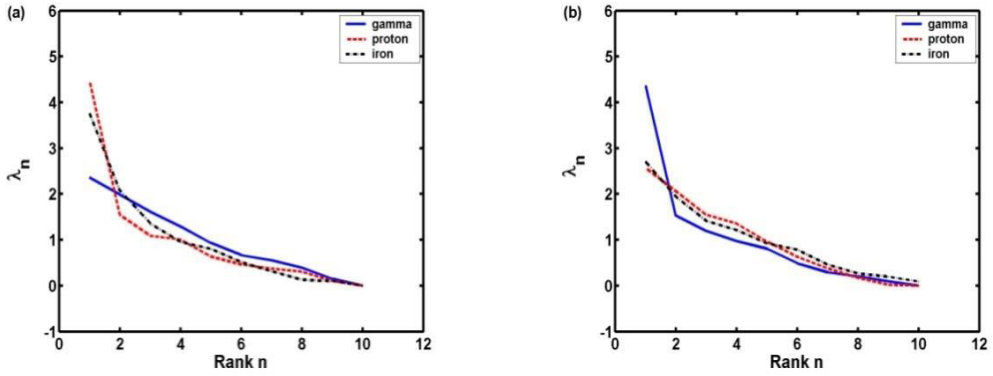

Fig. 5.11 Decreasing ordered eigenvalue spectrum for ΔN_2 samples of photon, proton and iron primaries considering secondary **(a)** electrons and **(b)** muons.

From Fig. 5.11 (a), considering distribution of electrons, we found that proton and iron primaries show larger variance of about 45% and 38% respectively by possessing dominant eigenvalues. Whereas for photon primary, the eigenvalue spectrum is smoothly distributed among all the ranks. The first component of gamma primary carries only about 24% of total variance. Thus we observed that gamma primary shows minimum variance for secondary electrons. In case of muons however, just the opposite is observed (Fig. 5.11 (b)). The first component of gamma shower possesses a dominant eigenvalue and hence shows largest variance of about 44%. But the variation is less for proton and iron series with 26% and 27% respectively. In order to estimate the separation power between gamma and hadrons, quality factor, Q is evaluated as [17]

$$Q = \frac{k_\gamma}{\sqrt{k_h}} \tag{5.3}$$

Where $k_\gamma = \frac{N_\gamma^{cut}}{N_\gamma}$ and $k_h = \frac{N_h^{cut}}{N_h}$

N is the total number of particles and N_{cut} is the number of particles remaining after the cutting procedure have been applied. k_γ is the fraction of photon and k_h is the fraction of hadron i.e. proton (k_p) and iron (k_{Fe}) falling within the selected radial distance of 100 m. Table 5.2 shows the values of quality factor Q corresponding to different ΔN_s bins. Here $Q_{\gamma p}$ describes the quality factor between gamma and proton primary and $Q_{\gamma Fe}$ describes the quality factor between gamma and iron primary

The maximum value of separation power between gamma and proton $Q_{\gamma p}$ is found to be 1.16 and between gamma and iron primary $Q_{\gamma Fe}$ is found to be 1.13 for electron component. For muon component, these values are 1.11 and 1.10 respectively. Thus, gamma-proton discrimination power is more compared to gamma-iron discrimination power.

Table 5.2 The quality factor Q corresponding to ΔN_s bins for both electron and muon components

ΔN_s	Electron					Muon				
	k_γ	k_p	k_{Fe}	$Q_{\gamma p}$	$Q_{\gamma Fe}$	k_γ	k_p	k_{Fe}	$Q_{\gamma p}$	$Q_{\gamma Fe}$
ΔN_1	0.39	0.14	0.12	1.04	1.13	0.99	0.83	0.81	1.09	1.10
ΔN_2	0.41	0.13	0.14	1.14	1.10	0.97	0.86	0.82	1.05	1.07
ΔN_3	0.38	0.12	0.13	1.09	1.05	0.93	0.77	0.79	1.06	1.05
ΔN_4	0.42	0.13	0.14	1.16	1.12	0.98	0.78	0.83	1.11	1.08

5.5 Conclusion

We have studied shower to shower fluctuation of secondary cosmic ray charged particles (i.e. electrons and muons) for different primary particles, using simulated data. Simulation has been carried out for primary energies 10^{14} eV, 10^{15} eV and 10^{16} eV with pure primary compositions (gamma, proton and iron nucleus). In this work, an effort has been made to find out parameters that are sensitive for gamma hadron separation. Considering the longitudinal profile (first section), $\sigma/\overline{\mathrm{N}}$ is found to be minimum at depth of shower maximum. For secondary electrons, the relative fluctuation is maximum for hadron primaries i.e. proton and iron, whereas, for muon component, gamma primary shows maximum fluctuation. Longitudinal fluctuation in muon component is found to be more for gamma primary compared to hadron primary. From the lateral profile (second section), the relative fluctuation of secondary particles is found to increase with core distance (r) for all the cases considered. Fluctuation of the lateral distribution of the muon component is also found to be maximum for gamma induced showers. Hence, lateral and longitudinal fluctuation in muon number may be used to distinguish gamma primaries from hadron primaries.

In the third section we have made an attempt to separate gamma and hadron primaries by applying the variable reduction method known as the Principle Component Analysis (PCA) method. Here, fluctuation of secondary electrons and muons is distributed in polar angle bins and co-variance matrix is formed. By comparing eigen values plotted as

function of rank of the co-variance matrix, it has been observed that for electron component, hadrons show larger variation than gamma photons. However considering muon component, gamma photon shows maximum variation compared to hadrons. The proton primary carries maximum variation of 45% for electron component. However for muon component, gamma photon shows maximum variation of about 44%. The quality factor Q, showing separation power between gamma and hadrons have been evaluated. It is found that PCA method is more effective in discriminating gamma from proton, compared to that from iron primaries. From this work, we can conclude that the study of fluctuation in secondary particle number can help in separation of gamma photons from the cosmic ray background.

REFERENCES

[1] P. M. Hansen, J. Alvarez Muniz and R. A. Vazquez, *Astroparticle Physics,* **34,** 503 (2011)

[2] P. M. Hansen, R. A. Vazquez and J. Alvarez Muniz, *Proceedings of the 31st ICRC, LODZ,* (2009)

[3] P. K. F. Greider, *Cosmic rays at earth: Researcher's Manual and Data Book,* (2001)

[4] F. Catalani and V. de Souza, *Proceedings of the 31st ICRC, LODZ,* (2009)

[5] F. Catalani *et al., arXive:astro-ph/0703582v1,* (2007)

[6] N. Inoue *et al., J. Phys. G: Nucl. Phys.,* **11,** 669, (1985)

[7] T. Antoni *et al., Astropart. Phys.,* **14,** 245, (2001)

[8] V. de Souza *et al., Proceedings of the 31st ICRC, LODZ,* (2009)

[9] D. C. Hoyle and M. Rattray, *PHYSICAL REVIEW E,* **69,** (2004)

[10] E. Faleiro *et al., Astropart. Phys.,* **26,** 50, (2006)

[11] K. Boruah, *Phys Rev. D,* **56,** 7376, (1997)

[12] U. D. Goswami and K. Boruah, *Indian J. Phys.,* **78,** 1253, (2004)

[13] D. Kalita and K. Boruah, *Indian J. Phys.,* **87(3),** 289, (2013)

[14] M. Rahman and K. Boruah, *Indian J. Phys.,* **90(3),** 253, (2015)

[15] D. Heck and T. Pierog, *Extensive Air Shower Simulation with CORSIKA: A users guide version 6.990,* [Karlsruhe, Germany: Karlsruher Institut Fur Technologie (KIT)], (2011)

[16] A. Ferrari, P. R. Sala, A. Fasso and J. Ranft, *"FLUKA: a multi-particle transport code" Report CERN-2005-10(2005) INFN/TC_05/11 SLAC-R-773*

[17] E. Faleiro *et al., The Astrophysical Journal Supplement Series,* **155,** 167, (2004)

CHAPTER 6

SIMULATION STUDY ON LATERAL DISTRIBUTION OF CHERENKOV PHOTONS FOR DIFFERENT PRIMARIES

The high energy cosmic ray and gamma ray particles enter the earth's atmosphere isotropically from all directions. They interact with the atmospheric nuclei on their way and give rise to the phenomenon of extensive air shower (EAS) in the atmosphere. The secondary leptons can give rise to the radiation component of an air shower, viz., Cherenkov, Fluorescence and radio-emission. Cherenkov radiation is emitted by ultra-relativistic charged particles moving in a dielectric medium, when the charged particles move faster than the speed of light in that medium. Detection of Cherenkov radiation produced in the earth's atmosphere by EAS particles is a well established method for identification of very high energy cosmic ray particles [1]. The lateral distributions of Cherenkov photons contain valuable information on the development and propagation of the EAS in the atmosphere. The study of Cherenkov photons at the observation level helps to distinguish between gamma ray and hadron primaries. In this particular work, we have

studied the lateral distribution of Cherenkov photons emitted by gamma, proton and iron initiated showers at different primary energies using the Monte Carlo simulation code CORSIKA (version 6.990) [2].

6.1 Cherenkov Radiation Emission

The phenomenon of Cherenkov radiation can be observed when charged particles travel through dielectric medium, such as air, faster than the phase velocity of light in that medium ($v > c/n$) where v is the speed of the charged particles, c is the speed of light and n is the refractive index [3] of the medium. The secondary electrons and positrons are the main components of an extensive air shower that are responsible for the emission of Cherenkov radiation mostly in the visible region of electromagnetic spectrum. With much less absorption, Cherenkov light produced in the atmosphere can reach the ground level. So, it can provide valuable information on the origin and energy of primary particle [4]. The lateral spread of Cherenkov radiation on the ground is more symmetric around the shower axis for gamma ray induced showers compared to hadron induced showers. So, this can be an identification parameter between gamma and hadron induced showers.

The development of an EAS in the atmosphere is being effected by the random interactions of secondary particles with the atmospheric nuclei which give rise to fluctuation [5]. So the Monte Carlo simulation is the best way to study the extensive air shower [6-7]. The CORSIKA code is one of the important numerical methods that

simulates the lateral distribution of Cherenkov light emitted by atmospheric cascades initiated by different primary particles with certain Cherenkov option. In this work effort is made to distinguish between different primaries on the basis of their distribution of Cherenkov photons as a function of core distance. The Cherenkov lateral distribution shape parameter is obtained which is considered as a possible indicator of the type of a primary particle initiating the shower.

6.2 The lateral distribution of Cherenkov radiation

Number of Cherenkov photons falling per unit area (density) on the ground, as a function of core distance gives the Lateral Distribution Function (LDF) of Cherenkov radiation. From this lateral distribution, information on the development of longitudinal profile of a shower can be obtained. Since the emission of Cherenkov radiation occurs through a cone, its lateral spread depends on the height of production. Therefore, its lateral distribution carries signature of longitudinal shower development, and the depth of shower maximum can be estimated from the LDF of Cherenkov light. Generally, the LDF of Cherenkov photons is fitted by two functions, one is the power law function and the other is exponential function. In order to identify the Cherenkov radiation parameters that are sensitive to longitudinal development of air showers, Protheroe and Turver [8] carried out detailed Monte Carlo simulations of air showers. From their work they found that the lateral distribution of Cherenkov photons can be fitted with a power law function intregated over all zenith angles. Here we have fitted the average lateral density distribution of

Cherenkov photons found from our simulation, using the power law function [9] given by Protheroe and Turver [8]

$$Q(r) = C(r + 50)^{-\delta} \qquad (6.1)$$

Where $Q(r)$ is the Cherenkov photon density at core distance, r from the shower axis and δ is the Cherenkov lateral distribution shape parameter and it is related to the depth of shower maximum (X_m) and C is a constant. The relation between δ and X_m at sea level is given by [8],

$$\delta = 0.001\, X_m + 1.6 \qquad (6.2)$$

6.3 Simulation of Cherenkov photons

The simulation of Cherenkov radiation from EAS was performed using the CORSIKA 6.990 code [2] with two models: QGSJET (Quark Gluon String model with JETs) code [10] for interactions of hadrons at higher energies and FLUKA code [11] for lower energies with Cherenkov standard option. The lateral distribution of atmospheric Cherenkov light is obtained at fixed primary energy 10^{14} eV, 10^{15} eV and 10^{16} eV for various primary particles, namely, gamma, proton and iron nuclei. Considering ground level as the observation level, 1000 vertical showers have been generated for each primary particle at each primary energy. The obtained particle output file from CORSIKA code is

decoded with available FORTRAN code. The lateral density of Cherenkov photons have been obtained considering core distance up to 200m for all the primaries.

6.4 Results and Discussion

In order to find the density, the number of Cherenkov photons is counted as a function of core distance. Considering annular rings of 5 meters, the lateral density distribution of Cherenkov photons is obtained up to a radial distance of 200 meters.

The lateral density profile is parameterized with the above mentioned power law function [Eqn. 6.1]. In Fig. 6.1 (a) – (i), the average lateral density distribution with the fitted function are shown as a function of core distance, corresponding to primary particles (gamma, proton and iron nuclei) at primary energy 10^{14} eV, 10^{15} eV and 10^{16} eV respectively. The values of δ and C are tabulated in Table 6.1. It has been found that, the value of δ increases with energy of primary particles. Again these values are systematically larger for gamma induced showers compared to the hadron induced showers.

The values of the shape parameter (δ) are plotted as function of corresponding depth of shower maximum as shown in Fig. 6.2. It is found to follow a linear relation as expected from equation (6.2).

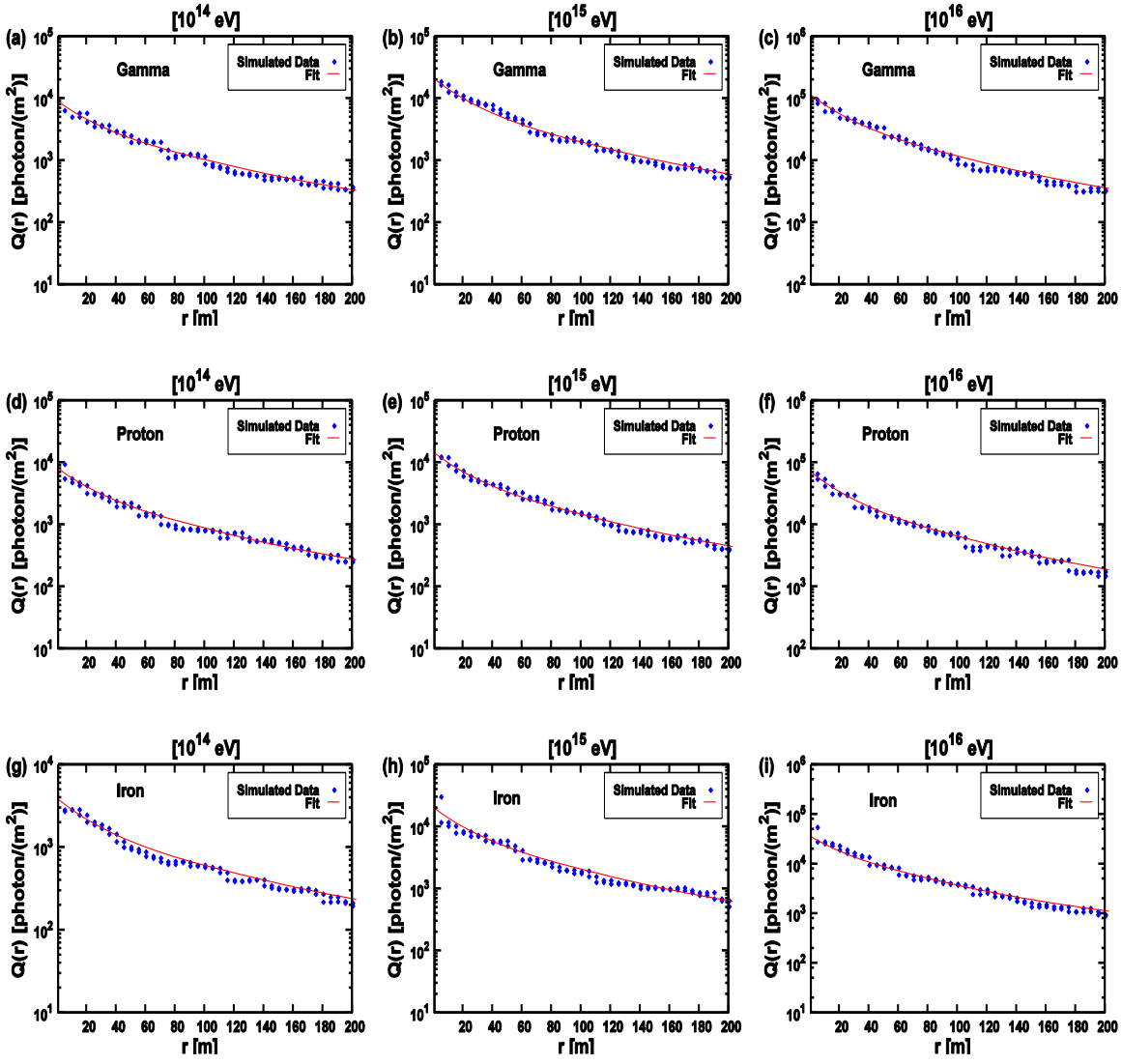

Fig. 6.1

(a)-(c): Average lateral density distribution of Cherenkov photons for gamma induced showers at primary energies 10^{14} eV, 10^{15} eV and 10^{16} eV respectively.

(d)-(f): Average lateral density distribution of Cherenkov photons for proton induced showers at primary energies 10^{14} eV, 10^{15} eV and 10^{16} eV respectively.

(g)-(i): Average lateral density distribution of Cherenkov photons for iron induced showers at primary energies 10^{14} eV, 10^{15} eV and 10^{16} eV respectively.

Table 6.1: Values of the Cherenkov lateral distribution shape parameter (δ) and amplitude parameter C for gamma, proton and iron nuclei at primary energy 10^{14} eV, 10^{15} eV and 10^{16} eV.

Primary Particle	Cherenkov lateral distribution shape parameter (δ)			Parameter C		
	10^{14} eV	10^{15} eV	10^{16} eV	10^{14} eV	10^{15} eV	10^{16} eV
Gamma	2.08	2.2	2.26	2.28×10^{7}	1.25×10^{8}	5.51×10^{8}
Proton	1.98	2.16	2.23	3.06×10^{7}	6.87×10^{7}	5.12×10^{8}
Iron	1.96	2.06	2.14	9.74×10^{5}	5.59×10^{7}	1.56×10^{8}

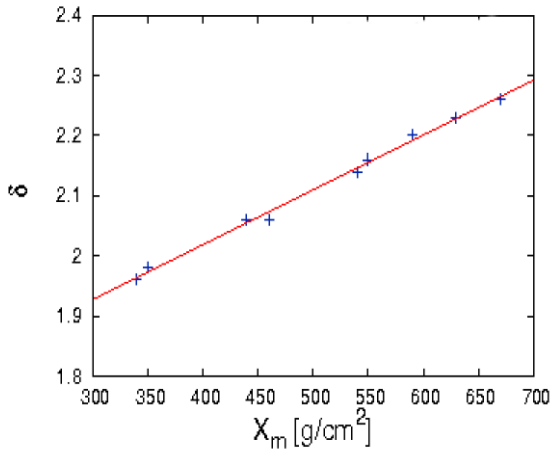

Fig. 6.2 Variation of lateral distribution parameter, δ with depth of shower maximum, X_m.

6.5 Conclusion

The lateral distribution of Cherenkov photons is well fitted by the power law function for all primaries (gamma, proton and iron). The exponent of the function, δ increases with energy and decreases with primary mass number. So, the lateral distribution parameter, δ is found to be dependent on primary energy and particle type. This parameter is found to be linearly correlated with the depth of shower maximum in the atmosphere i.e. X_m, which is different for different primary mass compositions. Hence the shape parameter of the Cherenkov lateral distribution function can be used to infer the primary mass composition and also to distinguish between gamma and hadron induced showers.

REFERENCES

[1] A. A. Watson, *Nuclear Physics B (Proceeding supplements),* 212-213, 13-19, (2011)

[2] D. Heck and T. Pierog, *Extensive Air Shower Simulation with CORSIKA: A users Guide version 6.990*, [Karlsruhe, Germany: Karlsruher Institut Fur Technologie (KIT)], (2011)

[3] M. V. S. Rao and B. V. Sreekantan, *Extensive Air Shower*, World Scientific (1998)

[4] Heike Prokoph, Ph. D Thesis, "Investigations on gamma-hadron separation for imaging Cherenkov telescopes exploiting the time development of particle cascades", Leipzig University, (2009)

[5] A. Hillas, *Space Science Review*, **75**, 17, (1996)

[6] K. Boruah, *Phys Rev. D*, **56**, 7376, (1997)

[7] D. Kalita and K. Boruah, *Indian J. Phys*., **87(3),** 289, (2013)

[8] R. J. Protheroe and K. E. Turever, *Nuo. Cim*, **51A**, 277, (1979)

[9] J. D. Kuhlmann and R. W. Clay, *17th ICRC*, Paris, France, **6**, 96-99, (1981)

[10] N. N. Kalmykov and S. S. Ostapchenko, Yad. Fiz, **56**, 346, (1993)

[11] A. Ferrari, P. R. Sala, A. Fasso and J. Ranft "*FLUKA: a multi-particle transport code",* Report CERN-2005-10(2005) INFN/TC_05/11 SLAC-R-773

CHAPTER 7

DISCUSSION AND CONCLUSION

Different properties of photon induced cosmic ray air showers can be studied by ground based observation of various parameters like secondary charged particle lateral distribution, angular distribution, Cherenkov photon lateral distribution associated with EAS etc. The discovery of high energy cosmic gamma-ray sources has increased the interest for the study of the gamma induced air showers [1]. Cosmic gamma photons having energy > 1TeV can be detected only by the shower of secondary charged particles (EAS) they produce in the atmosphere. As photons are not deflected by electric or magnetic fields, they directly point back to their sources. To distinguish EAS produced by a photon from that produced by a hadron is a real challenge. Various properties of Cosmic Rays can be studied by different theoretical methodologies. One such significant methodology is the Monte Carlo (MC) simulation method [2] which is based on the phenomenological models of the High Energy hadronic interactions [3]. The main objective of this thesis is to study some properties of EAS produced in the atmosphere by high energy cosmic gamma photons and to investigate parameters useful for separating gamma rays from hadron showers. To perform the analysis we have used a library of showers simulated with the CORSIKA code (6.990 and 7.5000) built with different hadronic interaction models and different input parameters like primary nuclei, primary energy etc. [4]

7.1 Angular variation of secondary charged particles

The zenith angle distribution of secondary cosmic ray charged components for different primaries using simulated data have been studied. In this analysis, simulation is carried out assuming primary energy range (10TeV–1PeV) with pure primary nuclei (photon, proton and iron nucleus) as well as mixed primary mass compositions (92%p + 6%He + 2%Fe) & (80%p + 20%γ). Two different versions of high energy hadronic interactions model QGSJET have been tested considering threshold energies ($E\mu > 0.3$ GeV and $Ee > 0.003$ GeV) and ($E\mu > 0.1$GeV and $Ee > 0.001$ GeV) of the secondary particles. The differential zenith angle distributions have been derived from 2000 simulated showers for each set which are fitted with a power law in $\cos(\theta)$. The power index [n] is related with the asymmetry of an EAS. The variation of the shower rate [$F(\theta)$] with zenith angle (θ) gives valuable information about attenuation of EAS in the atmosphere beyond shower maximum. From the simulated data, attenuation lengths (λ) have been calculated assuming different primary compositions. The results are found to agree with a proton dominant mixed composition within experimental error. In this work we compare the two versions of hadronic interaction model viz., QGSJET and QGSJETII. However, no significant difference is observed between the two. In a real experiment, if the composition is measured by other means, then the present method can be used to test any hadronic interaction model. A correlation between the two parameters (n & λ) completely based on CORSIKA Simulation is presented. Pure gamma showers show a negative correlation, whereas hadron showers show a slight positive correlation. When showers with a mixed

composition (92%p + 6%He +2%Fe) is compared with proton showers, the change of the value of 'n' is found to be only about 0.4% to 1% for lower attenuation lengths (< 220 g/cm^2), corresponding to higher atmospheric depths (> 850 g/cm^2, lower altitude). Whereas for higher attenuation lengths (lower atmospheric depths, higher altitude) the change in 'n' varies from about 7% to 10%. Our simulation study shows that the arrays situated at lower atmospheric depths (higher altitudes) are in a better position to infer about average mass composition based on zenith angle distribution.

7.2 Longitudinal and Lateral Profile of showers

This work comprises of longitudinal and lateral distribution of photon induced shower. The depth of shower maximum and number of particles at maximum depth are higher for gamma induced showers compared to proton induced showers. Based on this analysis it is found that shower longitudinal development is well fitted by the Gaisser-Hillas function, and the interaction length is evaluated at different energies. The interaction length, λ_i decreases with energy and its value is more for photon showers than proton showers which shows that λ_i depends on primary energy and mass.

The lateral distribution of photon induced showers is fitted with the NKG function. The variation of lateral shower age, as measured by χ^2- minimisation technique is studied

and it is found that the lateral shower age parameter increases with the zenith angle. The variation of mean lateral shower age with the shower size is studied considering an energy range of 10^{12} to 10^{15} eV, for all the primary compositions. It is found that the lateral shower age decreases with the shower size and takes higher values for heavy nuclei (iron) compared to that of lighter nuclei (proton) and gamma ray primaries. Another parameter relevant for ground based experimental array is the Local Age Parameter (LAP). From our simulation study, it is found to have lower value for gamma shower compared to hadron (proton & iron) shower and remain constant over a large range of core distances beyond about 100m. For hadron showers, this value decreases for larger core distances (~300m). Hence, it can be used for gamma hadron discrimination.

7.3 Study on Fluctuation of showers

In chapter 5, shower to shower fluctuation of secondary cosmic ray charged particles (i.e. electrons and muons) for different primary compositions have been studied. Simulation has been carried out for primary energy 10^{14} eV, 10^{15} eV and 10^{16} eV with pure primary compositions (photon, proton and iron nucleus).

From the study of the longitudinal and the lateral profiles induced by different primaries, the relative fluctuation $(\sigma/\bar{N})$ for electron component is found to be minimum at depth of shower maximum. Longitudinal fluctuation in muon component is found to be

more for gamma primary compared to hadron primary. Fluctuation of the lateral distribution of the muon component is also found to be maximum for gamma induced showers. Hence, lateral and longitudinal fluctuation in muon number may be used to distinguish gamma primaries from hadron primaries.

Again we have made an attempt to find separation between gamma and hadron primaries by applying the variable reduction method known as the Principle Component Analysis (PCA) method. In this method the covariance matrix is being constructed to observe the correlation between the variables. By computing the eigen value equation, it is observed that muon component shows larger variation for gamma shower while electron component shows larger variation for hadron shower. The discrimination power between gamma and hadron primaries are studied separately, by a parameter called quality factor. Such study can help in separation of gamma photons from the cosmic ray background.

7.4 Cherenkov Lateral Distribution Profile

Optical Cherenkov radiation is emitted by the ultra-relativistic charged particles (mainly electrons and positrons) of an EAS in the atmosphere. In chapter 6, the average lateral density distribution of Cherenkov photons have been studied for primary particles (Gamma, Proton and Iron) at primary energy 10^{14} eV, 10^{15} eV and 10^{16} eV, using 'Cherenkov' option in running CORSIKA Code. Simulated data are fitted with the power

law function, $Q(r) = C(r + 50)^{-\delta}$, where $Q(r)$ is the photon density at core is distance (r) from the shower axis and δ is the Cherenkov lateral distribution shape parameter which is found to be linearly related to the depth of shower maximum (X_{max}). It is found that, δ increases with energy of primary particles and is larger for gamma induced showers compared to the hadron induced showers. Hence the shape parameter of the Cherenkov lateral distribution function can be used to distinguish between gamma and hadron induced showers.

7.5 Future work plan

CORSIKA is the most widely used simulation code to study the different components associated with the development of an EAS in the atmosphere. It is proposed to extend our study on fluctuation using PCA method for Cerenkov photon distributions in the extensive air showers, considering energy range of some hundred GeV to few TeV, as the atmospheric Cherenkov technique is used extensively within this energy range. Such study is expected to help in rejecting large cosmic ray hadronic background in ground based gamma-ray astronomy setup.

REFERENCES

[1] B. D'Ettorre Piazzoli and G. Di Sciascio, *Astroparticle Physics,* 199, (1994)

[2] N. Metropolis and S. Ulam, *Journal of Am. Stats. Asso*., **Vol. 44**, No. 247 (1949), p. 335-341

[3] M. V. S Rao & B. V. Sreekantan, *Extensive Air Showers*, World Scientific, (1998)

[4] D. Heck and T. Pierog, *Extensive Air Shower Simulation with CORSIKA: A users guide version 6.990,* [Karlsruhe, Germany: Karlsruher Institut Fur Technologie (KIT)], (2011)

LIST OF PUBLICATIONS

1. Study of longitudinal development of EAS produced by 1 PeV Primary Cosmic Ray gamma photon published in **HORIZON – a journal of Physics, Volume-1, November, 2011, ISBN: 2250-0871.**

   Author: Punam Patgiri and K. Boruah

2. Simulation study on Shower to Shower Fluctuations of Longitudinal Profile published in **Journal of Gauhati University Research Scholars' Association, Volume-V (2011-12) ISSN: 2250-0456.**

   Author: Punam Patgiri, K. Boruah

3. Study of Longitudinal and Lateral Profile of Photon induced EAS using CORSIKA code published in **Proceedings of the National seminar on recent development in natural sciences held at DKD college on 20th to 21th January, 2012, ISBN-13: 978-81-924389-0-0.**

   Author: Punam Patgiri, K. Boruah

4. Study on angular variation of cosmic ray secondary particles with atmospheric depth using CORSIKA code published in **Indian Journal of Physics, Volume 91, Issue 4 (2017) pp 351-358.**

   Author: Punam Patgiri, D. Kalita & K. Boruah

5. A comprehensive study on fluctuation of secondary charged particles for gamma hadron primaries published in **International Journal of Applied Physics, Volume 6, Issue 2, (2016) ISSN: 2249-3174.**

   Author: Punam Patgiri, K. Boruah

6. Gamma hadron discrimination using Local Age Parameter of Cosmic Ray Extensive Air Showers accepted for publication in **proceedings of X^{th} Biennial National Conference of PANE on "Recent Advances in Physics Research and its Releavance" held on 10^{th} to 12^{th} November 2016, Department of Physics, St. Anthony's College.**

   Author: Punam Patgiri, D. Kalita & K. Boruah

CONFERENCE, SEMINAR & WORKSHOP

PARTICIPATED

1. EXPLORING THE COSMOS: 100 years of Cosmic Ray Physics, A Conference on Astrophysics and Astroparticle Physics, 15th to 16th December 2011, High Energy & Cosmic Ray Research Centre, University of North Bengal.
2. RECENT DEVELOPMENT ON NATURAL SCIENCES: A National Seminar, 20th to 21th January 2012, DKD College, Dergaon.
3. Assam Science Society, 57th technical session, 16th March 2012.
4. 2nd Theme meeting on Very High Energy Gamma Ray Astronomy, 29th to 30th March 2012, BARC, Mount Abu.
5. One day UGC SAP National Seminar on new Frontiers in Physics, 11th May, 2012, Department of Physics, Gauhati University.
6. Centenary Seminar 2012: Discovery of Cosmic Ray, 6th August, 2012, Department of Physics, Gauhati University.
7. System Administration using Linux: Summer Training Programme, 23th to 25th July 2012, Electronic Scientists & Engineers Society, Assam.
8. Contemporary Science & Technology: Research & Education, 9th to 10th November 2012, Electronic Scientists & Engineers Society, Assam.

9. CURRENT ISSUES IN COSMOLOGY, ASTROPHYSICS AND HIGH ENERGY PHYSICS (CICAHEP): A National Conference, 2^{nd} to 5^{th} November, 2015, Dibrugarh University.

10. X^{th} Biennial Natinal Conference of PANE on Recent Advances in Physics Research and its Relevance, 10^{th} to 12^{th} November 2016, Department of Physics, St. Anthony's College, Meghalaya.